GEOLOGICAL SURVEY OF CANADA

DEPARTMENT OF ENERGY, MINES AND RESOURCES

BULLETIN 149

STUDIES OF ROCK-FORMING MICAS

J. H. Y. Rimšaite

Price $2.50

1967

STUDIES OF ROCK-FORMING MICAS

2,000— 1966—5452

Chief Scientific Editor
PETER HARKER

Technical Editor
S. E. JENNESS

Production Editor
H. D. MARKELL

Printed on ANCASTER BOOK AND
NO. 1 OFFSET ENAMEL

Set in Times Roman with
20th Century captions by
RYERSON PRESS, TORONTO

Artwork by CARTOGRAPHIC UNIT, GSC

GEOLOGICAL SURVEY
OF CANADA

BULLETIN 149

STUDIES OF ROCK-FORMING MICAS

By

J. H. Y. Rimšaite

DEPARTMENT OF
ENERGY, MINES AND RESOURCES
CANADA

Available by mail from the Queen's Printer, Ottawa,
from Geological Survey of Canada,
601 Booth St., Ottawa,
and at the following Canadian Government bookshops:

OTTAWA
Daly Building, corner Mackenzie and Rideau

TORONTO
221 Yonge Street

MONTREAL
Æterna-Vie Building, 1182 St. Catherine St. West

WINNIPEG
Mall Center Bldg., 499 Portage Avenue

VANCOUVER
657 Granville Street

or through your bookseller

A deposit copy of this publication is also available
for reference in public libraries across Canada

Price $2.50 Catalogue No. M42-149

Price subject to change without notice

ROGER DUHAMEL, F.R.S.C.
Queen's Printer and Controller of Stationery
Ottawa, Canada
1967

PREFACE

The study of micas reported here was initiated because of their increasing geological significance for isotopic dating. Micas are the most important carriers of potassium and rubidium, and are stable under diverse geological conditions.

This report contains the results of detailed mineralogical and petrographic studies of forty-eight mica concentrates and of their host rocks, carried out by the author on samples selected from amongst several hundreds that were submitted for age determination by the Geological Survey. These studies contribute to a better understanding of relationships between chemical composition and physical properties of micas, and of paragenetic relations of micas and other minerals. A probable relationship between chemically abnormal, partly dehydrated micas and their isotopic age is also indicated.

J. M. HARRISON,
Director, Geological Survey of Canada

OTTAWA, April 7, 1964

BULLETIN 149 — Studien über gesteinsbildende Glimmer.

Von J. H. Y. Rimšaite

Dieser Bericht enthält ausführliche mineralogische und petrologische Angaben űber gesteinsbildende Glimmer und Schlussfolgerungen űber die Beziehungen der chemischen Zusammensetzung des Glimmers zur Art des primären Gesteins, den Ablauf der Kristallisation und die Begleitmineralien.

БЮЛЛЕТЕНЬ 149 — Исследования породообразующих слюд.

Я. Х. Римсайте

Отчет излагает результаты детального минералогического исследования породообразующих слюд. Также излагаются выводы о взаимоотношениях между химическим составом слюды и типом вмещающей породы, последовательности кристаллизации и сопутствующих минералах.

CONTENTS

Illustrations

STUDIES OF ROCK-FORMING MICAS
Physical Properties, Chemical Compositions, and Paragenesis

Abstract

Mineralogical and petrological studies of forty-eight mica concentrates and of their host rocks were carried out in order to establish the relationship between the chemical composition of fresh micas and the following physical properties: optical and X-ray diffraction properties, specific gravity and specific magnetic susceptibility, and stability on heating. This relationship is illustrated in fifteen working curves. The chemical composition of mica is related to the type of host rock, sequence of crystallization, and associated minerals. A special emphasis is placed on rocks containing more than one generation of micas.

Résumé

L'auteur a entrepris l'étude minéralogique et pétrologique de quarante-huit concentrés de mica et de leur roche encaissante pour déterminer la relation qui existe entre la composition chimique des micas frais et les propriétés physiques suivantes: propriétés de diffraction des rayons lumineux et des rayons X, poids spécifique et susceptibilité magnétique spécifique, et stabilité à la chaleur. Quinze courbes illustrent cette relation. La composition chimique du mica varie selon la roche encaissante, le mode de cristallisation et les minéraux associés. L'auteur a accordé une attention spéciale aux roches qui renferment plus d'une génération de mica.

Chapter I

INTRODUCTION

This report is a result of the writer's mineralogical and petrological studies, carried out in addition to the general examination of the mica concentrates prepared for K-Ar dating (Lowdon, 1960, 1961, 1963). The present study is concerned with determining the homogeneity of each mica concentrate, establishing the type or types of mica present, correlating physical and chemical properties of the micas, and establishing the relationship between the type of mica and the type of its host rock. A summary of this study has already been presented at the Third General Meeting of the International Mineralogical Association in Washington (Rimsaite, 1962).

The term 'rock-forming micas' refers to the common mica varieties, which are essential components of diverse rock types.

Summary of Previous Related Studies

The advantage of relatively rapid physical methods over time-consuming chemical analyses for the identification and classification of mineral species has been realized by mineralogists in the past century. While optical and X-ray diffraction methods for identification of chemically simple mineral species are well established, accurate identification of chemically complex minerals is not yet possible without a complete chemical analysis. Extensive studies are required in the search for suitable physical properties that would permit quantitative determination of all ions composing chemically complex minerals.

During the past six decades many attempts have been made to correlate physical properties of natural and synthetic micas with their chemical composition. A detailed summary of the most important studies of natural micas over a period from 1855 to 1953 was made by Heinrich *et al.* (1953), who also included a description of over one hundred names given to diverse members of the mica family. More recently, Deer, Howie, and Zussman (1962) published a comprehensive description of the mica family, including data on synthetic micas.

An optical method for the rapid identification of the most important mica groups has been proposed by Burckhardt (1943). On the basis of refractive index γ and optic angle 2V, he constructed a diagram for distinguishing muscovite, iron-rich muscovite, phengite, lepidolite, zinnwaldite, phlogopite, biotite, and lepidomelane. Burckhardt also noticed that changes in optic angle may take place during heat treatment at temperatures of 100° to 150°C, which may be reached in the preparation

MS. received December, 1963.

of thin sections. This confirmed earlier observations of Rinne (1924) that the micas lose water during heat treatment and are susceptible to oxidation. Winchell (1935, 1951) correlated the optical properties of biotite with the molecular percentages of four end-members: phlogopite, eastonite, annite, and siderophyllite. However, his diagram does not account for the effect of Ti, Na, and other ions. Kunitz (1924) pointed out that the composition of biotites is much too complex to be expressed by the molecular percentages of three or four end-members. He later showed that an increase of one per cent TiO_2 (by weight) raises the refractive index by 0.01 (Kunitz, 1936).

Nagelschmidt (1937) was the first to apply an X-ray diffraction method to distinguish biotite from muscovite in clays by measuring the spacing b_0. Harder (1956) found a relationship between the spacing $c_0 \sin\beta$ and the sodium content in muscovite and paragonite. Gower (1957) developed an X-ray diffraction method for quantitative determination of the amount of iron occupying octahedral positions in biotites. The method is based on variations in the phase angles and scattering powers of the Mg and Fe ions, which contribute to the intensities of basal reflections (004) and (005). He pointed out that the method is not suitable for the detection of Mn, Ti, Al, and Li, which may substitute for Mg and Fe in octahedral coordination. Gower also attempted to correlate the size of the unit cell with the composition. His results showed that the spacing $c_0 \sin\beta$ decreases with increasing iron content.

A similar relationship was also observed by von Engelhardt (1943) in chlorites and other layer minerals. Von Engelhardt studied this phenomenon from the structural viewpoint. He considered the polarizing factor of Al, Mg, and Fe cations. In the octahedral layer these cations are exposed to strain, which results from mutual intercationic repulsion and a strong attraction to the (OH) layer. The polarizing effect increases in the order Al < Mg < Fe and causes a proportionate deformation of the octahedral layer, thus affecting the spacing c_0. Studies of synthetic annite by Eugster and Wones (1962) showed that optical properties and unit cell dimensions depend on conditions of synthesis; i.e., temperature, pressure (P_{H_2O}, P_{H_2}) and fugacity of oxygen.

Previous attempts to correlate physical properties and chemical composition of micas have shown that the main factors affecting the correlation are variability of chemical composition, homogeneity of analyzed samples, structure of the micas, conditions of crystallization, and post-crystallization alterations. The occurrence of more than one type of biotite in fine-grained rocks is commonly overlooked because of optical similarity in thin section. Chemical analysis of a concentrate that is composed of more than one type of mica cannot be properly evaluated and would lead to incorrect correlation of properties. Because no mica concentrate can be completely homogeneous, the relationship between chemical composition and any one of the physical properties can be only a close approximation. Obviously, the determination of a single physical property will not be sufficient to characterize the chemical composition of a given mica.

Hirschi (1901) and Schauberger (1927) found that iron-rich biotites occur in granitic rocks, and magnesium-rich micas occur in basic rocks. Heinrich (1946) studied the relationships between some of the major chemical components of biotite

and the type of the host rock, and using published analyses, plotted percentages of $(Fe_2O_3+TiO_2)$-MgO and (FeO+MnO) of biotites on triangular diagrams. Nockolds (1947) made similar diagrams using total iron as FeO-MgO and Al_2O_3, and found that biotites associated with aluminum-rich minerals contain considerable quantities of octahedral aluminum. Foster (1960) made a similar study by plotting the octahedral Mg-(Fe'', Mn) and (Al, Fe''',Ti) of trioctahedral micas and confirmed the previous observations. The compositional field of trioctahedral micas from granitic rocks was found to be the largest, enclosing micas from schists, gneisses, and diorites. Micas from basic rocks, pegmatites, and limestones showed narrower compositional fields on triangular diagrams and thus a more definite relation to the host rock. The wide compositional field of micas from granitic rocks has been attributed to diverse definitions of the term 'granite' (Foster, 1960) and also to impure samples (Nockolds, 1947). To the writer's knowledge, however, no systematic study has yet been performed on the position of biotites in the sequence of crystallization of diverse rock types, and this might possibly account for the wide range of variations in chemical composition of micas from such rocks as 'granite'. This is one of the objectives of the present study.

The stability ranges and the conditions of crystallization of the principal mica types have been extensively studied at the Carnegie Institution by Yoder and Eugster (1954, 1955) and Eugster and Wones (1962). Yoder and Eugster (1955) compared the upper stability curve of muscovite with the minimum melting curve of 'granite' (after Bowen and Tuttle, 1953) and concluded that muscovite can form during

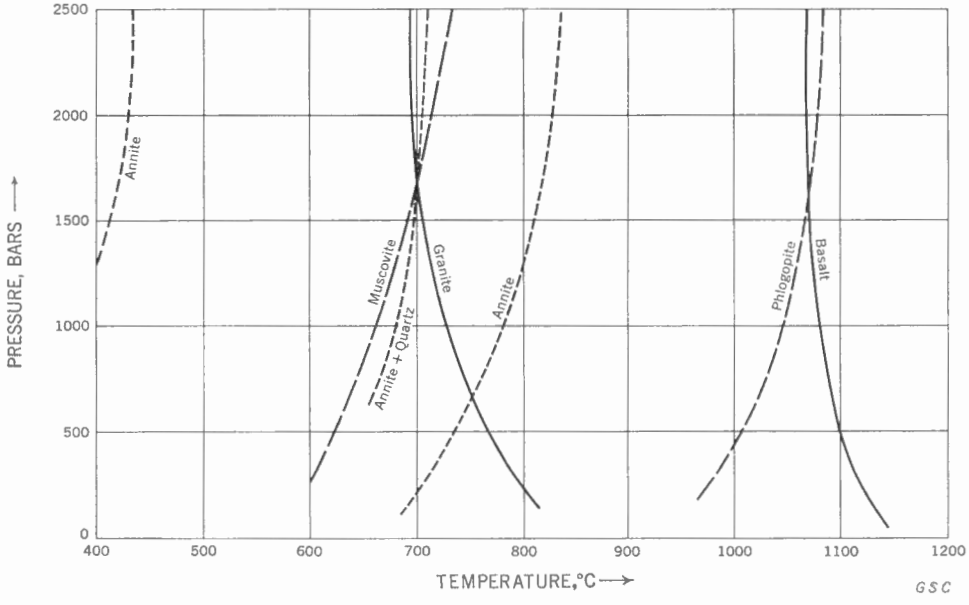

FIGURE 1. Upper stability curves of phlogopite, muscovite, and annite in relation to minimum melting curve of 'granite' and basalt. Stability of annite (three curves reproduced) depends on fugacity of oxygen. [Curves from Yoder and Eugster (1954, 1955) and Eugster and Wones (1962).]

crystallization of granite above 1,500 atm. water pressure, provided some alumina is still available after crystallization of alkali feldspar. The early muscovite formed during crystallization of 'granite' is relatively rare. The later muscovite, which forms in a solid state below 1,500 atm. water pressure as an alteration product of feldspars, and muscovite formed during metamorphic reactions are more common. Eugster and Wones (1962) found that stability of Fe-Mg biotites is a factor of temperature, water pressure, and fugacity of oxygen. They also observed that iron-rich biotite is very sensitive to environmental changes and breaks up into a biotite that contains less iron, plus iron oxides. Results of these experimental studies, showing the upper stability curves of the principal mica types in relation to the minimum melting curves of 'granite' and basalt, are summarized in Figure 1.

These experimental studies have made a very important contribution to petrology. Natural conditions of crystallization, however, are much more complicated as a result of the presence of mineralizers and more complex chemical systems (Goldschmidt, 1954). The role of mobile alkalis on mineral paragenesis has been recently discussed by Korzhinsky (1960) and Szádeczky-Kardoss (1960). According to Korzhinsky, paragenesis and the Fe/Mg ratio in ferromagnesian minerals depend on the alkalinity of magma. A higher activity of alkaline metals causes an early precipitation of strong inert bases, whereas residual alkaline magma is enriched in silica and weak bases. The basicity of oxides decreases in this order: K_2O, $Na_2O > Li_2O > CaO > MgO > FeO > Al_2O_3 > Fe_2O_3 > SiO_2$. Thus, paragenesis of biotite-plagioclase becomes unstable with increasing alkalinity and is replaced by paragenesis of orthoclase and hornblende and, with further increase in potassium activity, by orthoclase and pyroxene.

Szádeczky-Kardoss (1960) pointed out the natural abundance of altered igneous rocks (neglected in most of the earlier petrological classifications), and the scarcity of 'fresh rocks', which were subjected to intensive studies and served as a basis for the classification of igneous rocks. He included this most abundant group of 'altered rocks', containing volatile-bearing minerals, in his system of igneous rocks, and pointed out the importance of volatile migration (transvaporization) during the interaction of magma and surrounding masses. These altered rocks are his hemiorthomagmatites, formed, after a prolonged high-viscous stage, by long-lasting ionic differentiation. They include residual rocks, such as anorthosite, at the deeper parts of sialic crust; and alkaline igneous rocks, granites, aplites, and lamprophyres, which are characterized by transitions into metamorphic and metasomatic granitoid rocks at higher levels.

The effect of volatiles H_2O, NH_3, HCl, and HF on the sequence of crystallization of the obsidian melt was studied in laboratory experiments by von Platen and Winkler (1961). Results of these studies showed that these volatiles affect the sequence of crystallization of alkali feldspar, plagioclase, and quartz and also the temperature of crystallization. In the presence of NH_3, magnetite is the stable iron-bearing mineral, and the biotite does not form at all. In the presence of HF, biotite crystallizes during the late stage.

The importance of textural studies in distinguishing between the magmatic and metasomatic origin of rocks has been shown by Goodspeed (1959). Ramberg (1952) discussed in detail chemical reactions, which include formation and decomposition of micas during metamorphic processes.

The present report is based chiefly on the writer's thin section and petrological studies, which were carried out with a knowledge of the above-mentioned results.

Abbreviations

The following abbreviations have been used in the tables, illustrations, and in part in the text:

α, β, γ	= least, intermediate, and greatest refractive indices; also the vibration directions of the fast, intermediate, and slow rays.
OAP	= optic axial plane
$2V^\circ$	= optic angle
$I_{(004)}$	= measured X-ray intensity of the fourth order basal reflection
$I_{(005)}$	= intensity of the fifth order reflection
1M	= one-layer monoclinic mica (abbreviation proposed by Smith and Yoder, 1956)
1Md	= one-layer disordered mica
2M	= two-layer monoclinic mica
DTA	= differential thermal analysis
TGB	= thermogravimetric balance
ΣoctFe	= total octahedral iron
%ΣFeGrMe	= per cent of total iron group metals
Sp. G.	= specific gravity
pl H	= pleochroic haloes

Minerals:

Ab, Alb	= albite
Ap	= apatite
B, Bio	= biotite
Ca	= calcite
Ch, Chl	= chlorite
chlorit	= (chloritized, partly altered to chlorite)
Ep	= epidote
H	= hornblende
Ilm	= ilmenite
Mgn	= magnetite
M, Mu	= muscovite
Ph, Phl	= phlogopite
Pl	= plagioclase
Py	= pyroxene
Q	= quartz
Ru	= rutile
Sph	= sphene
Zr	= zircon

Acknowledgments

The writer gratefully acknowledges kind cooperation and helpful criticism by fellow officers of the Geological Survey of Canada, especially to Dr. R. J. Traill who read the manuscript. Three summer assistants, Miss Mabel Corlett, Mrs. N. F. H. Bristol, and Miss C. M. Hunt, gave valuable assistance. Mica concentrates, chemical analyses, and X-ray spectrographic analyses were made by the Geological Survey staff. Differential thermal analysis and thermogravimetric balance tests were made by the staff of the Physical Chemistry section, Mines Branch.

Chapter II

EXPERIMENTAL PROCEDURES AND RESULTS

Selection of Samples

Fifty micas were selected for the present study from several hundred concentrates prepared for age determination. The choice was made on the basis of physical properties, origin, age, and quantity available. Seven chemical analyses of coarse micas (*3*, *4*, *6*, *7*, *10*, *13*, and *31* in Table III) from the crystalline limestones, gneisses, and pegmatites of the Grenville subprovince, Bancroft area, Ontario, were made available for the present study by S. C. Robinson. Concentrate *31* was present in sufficient quantity for further mineralogical studies. However, since the other samples were used up in chemical analysis, the mineralogical studies were carried out on newly prepared concentrates from the same rocks. J. E. Reesor kindly permitted the use of six analyzed concentrates (*14*, *16*, *17*, *22*, *23*, and *25* in Table III) from granodiorites and quartz monzonites of the White Creek Batholith, British Columbia (Reesor, 1958). The locality and source of all samples are given in Figure 2 and in Table I. Thirty-two of the micas were of Precambrian age and were collected from the northeastern, southern, and western margins of the Canadian Shield. The host rocks included: one picrite, one anorthosite, one porphyritic basalt, two lamprophyres, three granodiorites, four quartz monzonites, two pegmatites, two radioactive orebodies, one pyroxenite gneiss, four marble pyroxenites, four gneisses, three paragneisses, and one cordierite schist. Late Cretaceous and Tertiary micas from the Canadian southern Cordillera were concentrated from five quartz monzonites, six granodiorites, and one porphyroblastic gneiss. Two micas of Cretaceous age were separated from anorthositic gabbro and granodiorite from the Mount Megantic complex, Quebec.

Homogeneity of the concentrates selected for chemical analysis was determined on the X-ray diffractometer and optically in oil immersion mounts. Large concentrates containing free mineral impurities were reconcentrated. In some cases, purification of the concentrates could not be performed because of insufficient quantity of material.

Description of the concentrates, quantity and nature of impurities, and homogeneity of the micas are summarized in Table II. Heterogeneity of a concentrate is caused by the presence of free mineral impurities and by physical and chemical variations of the mica flakes themselves. Chemical analyses can be corrected for the mineral impurities, but it is difficult to account for the variations in the flakes.

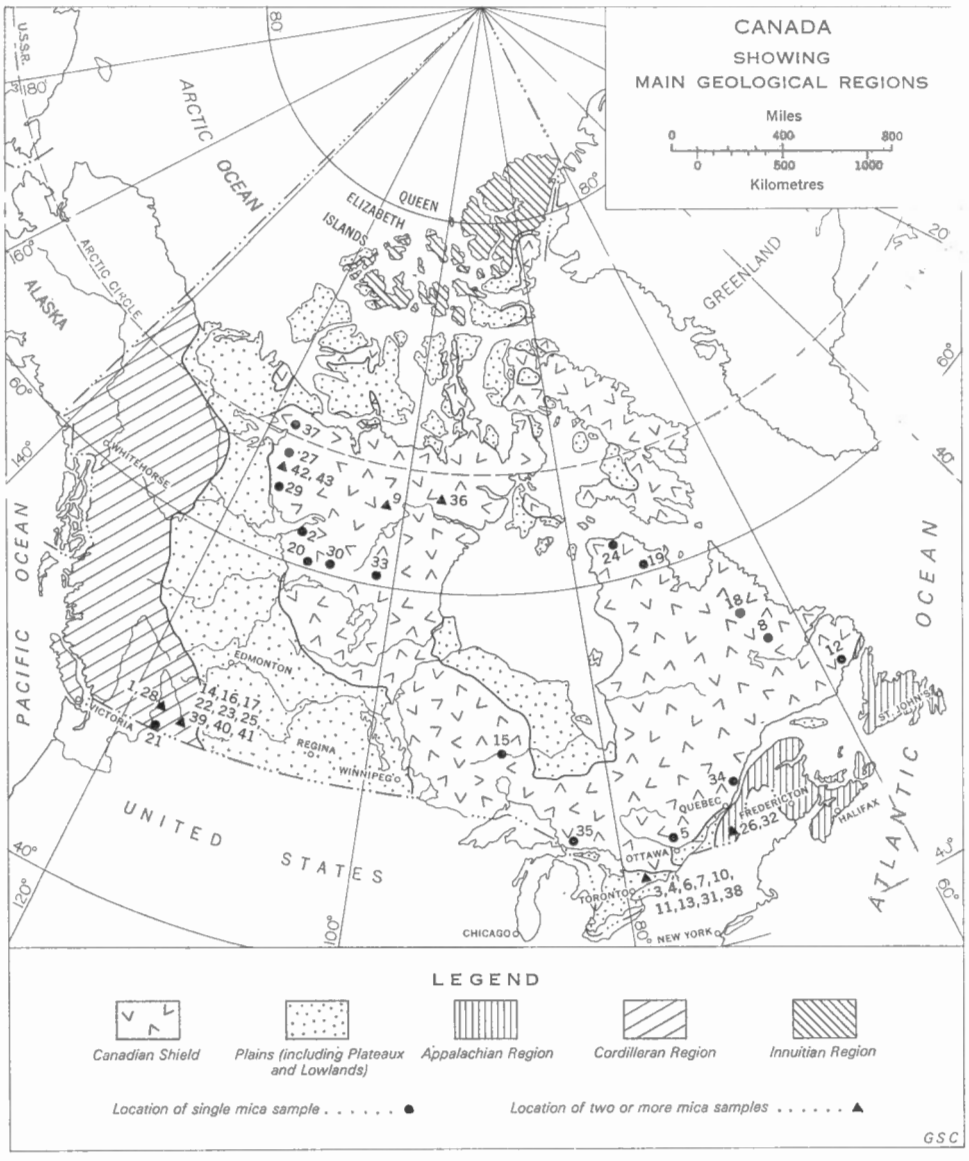

FIGURE 2. Index map showing location of samples (see Table I).

Optical Study

Optical study included examination of micas in thin sections and in oil immersion mounts. Thin section study provided valuable information on the relation of micas with other minerals, their origin, paragenesis, and general degree of alteration. The concentrates, on the other hand, contain the least altered and cleanest mica flakes that can be obtained from the rock. Both types of study are needed for proper evaluation of the mica properties.

Determinations of the refractive indices were carried out in oil immersion mounts using Shillaber's Certified Index of Refraction Liquids, which were periodically checked on the refractometer. Measurements of refractive indices were made on several hundred flakes from each selected concentrate. The average, as well as the extreme low and high, values for the majority of the flakes are reported in Table II. The average values were used in correlating refractive indices with chemical compositions. The accuracy of the determinations is ± 0.001, which is much less than the extreme variations obtained on a few individual flakes in the concentrate.

Measurements of the optic angle were carried out with a Zeiss auxiliary microscope with built-in micrometer plate, using Mallard's method. In order to calculate Mallard's constant, the optic axes of a few muscovite flakes were measured on the universal stage. The 2V values were determined from Troeger's table (Troeger, 1952, p. 122).

The colour (γ, β) of the flakes was determined in transmitted light using x100 magnification, by comparing the colour of the mica flake with Ridgway's (1912) colour standards. This procedure is very simple and allows rapid determination and recording of the characteristic colour of the majority of the mica flakes, and of their variations in colour.

Results of the optical examination show that none of the concentrates is entirely homogeneous. The heterogeneity can be summarized as follows:

(1) different abundance and nature of mineral inclusions (concs. *1*, *28*, *9B*, *7*, *5*; Pl. I-1, 3, 3a, 7; Pl. II-1, 2);

(2) presence of single and composite mica flakes (muscovite conc. *1*; Pl. I-1, 2);

(3) presence of more than one mica type in the concentrate (phlogopite conc. *9Ph* with a small amount of the biotite flakes *9B*; Pl. II-1, 2);

(4) local variations of the flake itself (oscillating zoning, Pl. II-1); apparent zoning as a result of alternating clear and inclusion-rich zones (phlogopite *5*, *5incl*; Pl. I-7, 8);

(5) presence of green and brown unchloritized flakes in the concentrate (most specimens from British Columbia);

(6) morphological variations within the flake (splitting along (001) planes, Pl. I-4; blistering, Pl. I-6; polygonal cracks, Pl. III-5);

(7) variable degree of γ,β pleochroism [γ brown, β green];

(8) different degree of alteration of the flakes and local alterations of a flake (biotite conc. *33*, Pl. III-3, 4).

Table III

No.	Concentrate (Field No.)	SiO_2	Al_2O_3	TiO_2	Fe_2O_3	FeO	MgO	MnO	Cr_2O_3	NiO
1	1955-165a-RA(Mu)	47.8	32.4		2.2	0.96	0.73			
2	SH-44-59	47.6	31.8		2.8	0.87	0.87			
3	56-RC-37	42.3	10.0	0.40	0.0	2.59	26.8	0.00		
4	56-RC-40	42.8	10.1	0.30	1.3	0.79	26.4	0.00		
5	B-JR-1	39.12	18.24	0.54	0.96	1.27	24.47	0.03	0.02	
6	55-SR-45	41.4	10.2	0.40	3.7	4.22	23.2	0.2		
7	56-RC-29	43.4	9.4	0.70	0.6	5.55	21.8	0.1		
8	WED-3-30	41.5	12.07	1.25	1.92	6.90	21.3	0.06	0.23	0.06
9	SH-101-59 (Ph)	41.34	14.94	1.43	1.82	6.15	18.11	0.07	0.93	0.03
10	56-RC-17	40.8	10.0	0.50	2.1	13.85	16.3	0.40		
11	60-RC-2 compact	41.92	10.4	0.90	6.31	10.50	14.3	0.50		
11B	60-RC-2 Blistered	41.96	9.81	1.04	6.95	10.87	14.48	0.51		
12	FB-3-59	39.12	12.49	3.57	1.28	14.61	15.14	0.21	0.02	0.02
13	56-RC-28	39.6	10.6	1.9	3.8	15.22	14.6	0.5		
14	W-58-RA-1A	37.78	15.39	1.66	3.28	15.22	12.55	0.32		
15	FB-28-59	36.11	18.5	2.63	1.46	16.62	10.5	0.33		
16	W-58-RA-14	36.20	17.04	1.93	3.13	15.80	12.14	0.45		
17	W-58-RA-1	36.66	15.12	1.81	3.62	15.70	11.96	0.34		
18	BL-9-157	36.50	15.80	2.05	3.95	16.70	11.34	0.34		
19	KG-306-59	36.70	15.10	4.10	2.83	15.90	11.82	0.21		
20	SH-40-59	37.00	17.2	3.4	0.98	18.44	9.9			
21	5-RA-4	36.40	14.6	4.0	3.06	16.50	12.28	0.25		
22	W-58-RA-9	35.70	16.0	2.38	3.54	17.05	11.04	0.40		
23	W-58-RA-19	36.20	15.97	2.52	3.72	17.08	10.32	0.38		
24	KG-58-59	36.70	16.10	2.83	3.37	18.68	9.16	0.23		
25	W-58-RA-21	34.70	16.38	2.93	3.67	18.99	8.87	0.47		
26	LA-2-59R	36.27	13.88	4.05	2.95	18.98	10.29	0.14	0.02	0.02
27	SH-52-59	35.2	19.8	3.1	1.9	20.82	6.40			
28	1955-165a-RA	35.5	18.1	2.5	2.1	21.67	6.0			
29	SH-58-59	35.3	14.9	2.71	3.67	22.63	7.56	0.43		
30	SH-90-59	36.11	14.41	4.29	2.37	23.18	6.78	0.20		
31	56-RC-41	32.8	16.8	1.5	7.2	22.36	5.8	0.9		
32	LA-1-59R	36.43	12.55	3.5	5.56	22.49	6.01	0.44		
33	SH-95-59	34.9	14.7	3.3	3.5	28.79	3.2			

*Analyses by G. Bender and S. Courville, Analytical Chemistry Section; analyses 1-4, 6-8, 10, 13, 27-29, 31, and 33 by rapid methods

*Chemical Analyses of Micas**

Li_2O	ZnO	K_2O	Na_2O	CaO	BaO	Rb_2O	SrO	H_2O^+	H_2O^-	F	P_2O_5	Total	Less F≡O	Net Total
		10.1	0.76	0.05				4.40		0.28		99.68	0.12	99.56
		10.2	0.76	0.35				4.10		0.19		99.54	0.08	99.48
		9.9	0.9	1.0	0.2			2.10	0.5	4.3	0.00	101.00	1.8	99.2
		9.7	0.5	1.3	0.3			2.15	0.35	4.21	0.00	100.2	1.8	98.4
		9.46	0.34	0.26	0.25			2.88	0.32	2.28	0.06	100.5	0.96	99.54
		10.0	0.3	0.9	0.3			1.85	0.35	4.2	0.00	100.9	1.8	99.1
		10.0	0.3	0.9	0.3			1.35	0.25	5.7	0.00	100.4	2.4	98.0
		9.55	0.39	0.40	0.27			1.40	0.04	3.33	0.05	100.72	1.4	99.32
		9.12	0.55	0.68	0.54		0.02	2.94	0.08	0.74	0.05	99.54	0.31	99.23
	tr	9.7	0.3	0.0	tr			1.92	0.88	3.73	0.00	100.5	1.6	98.9
0.71		9.9	0.12	0.22	0.05	0.74	Cs_2O 0.1	1.32	0.19	3.67	0.02	101.72	1.54	100.18
0.65		9.36	0.11	tr		0.73	Cs_2O 0.1	1.66	0.26	3.64	0.03	102.06	1.53	100.53
		9.52	0.23	0.18	0.11	0.1		1.32	0.04	2.80	0.03	100.69	1.18	99.51
		9.5	0.3	0.2	tr			1.5	0.35	3.63		101.7	1.5	100.2
		8.96	0.25	0.85	0.16			3.32	0.08	0.44	0.10	100.28	0.18	100.10
		9.54	0.1		0.11			3.05	0.05	0.55	0.08	99.63	0.23	99.40
		9.30	0.06	0.38	0.19			3.02	0.08	0.47	0.07	100.26	0.20	100.06
		9.35	0.1	0.58	0.14			4.07	0.10	0.50	0.10	100.15	0.21	99.94
		9.39	0.05	0.04	0.11			3.23	0.07	0.37	0.07	100.01	0.16	99.85
		9.42	0.13	0.03	0.28			2.64	0.06	0.59	0.05	99.86	0.25	99.61
		9.1	<0.2	0.65				3.30		0.23		100.40	0.10	100.3
		9.33	0.07	0.04	0.30			2.47	0.06	0.42	0.06	99.84	0.18	99.66
		8.58	0.04	0.11	0.09			3.90	0.10	1.18	0.19	99.67	0.50	99.17
		9.32	0.10	0.23	0.09			2.69	0.04	0.73	0.29	99.69	0.31	99.38
		9.39	0.05		0.18			2.90	0.10	0.31	0.04	100.04	0.13	99.91
		8.61	0.04	0.34	0.23			3.73	0.04	0.99	0.21	100.20	0.42	99.78
		8.39	0.27	0.48	0.38	0.02		2.92	0.20	0.18	0.05	99.47	0.08	99.39
		9.30	<0.2	0.27				3.70		0.51		101.2	0.21	100.99
		9.20	<0.2	0.12				3.50		0.83		99.72	0.35	99.37
		9.09	0.10	0.02	0.05			2.93	0.04	0.49	0.12	100.04	0.21	99.83
		8.21	0.14	0.46	0.91	0.05		2.80	0.10	0.59	0.03	100.58	0.25	100.33
		9.3	0.3	0.2	tr			3.02	0.63	0.55	0.00	101.4	0.2	101.2
		8.25	0.11	0.06	0.32	0.11		2.79	0.26	1.22	0.04	100.03	0.51	99.52
		8.2	<0.2	0.05				3.30		0.63		100.77	0.27	100.5

The refractive indices and the optic angle of individual flakes in the concentrate vary in relation to their heterogeneity. Extreme variations of the optical properties were observed in mica flakes of the following concentrates: *9B* and *9Ph*, which are composed of zoned flakes and different types of mica; concentrate *33*, which contains some flakes partly altered to chlorite with local segregations of iron; and concentrate *31*, in which mica alters along the fractures to a strongly pleochroic mica with γ, β orange-green, extremely high R.I. = 1.740, and relatively large 2V = 24°.

The optic angle of muscovites is about 40°. In composite grains, however, it may appear much less than 40°, as a result of random orientation of the individual flakes, and approaches 0° when the optic axis planes of the flakes are in perpendicular positions (Pl. I-2). Similarly, the optic angle of almost uniaxial biotite appears larger in areas containing muscovite inclusions (Pl. I-3), as a result of the relatively large 2V of the interfering muscovite.

In general, the optic angle of the biotites is small, but distinctly increases in pleochroic haloes that surround radioactive inclusions (Pl. I-3a). The large optic angle was also observed in flakes that exhibit a distinct γ, β pleochroism (and thus resemble pleochroic haloes) in the blistered areas and in altered flakes.

X-Ray Diffraction Study

All concentrates were scanned on a General Electric X-ray diffractometer in the 2θ range from 4° to 47° and from 58° to 62° in order to detect impurities and to measure the position of the $d_{(060)}$ reflection. The diffractometer was operated at 45 kilovolts and 16 milliamperes, using Ni-filtered copper radiation. The scan speed was 2° per minute. The samples for analysis were packed into aluminum holders and pressed with a glass slide in order to obtain a flat surface and a preferential (001) orientation of the mica flakes and other layer minerals. In order to estimate the quantity of impurities from X-ray diffractometer charts, the following standard mixtures were prepared and X-rayed for comparison: biotite-chlorite, biotite-hornblende, biotite-muscovite, muscovite-quartz-feldspar, and muscovite-calcite. X-ray diffraction results and optical estimates of impurities were in most cases in good agreement. The X-ray diffraction method for the detection of impurities is much less sensitive (*ca* 100 times) than the optical method, but it provides means for more accurate quantitative determination of impurities (> 1 %) present both in intergrowths with micas and as inclusions in mica flakes. The optical method is useful in determining the mode of occurrence of chlorite; i.e., whether chlorite occurs in separate flakes, in intergrowths with mica, or as a partial alteration of mica flakes.

Special care must be taken in the X-ray quantitative determination of impurities in heterogeneous mica concentrates. Concentrates containing more than one type of mica display broad and multiple basal reflections, and this results in the decreasing intensity of the peaks. X-ray determination of different mica types in a concentrate is possible when the difference between the positions of basal reflections is more than 0.005° and if different mica types are present in about equal amounts. In other cases the peaks are not resolved.

Further X-ray diffraction studies include determination of the intensity ratio (004) to (005) and the measurement of the position of basal reflections. The two values

of the intensity ratio reported in Table II were obtained (1) by measuring areas under the peak, and (2) by measuring intensity at the highest point of the peak. In order to measure the area under the peak, the sample was scanned at slow speed, 0.2° per minute, and the pulses counted on a scaler for a sufficient period of time to traverse the peak. The intensity of the background was counted for 100 seconds at a fixed position on each side of the peak, and the background area was obtained by multiplying average background counts by scanning time. The peak area (expressed as counts) was obtained by subtracting the background area counts from the total counts. In the second procedure, the 2θ position of the highest point of the peak was obtained by manual adjustment of the vernier on the diffractometer. The intensity at the top of each peak was counted for a period of 100 seconds. The slight difference in intensity ratios (004)/(005) between those obtained by areas and those obtained at the top of the peak can be explained by the difference in the width of the peaks (004) and (005). The best reproducibility was obtained in the range of intensity ratio approaching 1. The high intensity ratios are least reproducible (2.0 ± 0.1, peak counts; 2.0 ± 0.2, area counts) because of the high background intensity of iron-rich biotites and the decreasing net intensity of the (005) peak, which becomes less than the intensity of the background. Thus a slight variation in the intensity of the background has a considerable effect on the net intensity of the basal reflection (005). Reproducibility of the peak counts is somewhat better than that of net area counts.

Lattice spacings $d_{(010)}$ and $d_{(001)}$ were calculated from measurements of the positions of the (060) and (001) reflections on diffractometer charts. To test the errors in determining the peak locations, ground quartz was added to several mica concentrates, and positions of SiO_2 reflections (100) and (112) were measured on X-ray diffractometer charts. A comparison with α-SiO_2 spacings reported by Swanson and Fuyat (1953) showed a displacement of peak (100) by 0.03° and showed no displacement of peak (112). Adding up all errors arising from the instrument displacement, sample preparation, etc., which have been discussed in detail by Chayes and MacKenzie (1957), the accuracy of the spacings reported in Table II is about ± 0.01 Å.

To determine structural modifications of micas, several flakes of each concentrate were X-rayed using the conical Laue camera. The camera is described in detail by its designer O. Braitsch (1957) and was applied for study of structural modifications of micas by the writer (Rimsaite, 1957). A few Laue patterns of different mica polymorphs are illustrated by Hendricks and Jefferson (1939). Identification of the structural modifications is made by a comparison of Laue patterns of unknown micas with the standard patterns. One-, two-, and three-layer micas can readily be identified; other modifications can be selected for more accurate study with the Weissenberg camera.

No impurities were detected on the X-ray diffractometer charts of 30 concentrates. Twelve concentrates contained small quantities of chlorite, ranging from 1% to 4%. Two concentrates contained *ca* 10% and one *ca* 20% of chlorite, and the most impure concentrate *ca* 10% of chlorite and *ca* 15% of hornblende. Chemical analyses were corrected for these impurities.

Proportions of chlorite in relation to biotite, shown as chlorite/biotite in Table II, were determined according to a method devised by R. J. Traill. By measuring prepared standard mixtures, the relationship between the ratio of chlorite to biotite (by

weight) and the net intensity ratio of the fourth basal reflection of chlorite to the third basal reflection of the biotite is approximately: $\frac{\text{Chlorite}}{\text{Biotite}}\,(\text{by weight}) = \frac{\text{I Chl (004)}}{\text{I Bio (003)}} \times 4.5$; this method is semi-quantitative, because the intensities of the basal reflections vary with composition and with degree of alteration.

Intensity ratios (004)/(005) of micas determined by areas and by peak-counts are lowest in muscovites (<0.3) and highest in iron-rich biotites (>2). Although $I_{(004)}$ decreases with decreasing iron content, it is still distinct in the muscovites and even more prominent in the magnesium-rich phlogopites. The ratio $I_{(004)}/I_{(005)}$ in phlogopites (>0.3) was found to be slightly higher than that in muscovites (<0.3), and thus it can be used to distinguish between colourless phlogopite and muscovite.

The lattice spacings $d_{(001)}$ and $d_{(010)}$ are smallest in muscovite (9.97 Å and 9.03 Å, respectively) and increase in altered biotites to 10.10 Å and 9.25 Å. A more detailed discussion of the spacings will be given later in this report in relation to the chemical composition.

All muscovite flakes gave Laue patterns characteristic of 2-layer monoclinic muscovite 2M (Smith and Yoder, 1956). All biotites were found to be one-layer or one-layer disordered micas (shown as 1M or 1Md in Table II).

Specific Gravity

The specific gravity of the micas was determined by suspension in heavy liquids. A biotite concentrate was placed in a glass beaker containing a mixture of methylene iodide (Sp. G. = 3.33) and bromoform (Sp. G. = 2.85). Bromoform or methylene iodide was then added to the heavy liquid mixture as required to hold the biotite in suspension. The biotite suspension was filtered, and the specific gravity of the heavy liquid measured on the Westphal balance. Homogeneous samples gave a uniform suspension, whereas heterogeneous concentrates separated into 'float', 'sink', and 'suspension' fractions. To determine the variation in specific gravity of mica flakes composing a heterogeneous concentrate, the 'float' and 'sink' fractions were separated and their specific gravities measured by repeating the procedure. Specific gravities of the phlogopites and muscovites were measured in bromoform-dimethyl sulfoxide (Sp. G. = 1.099) mixtures using the same procedure. Results of the specific gravity measurements are summarized in Table II.

Micas ranged in specific gravity from 2.675 for phlogopite to 3.250 for iron-rich biotite. The specific gravity of individual flakes in a concentrate is affected by inclusions, variations in chemical composition, morphological features, and degree of alteration. Compact flakes are heavier than the blistered ones and those which exhibit (001) splitting (Pl. I-4, 6). Extreme variations in specific gravity (2.956-3.030) were observed in concentrates *9Ph* and *9B*, which are composed of different types of micas (Pl. II-1, 2) and in concentrate *33* (3.250-3.155), in which some flakes are partly altered to chlorite (Pl. III-3, 4).

Magnetic Susceptibility

The specific magnetic susceptibility of micas was measured with a Frantz isodynamic separator, applying the method devised by McAndrew (1957), who showed

the relationship between the magnetic susceptibility and the critical current. In the present study, the Frantz separator was not calibrated, thus magnetic susceptibilities are expressed in terms of the currents measured. A record was made of: (1) maximum current at which $<10\%$ of the flakes separate as a non-magnetic fraction; (2) critical current; and (3) minimum current at which $<10\%$ of the flakes separate as a magnetic fraction. The accuracy of the current measurements reported in Table II is $= 0.02$ amp.

The measurements of critical current and of maximum and minimum currents at which the separation commences provide valuable information on the homogeneity of a concentrate. The range between the minimum and maximum currents varied from 0.03 ampere for homogeneous concentrates to 0.48 ampere for heterogeneous concentrates. The magnetic susceptibility of blistered flakes is lower than that of compact micas, and it is also strongly affected by the degree of alteration of the micas. In general, mica flakes partly altered to chlorite display higher magnetic susceptibility than the fresh flakes, perhaps due to the separation of iron.

Chemical Analyses

The chemical analyses of 34 micas were made by classical and rapid methods, and by means of a flame photometer (alkali metals) and emission spectroscopy (some trace elements). Total water content was determined by the Penfield method (Courville, 1962). The method for the determination of potassium is described by Abbey and Maxwell (1960). Chemical analyses were carried out by G. Bender and S. Courville. Some fluorine determinations were performed by R. P. Hollingsworth. J. A. Maxwell checked fluorine and water contents in micas containing the deficient (OH,F) group. The results of chemical analysis are reported in Table III.

Quantitative determinations, in about 50 micas, of the oxides Cu, Cr, Fe, Mn, Ni, Ti, Zn, Ga, Ba, Ca, Cs, K, Rb, and Sr were made by G. R. Lachance on a Philips X-ray vacuum spectrograph. Traces of As and Pb were present in a few concentrates, but in most samples these and other minor elements were not detected. All determinations were performed on the same fraction in order to correlate the trace elements with the major components. Results are reported in Table IV.

The analyzed micas show considerable differences in chemical composition. The both muscovites are similar in chemical composition, and contain more SiO_2 (47.8%), Al_2O_3 (32.4%), K_2O (10.2%), and H_2O (4.40%) than the members of the biotite group. The lowest silica content is found in the biotite *31*, from a syenite pegmatite. In the biotites, alumina ranges from 9.4% in phlogopite *7*, from a calcite-fluorite vein, to 19.8% in biotite *27*, from a cordierite schist. Titania is lowest in the phlogopite from crystalline limestone (0.3%) and highest in biotite *30* from quartz monzonite (4.29%). Ferric iron ranges from 0.0% Fe_2O_3 in phlogopite *3* to 7.2% in biotite *31*, and in the muscovites it exceeds the amount of ferrous iron. Ferrous iron ranges from 0.79% FeO in phlogopite *4* to 28.8% in biotite *33*. The lowest magnesia content is found in muscovites (below 1%) and in biotite *33* (3.2%), and the highest in phlogopite *3* (26.8%). BaO, MnO, and Na_2O in all concentrates is less than 1%. K_2O in biotites ranges from 7.2% to 10%, depending to some extent on the impurities present, and on the state of alteration of mica. The CaO content shows rather erratic variations, in part due to the

Table IV

X-Ray Spectrographic Analyses of Micas

Concentrate		Weight %							ppm						
No.	(Field No.)	Total iron as FeO	TiO_2	Cr_2O_3	MnO	K_2O	CaO	BaO	SrO	Rb_2O	Ga_2O_3	NiO	CuO	ZnO	Other traces
1	1955-165a-RA Mu	2.0	0.65*	<0.05	0.05*	9.8	0.05	<0.05	50	775*	190	100	<50	50	
2	SH-44-59	2.3	0.80*	<0.05	<0.05	10.0	0.10*	<0.05	20	625	190	50	<50	50	
3	56-RC-37	<0.5	0.35	<0.05	<0.05	10.4	0.10*	0.10	40	1275*	20	200	<50	300	
4	56-RC-40	1.4	0.50	<0.05	<0.05	9.8	0.60	0.20	60	825	30	100	<50	250	
5a	B-JR-1 (with inclusions)	2.0	0.90**	<0.05	0.05	10.4	0.40	0.25	70	570	30	100	<50	400	
6	55-SR-45	8.1	0.35	<0.05	0.25	9.2	1.20	0.10	10	850	20	350	<50	700	As, Pb
7	56-RC-29	5.4	0.7	<0.05	0.10	10.1	<0.05	0.15	10	1100*	50	150	<50	650	
8	WED-3-30-59	8.6	1.2	0.25	0.05	9.2	0.55	0.20	60	850*	<20	1000*	<50	150	
9	SH-101-59 Ph	9.8	1.7	0.70	0.10	8.8	1.3	0.50	250*	700*	<20	450*	<50	200	
9b	SH-101-59 B	16.0	3.1	0.10	0.15	7.6	2.5	0.80	420	570	30	100	<50	300	
10	56-RC-17	16.0	0.55	<0.05	0.45	9.7	<0.05	0.05	<10	2100*	70	350	<50	2000	
11	60-RC-2 Compact	15.8	1.1	nd	0.40	9.5	0.2*	0.1*	<10	6000	100	1500*	nd	1200	
11Bl	60-RC-2 Blistered	15.8	1.2	nd	0.40	9.3	0.1*	0.1*	<10	6000	100	1500*	nd	1200	
12	FB-3-59	14.1	3.7	<0.05	0.20	9.5	0.15	0.20	<10	1060*	<20	300	<50	350	
13	56-RC-28	17.5	1.8	<0.05	0.50	9.1	0.10	0.20	10	2700*	70	350	50	2000*	
14	W-58-RA-1A	17.6	1.3	<0.05	0.35	8.3	1.90	0.10	10	650	20	200	<50	400	As, Pb
15	FB-28-59	18.0	2.5	<0.05	0.30	9.6	0.10	0.15	10	775	20	100	<50	700	
16	W-58-RA-14	18.2	1.7	<0.05	0.40	9.4	0.40	0.15	10	675	20	100	<50	500	
17	W-58-RA-1	19.2	1.6	<0.05	0.35	9.2	0.25*	0.10	<10	750	20	150	<50	500	
18	BL-9-157	20.3	2.2	0.05	0.35	9.0	0.20	0.10	10	460	50	100	<50	550	
19	KG-306-59	18.0	3.7	<0.05	0.20	9.8	<0.05	0.25	20	550	40	50	<50	850	
20	SH-40-59	19.7	2.9	<0.05	0.15	9.1	0.40	0.20*	10	450	50	50	<50	300	
21	5-RA-4	18.0	3.6	<0.05	0.25	9.4	0.10	0.30	10	590*	40	50	<50	500	
22	W-58-RA-9	21.0	2.4	<0.05	0.50	9.0	0.15	0.15	<10	1000*	70	150	<50	700	
23	W-58-RA-19	21.0	2.7	<0.05	0.45	8.8	0.70	0.25	10	675	70	50	<50	800	
24	KG-58-59	20.3	2.8	<0.05	0.20	9.1	0.05	0.20	<10	550	60	100	<50	700	
25	W-58-RA-21	21.0	2.0	0.05	0.40	8.8	1.0	0.25	10	550	20	50	<50	400	
26	LA-2-59R	22.0	5.7	0.05	0.15	8.4	0.9	0.50	40	220	<20	150	<50	450	
27	SH-52-59	23.4	3.5	0.15*	0.05	8.9	<0.05	0.15*	<10	740*	60	250	<50	450	
28	1955-165a-RA (Bio)	23.9	2.8	0.05	0.70*	9.2	0.30	0.10*	<10	1125*	110	200	<50	1300*	
29	SH-58-59	27.0	2.9	0.05	0.50	8.8	0.40	0.10*	<10	1000*	60	150	<50	300	
30	SH-90-59	25.0	5.1	0.05	0.20	8.1	0.60	0.95	30	500	<20	50	<50	400	
31	56-RC-41	25.7	1.7	0.05	0.90	8.3	0.10	0.10*	<10	625	<20	50	200	1800	
32	LA-1-59R	27.9	4.1	0.05	0.60	8.3	0.20	0.15	<10	1130*	90	250	<50	700	

*Included in calculations of structural formulae.

Concentrate		Weight %							ppm						
No.	(Field No.)	Total iron as FeO	TiO_2	Cr_2O_3	MnO	K_2O	CaO	BaO	SrO	Rb_2O	Ga_2O_3	NiO	CuO	ZnO	Other traces
33	SH-95-59	29.3	3.3	<0.05	0.50*	8.3	0.20	0.10*	10	1200*	90	50	<50	800	
34	RG-59-1	5.6	3.0	0.15	<0.05	8.3	<0.05	0.20	30	450	70	1500	150	200	
35	PH-277-57	7.0	2.2	0.65	0.08	9.4	0.75	0.70	210	625	<20	1000	<50	150	
36Ph	DA-260	7.2	5.2	0.60	0.05	8.6	0.25	0.30	20	350	20	2300	<50	50	
36B	DA-260	14.4	2.8	0.20	0.10	8.0	1.40	0.25	180	1250	20	200	<50	250	
37	SDC-59-1177	10.5	5.2	0.65	0.05	8.0	0.50	0.25	30	400	50	2100	250	700	
38c	60-RC-1	16.6	1.3	nd	0.60	9.3	0.60	0.10	nd	6000	100	1000	nd	1400	As, Pb
38bl	60-RC-1	16.2	1.0	nd	0.50	8.3	2.00	0.10	10	7000	100	1000	nd	1300	As, Pb
*40***	W-58-RA-22	19.4	2.0	nd	0.30	8.7	2.	0.2	40	650	40	150	nd	400	
41B	W-58-RA-20	23.4	3.3	tr	0.75	8.4	0.4	0.13	nd	1800	120	400	nd	1400	CS?
41M	W-58-RA-20	2.3	0.8	nd	0.04	10.2	0.1	0.03	20	1200	200	250	nd	150	
42B	MCB-60	23.9	0.3	nd	0.55	7.2	0.1	0.05	10	2800	140	550	nd	900	Sc, Cs
42M	MCB-60	4.5	nd	nd	0.10	10.1	0.1	0.03	10	2000	260	350	nd	500	

**Chemical analysis of a portion containing needle-like inclusions gave TiO_2=0.83%.
***H_2O=3.15%, F=0.4% (determined by the Penfield Method).

presence of inclusions, mainly apatite and epidote, and in only a few micas exceeds 1%. The amount of constitutional water in the biotites shows a distinct variation from 1.34% to 4.07%, owing to substitution by fluorine, partial dehydration, and incipient chloritization of some micas. Fluorine is present in all micas. It is lowest in the muscovites and in biotite *20* (0.2%), and highest in the phlogopites, reaching 5.7% in phlogopite *7*. Li_2O was detected in biotite *11* from a radioactive orebody. Cs, Cr, Cu, Ni, Rb, and Sr are generally present in small quantities in all micas and show relatively distinct variations. The abundance of minor elements does not appear to be directly related to major components, but depends on the origin of micas and their environment.

In Chapter III, the correlation between physical properties and chemical composition is made on the basis of the composition of the octahedral layer. Structural formulae of micas were calculated, applying three methods:

(a) on the basis of 44 anionic and cationic valencies of the unit cell of the ideal mica (Stevens, 1946; Foster, 1960),

(b) on the basis of 24 anions (Shell and Craig, 1956), and

(c) on the basis of 20 oxygens (excluding the (OH,F) group).

When the unit cell contents of natural micas are equivalent to those of the ideal mica (Fig. 3, *in pocket*), structural formulae calculated by the above methods are the same. However, in micas that contain a deficient (OH,F) group, the structural formulae obtained by these three methods are different and are distorted to a greater or lesser extent. Biotite *21* [(OH,F) = 2.67] illustrates the differences in the half unit cell contents calculated by three different methods. Structural formulae and unit cell contents, expressed as occupancy percentages of IV, VI, and XII layers, and calcu-

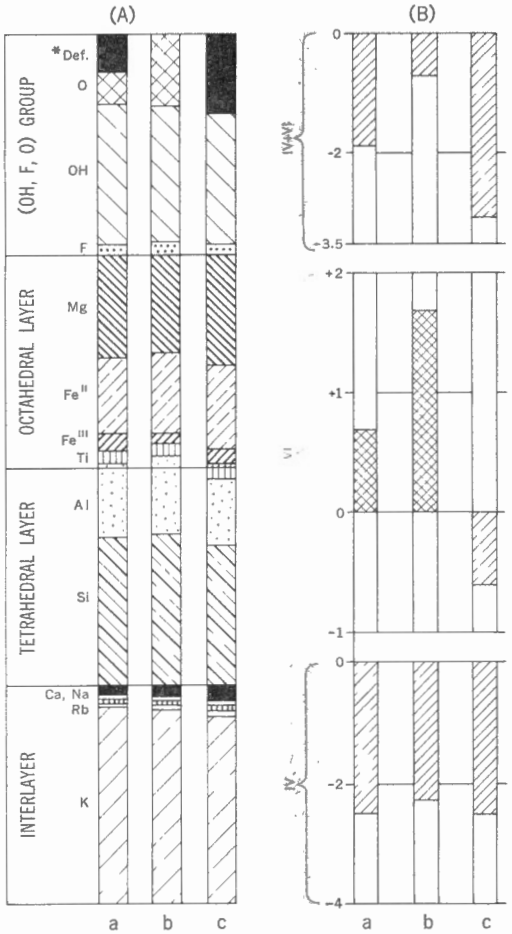

FIGURE 4. Variations in unit cell contents (A) and layer charges (B) of dehydrated biotite resulting from method of calculation.

Table V

Calculated structural formulae of OH deficient biotite 21.

FORMULA BASED ON:

a: 44 Cationic Valences b: 24 Anions $[O^{=}+(OH,F)^{-}]$ c: 20 Oxygens, excl. (OH,F)

a: $\{(Al_{.02}\ Ti_{.23}\ Fe'''_{.17}\ Fe''_{1.03}\ Mg_{1.37}\ Mn_{.02})^{+0.33}_{2.84}\ (Si_{2.73}\ Al_{1.27})^{-1.27}_{4.00}\ O_{10.33}^{-0.66}\ [(OH)_{1.24}\ F_{.10}]^{+0.66}_{1.34}\}^{-0.94}\ (K_{.90}\ Na_{.01}\ Ba_{.01}\ Rb_{.01})^{+0.94}_{0.93}$

b: $\{(Al_{.13}\ Ti_{.23}\ Fe'''_{.18}\ Fe''_{1.06}\ Mg_{1.41}\ Mn_{.02})^{+0.83}_{3.03}\ (Si_{2.82}\ Al_{1.18})^{-1.18}_{4.00}\ O_{10.61}^{-1.22}\ [(OH)_{1.27}\ F_{.10}]^{+0.63}_{1.37}\}^{-0.94}\ (K_{.91}\ Na_{.01}\ Ba_{.01}\ Rb_{.01})^{+0.95}_{0.94}$

c: $\{(Al_{.00}\ Ti_{.09}\ Fe'''_{.17}\ Fe''_{1.00}\ Mg_{1.33}\ Mn_{.02})^{-0.33}_{2.61}\ (Si_{2.62}\ Al_{1.25}\ Ti_{.13})^{-1.25}_{4.00}\ O_{10}\ [(OH)_{1.20}\ F_{.10}]^{+0.70}_{1.30}\}^{-0.88}\ [K_{.86}\ Na_{.01}\ (Ba, Rb)_{.01}]^{+0.89}_{0.88}$

IONIC PERCENTAGES IN MICA LAYERS

	Al	Ti	Fe'''	Fe''	Mg	Mn	Si	Al	Ti	OH	F	Def.*	K	Na	Ba	Rb
a:	0·9	8·0	6·1	36·3	48·1	0·6	68·5	31·5	0·0	61·7	4·9	33·4	89·2	1·0	0·9	0·5
b:	4·4	7·6	5·8	35·0	46·7	0·5	70·2	29·8	0·0	63·4	5·1	31·5	90·7	0·9	0·9	0·5
c:	0·0	3·4	6·4	38·5	51·1	0·6	65·5	31·3	3·2	57·8	4·8	37·4	85·7	0 9	0·8	0·4

* Def.= per cent deficiency of the (OH,F) group

GSC

lated on the basis of formulae (a), (b), and (c) are shown in Table V. Occupancy of the unit cell and layer charges are compared graphically in Figure 4.

Results obtained in calculating structural formulae of mica that has a deficient (OH,F) group, on the basis of methods (a), (b) and (c), can be summarized as follows:

(1) The (OH,F) group is deficient, regardless of the method of calculation.

(2) The excess of oxygen (0.33) in the formula calculated by method (a) is exactly the same as that required to balance the deficiency in the negative charge, which is a result of the deficient (OH,F) group (0.66).

(3) The excess of oxygen (0.66) in the formula calculated by method (b) is the same as that required to fill the unoccupied (OH,F) positions (0.66); i.e., to replace the $(OH,F)^-$ ions by $O^=$ ions, and this proportionately increases the total negative charge.

(4) The occupancy and the positive charge of the octahedral layer in structural formula (b) are very high. The negative charge carried by the tetrahedral layer is insufficient to balance the high positive charge of the octahedral layer.

(5) The ferric iron content in formulae calculated by methods (a) and (b) is much lower than that required to account for the excess of oxygen. It is thus assumed that the constitutional water is lost, at least in part, as H_2O, according to the equation:

$$4(OH) \longrightarrow H_2O + O + 2(OH).$$

(6) In the structural formula calculated by method (c) the occupancy of the octahedral layer is the lowest and it carries a negative charge. The (OH,F) group is not fully occupied and contains 0.70 unoccupied positions.

(7) Silica, which is the major constituent by weight, is affected more than any other constituent by the method of calculation. The number of tetrahedral positions occupied by Si ions in formulae (a), (b), and (c) varies from 2.62 to 2.82. The different quantities of Al and Ti ions that remain after filling the tetrahedral positions affect the content of the octahedral layer.

These observations suggest that: (1) the structural formula calculated on the basis of 44 valencies is perhaps least distorted; (2) deficiency in the (OH,F) group is a result of partial dehydration of natural micas. Therefore, the structural formula of the unit cell of mica *21* can be written:

$$\underset{+0.67}{\left\{\left(\underset{0.05}{Al}\ \underset{0.45}{Ti}\ \underset{0.34}{Fe'''}\ \underset{2.07}{Fe''}\ \underset{2.75}{Mg}\ \underset{0.03}{Mn}\right)\right.}\ \underset{5.69}{}\ \underset{-2.53}{\left(\underset{5.47}{Si}\ \underset{2.53}{Al}\right)}\ \underset{8.00}{}\ O_{20}\ \underset{3.33}{\left[\underset{2.47}{(OH)}\ \underset{0.20}{F}\ \underset{0.66}{O}\right]}\ \underset{-1.86}{\left.\right\}}\ \underset{+1.86}{\left(\underset{1.79}{K}\ \underset{0.02}{Na}\ \underset{0.02}{Ba}\ \underset{0.01}{Rb}\right)}\ \underset{1.84}{}$$

The resulting negative charge of the tetrahedral and octahedral layers (−1.86) is balanced by the positive charge (+1.86) of the interlayer. The sum of the negative charges $O^{=}_{20} + (OH,F,O)^{3.99} = 43.99$. The total number of anions is 23.33; i.e., 0.67 less than the 24 anions present in the unit cell of the ideal mica. Considering that water can escape from mica on heating (which has been proved already by Brun (1913), in laboratory experiments), partial dehydration and thus a small deficiency of anions in

Table VI

Concentrate No.		CATIONS													
		Tetrahedral Layer (IV)				Octahedral Layer (VI)									
		Si	Al	Ti	Fe^{3+}	Al	Ti	Fe^{3+}	Fe^{2+}	Mg	Mn	Cr	Ni	Li	Zn
1	1955-RA	6.36	1.64			3.44	0.06	0.22	0.12	0.14	0.06				
1c	1955-RA corr 2% B	6.39	1.61			3.51	0.015	0.22	0.06	0.12	0.06				
2	SH-44-59	6.34	1.66			3.33	0.08	0.28	0.097	0.17					
3	56-RC-37	6.10	1.70	0.04	Fe^{2+} 0.16				0.15	5.75					
4	56-RC-40	6.14	1.70	0.04	Fe^{3+} 0.12			0.02	0.10	5.64					
5	B-JR-1	5.50	2.50			0.52	0.06	0.10	0.14	5.12	.004				
6	55-SR-45 (IV p. filled)	6.02	1.74	0.04	0.20			0.20	0.51	5.02	0.02				
6a	55-SR-45 (IV p. not filled)	6.01	1.74				0.04	0.40	0.51	5.02	0.03				
7	56-RC-29	6.36	1.62	0.02			0.06	0.06	0.68	4.76	0.02				
8	WED-3-30	5.95	2.04	0.01			0.12	0.21	0.83	4.55	0.01	0.03	0.01		
9	SH-101-59	5.92	2.08			0.44	0.15	0.19	0.74	3.86	0.01	0.10	0.003		
9c	SH-101-59 corr 2% Q, Ch; 3% Alb	5.74	2.26			0.27	0.17	0.20	0.77	4.08	0.004	0.12	0.003		
10	56-RC-17	6.20	1.78	0.02			0.03	0.24	1.75	3.68	0.05				
11	60-RC-2 Compact	6.16	1.82	0.02			0.07	0.70	1.28	3.12	0.06		0.02	0.40	0.01
11Bl	60-RC-2 Blistered	6.17	1.70	0.11	0.02			0.76	1.34	3.18	0.06		0.02	0.38	0.01
11Bla	60-RC-2 Blistered (IV p. not filled)	6.17	1.70				0.11	0.77	1.34	3.17	0.06		0.02	0.38	0.01
12	FB-3-59	5.79	2.18	0.03			0.37	0.14	1.81	3.34	0.03				
13	56-RC-28	5.94	1.87	0.19			0.02	0.43	1.91	3.27	0.06				0.02
14	W-58-RA-1A	5.64	2.36			0.34	0.18	0.36	1.90	2.79	0.04				
14c	W-58-RA-1A; corr 10% Ch, 15% H	5.66	2.34			0.36	0.21	0.31	1.96	2.67	0.04				
15	FB-28-59	5.44	2.56			0.72	0.29	0.15	2.08	2.34	0.05				
15c	FB-28-59; corr 2% Ch, 1% Fe_2O_3	5.48	2.52			0.78	0.29	0.06	2.10	2.35	0.03				
16	W-58-RA-14	5.42	2.58			0.43	0.22	0.35	2.00	2.70	0.05				
16c	W-58-RA-14; corr 4% Ch, 2% H	5.39	2.61			0.33	0.22	0.35	1.99	2.68	0.04				
17	W-58-RA-1	5.58	2.42			0.29	0.21	0.41	2.00	2.71	0.05				
17c	W-58-RA-1 corr 4% Ch	5.65	2.35			0.31	0.21	0.42	1.96	2.68	0.04				
18	BL-9-157	5.52	2.48			0.34	0.23	0.45	2.09	2.55	0.04				
18c	BL-9-157 corr 4% Ch, Ap	5.56	2.44			0.36	0.24	0.45	2.08	2.50	0.03				
19	KG-306-59	5.50	2.50			0.16	0.47	0.33	1.98	2.64	0.03				
20	SH-40-59	5.40	2.60			0.67	0.37	0.11	2.26	2.15	0.02				
20c	SH-40-59 corr 5% Ch	5.57	2.43			0.58	0.39	0.09	2.33	2.11	0.01				
21	5-RA-4	5.47	2.53			0.05	0.45	0.35	2.07	2.75	0.03				
22	W-58-RA-9	5.46	2.54			0.35	0.27	0.41	2.18	2.52	0.05				
22c	W-58-RA-9 corr 12% Ch	5.62	2.38			0.38	0.29	0.40	2.09	2.37	0.03				

Unit Cell Content, Occupancy and Layer Charge

CATIONS					ANIONS							Occupancy and Layer Charge					
Interlayer (XII)					Oxygen		(OH,F) Group					Layer: IV		VI		XII	
Na	Ca	K	Ba	Rb	Number	Charge diff fr. 40	OH	F	Σ (OH, F)	(OH,F) diff fr. 4	$O^{=}$ diff fr. 20	Occ.	Charge (−)	Occ.	Charge	Occ.	Charge (+)
0.19	.007	1.715		0.006	19.99	0.02	3.89	0.11	4.00		0.01	8	1.64	3.96	−0.34	2.01	2.02
0.20	.007	1.73		0.006	19.99	0.02	3.90	0.10	4.00		0.01	8	1.61	3.94	−0.32	1.94	1.95
0.20	.014	1.73			20.13	0.26	3.64	0.08	3.72	0.28	0.13	8	1.66	3.96	−0.22	1.95	1.96
0.24	.016	1.90	0.01	0.01	20.01	0.02	2.02	1.96	3.98	0.02	0.01	8	2.02	5.90	−0.20	2.18	2.22
0.14	0.20	1.78	0.02		20.03	0.06	2.06	1.92	3.98	0.02	0.03	8	1.82	5.76	−0.46	2.14	2.36
0.10	0.04	1.70	0.02		20.14	0.28	2.70	1.02	3.72	0.28	0.14	8	2.50	5.94	+0.62	1.86	1.90
0.08	0.14	1.84	0.02		20.14	0.28	1.78	1.92	3.70	0.30	0.14	8	1.94	5.76	−0.28	2.08	2.24
0.09	0.14	1.85	0.02		20.14	0.28	1.79	1.93	3.72	0.28	0.14	7.75	2.74	6.00	+0.48	2.10	2.28
0.08	0.14	1.86	0.02	0.01	20.02	0.04	1.32	2.64	3.96	0.04	0.02	8	1.62	5.58	−0.66	2.11	2.27
0.11	0.06	1.74	0.015	0.01	20.58	1.16	1.34	1.50	2.84	1.16	0.58	8	2.04	5.76	0.00	1.935	2.03
0.15	0.10	1.66	0.03	0.01	20.45	0.90	2.80	0.33	3.13	0.87	0.45	8	2.08	5.49	+0.01	1.95	2.08
0.08	0.09	1.78	0.03	0.01	20.41	0.82	2.82	0.36	3.18	0.82	0.41	8	2.26	5.61	+0.15	1.99	2.12
0.09		1.88		0.02	20.13	0.26	1.94	1.79	3.73	0.27	0.13	8	1.78	5.74	−0.20	1.99	1.99
0.04	0.02	1.86	+Cs 0.01	0.06	20.50	1.00	1.29	1.70	2.99	1.01	0.50	8	1.92	5.66	−0.04	1.99	2.01
0.03	0.02	1.76	+Cs 0.01	0.07	20.34	0.68	1.63	1.69	3.32	0.68	0.34	8	1.72	5.75	−0.12	1.89	1.91
0.03	0.02	1.76	+Cs 0.01	0.07	20.34	0.68	1.63	1.69	3.32	0.68	0.34	7.87	2.22	5.86	+0.33	1.89	1.91
0.07	0.03	1.80	0.006	0.01	20.73	1.46	1.31	1.23	2.54	1.46	0.73	8	2.18	5.69	+0.26	1.92	1.95
0.09	0.03	1.82		0.03	20.39	0.78	1.49	1.72	3.21	0.79	0.39	8	1.87	5.73	−0.09	1.97	2.00
0.08	0.12	1.70			20.25	0.50	3.30	0.21	3.51	0.49	0.50	8	2.36	5.61	+0.28	1.90	2.02
0.09	0.01	1.99	0.01		20.53	1.06	2.67	0.27	2.94	1.06	0.53	8	2.34	5.56	+0.22	2.10	2.12
0.03		1.81	0.004		20.33	0.66	3.07	0.27	3.34	0.66	0.33	8	2.56	5.62	+0.70	1.85	1.86
0.03	0.01	1.88	0.005		20.42	0.84	2.95	0.27	3.22	0.78	0.42	8	2.52	5.61	+0.70	1.93	1.94
0.02	0.05	1.77			20.38	0.76	3.00	0.23	3.23	0.77	0.38	8	2.58	5.75	+0.72	1.84	1.89
0.02	0.06	1.89	0.02		20.42	0.84	2.93	0.23	3.16	0.84	0.42	8	2.61	5.61	+0.54	1.99	2.05
0.03	0.07	1.82	0.02		19.82	0.36	4.12	0.23	4.35	+0.35	−0.18	8	2.42	5.67	+0.57	1.94	2.03
0.03	0.04	1.87	0.01		19.96	0.08	3.84	0.24	4.08	+0.08	−0.04	8	2.35	5.62	+0.39	1.95	2.00
0.02		1.82	0.01		20.28	0.56	3.28	0.18	3.46	0.54	0.28	8	2.48	5.70	+0.66	1.85	1.86
0.01		1.87	0.01		20.45	0.90	2.93	0.18	3.11	0.89	0.45	8	2.40	5.66	+0.51	1.89	1.90
0.04		1.80	0.02		20.56	1.12	2.60	0.28	2.88	1.12	0.56	8	2.50	5.61	+0.65	1.86	1.88
	0.10	1.68	0.02		20.35	0.70	3.20	0.10	3.30	0.70	0.35	8	2.60	5.58	+0.68	1.80	1.92
	0.12	1.81	0.01		20.53	1.06	2.92	0.11	3.03	0.97	0.53	8	2.43	5.51	+0.49	1.94	2.05
0.02		1.79	0.02	0.01	20.66	1.32	2.47	0.20	2.67	1.33	0.66	8	2.53	5.70	+0.69	1.84	1.86
0.01		1.67	0.005	0.01	19.72	0.56	3.98	0.57	4.55	+0.55	−0.28	8	2.54	5.78	+0.86	1.70	1.70
0.01		1.88	0.006	0.01	20.16	0.32	3.04	0.64	3.68	0.32	0.16	8	2.38	5.56	+0.42	1.91	1.91

Table VI

Concentrate No.		CATIONS													
		Tetrahedral Layer (IV)				Octahedral Layer (VI)									
		Si	Al	Ti	Fe^{3+}	Al	Ti	Fe^{3+}	Fe^{2+}	Mg	Mn	Cr	Ni	Li	Zn
23	W-58-RA-19	5.51	2.49			0.37	0.29	0.43	2.17	2.34	0.05				
23c	W-58-RA-19 corr 3% Ch	5.55	2.45			0.38	0.29	0.42	2.15	2.29	0.03				
24	KG-58-59	5.55	2.45			0.42	0.32	0.39	2.36	2.04	0.04				
25	W-58-RA-21	5.38	2.62			0.37	0.34	0.43	2.46	2.05	0.06				
25c	W-58-RA-21 corr 10% Ch	5.51	2.49			0.38	0.37	0.42	2.41	1.87	0.06				
26	LA-2-59R	5.54	2.46			0.04	0.47	0.34	2.42	2.34	0.02	0.003	0.002		
27	SH-52-59	5.32	2.68			0.84	0.35	0.22	2.63	1.44	0.01	0.02			
27c	SH-52-59 corr 1% Q, 2% Ch	5.26	2.74			0.86	0.36	0.21	2.66	1.41		0.02			
28	1955-165a-RA	5.46	2.54			0.71	0.30	0.24	2.84	1.37	0.08				0.01
29	SH-58-59	5.47	2.53			0.20	0.33	0.43	2.94	1.77	0.04	0.02			
30	SH-90-59	5.58	2.42			0.21	0.50	0.28	3.00	1.56	0.03				
31	56-RC-41	5.15	2.85			0.26	0.18	0.85	2.93	1.40	0.12				
32	LA-1-59R	5.75	2.25			0.08	0.41	0.66	2.95	1.40	0.06				
33	SH-95-59	5.52	2.48			0.26	0.38	0.42	3.80	0.74	0.06				
33c	SH-95-59 corr 3% Ch	5.52	2.48			0.24	0.42	0.41	3.79	0.69	0.07				

natural micas seems to be not improbable. The mechanism of the rearrangement of anions in the octahedral layer of laboratory-dehydrated clay minerals was discussed by Bradley and Grim (1951).

Unit cell contents of all micas listed in Table VI were calculated on the basis of 44 valencies. The differences in the interlayer content (1.71 in biotite *33*; 2.18 in phlogopite *3*) can be accounted for by the proportionate differences in resulting negative charges of the tetrahedral and octahedral layers.

With the exception of muscovite *1*, which contained inclusions of biotite *28*, the chemical composition of impurities in the concentrates is not known. Thus, for correcting the analyses of impure concentrates, the chemical analysis of hornblende from Rankama and Sahama (1950, p. 149, No. 24) was used, and chlorite analyses were selected from Deer *et al.* (1962) on the basis of their optical properties. Chemical analysis of plagioclase was taken from Rankama and Sahama (1950, p. 136, No. 59). P_2O_5 and equivalent CaO to make apatite were subtracted from analyses. Formulae of the impure concentrates were calculated before and after corrections of the analyses were made. The latter are marked 'c' (= corrected) in Tables VI and VII. After correcting for chlorite, the main difference is in the (OH,F) content.

The occupancy percentages in the mica layers (Table VII and Fig. 5, *in pocket*) were calculated on the basis of the actual occupancy of the layer, with the exception of the (OH,F) group. In order to show the magnitude of variation in the content of the (OH,F) group, the percentages were calculated on the basis of the (OH,F) content (= 4) of the ideal micas.

Unit Cell Content, Occupancy and Layer Charge—continued

CATIONS					ANIONS							Occupancy and Layer Charge					
Interlayer (XII)					Oxygen		(OH,F) Group					Layer: IV		VI		XII	
Na	Ca	K	Ba	Rb	Number	Charge diff fr. 40	OH	F	Σ (OH, F)	(OH,F) diff fr. 4	$O^{=}$ diff fr. 20	Occ.	Charge (—)	Occ.	Charge	Occ.	Charge (+)
0.03		1.81	0.005		20.46	0.92	2.73	0.35	3.08	0.92	0.46	8	2.49	5.65	+0.68	1.85	1.85
0.04		1.86	0.006		20.58	1.16	2.49	0.36	2.85	1.15	0.58	8	2.45	5.55	+0.50	1.91	1.91
0.02		1.81	0.01		20.46	0.92	2.90	0.18	3.08	0.92	0.46	8	2.45	5.57	+0.59	1.84	1.85
0.01	0.01	1.70	0.01		19.83	−0.34	3.85	0.48	4.33	+0.33	−0.17	8	2.62	5.71	+1.00	1.73	1.75
0.02	0.01	1.87	0.01		20.22	0.44	3.02	0.54	3.56	0.44	0.22	8	2.49	5.51	+0.56	1.91	1.93
0.08	0.07	1.62	0.02		20.46	0.92	2.97	0.11	3.08	0.92	0.46	8	2.46	5.64	+0.60	1.77	1.86
	0.04	1.76	0.01	0.01	20.02	0.04	3.73	0.23	3.96	0.04	0.02	8	2.68	5.51	+0.80	1.82	1.87
	0.046	1.84	0.01	0.01	20.06	0.12	3.65	0.25	3.90	0.10	0.06	8	2.74	5.52	+0.85	1.91	1.95
	0.02	1.80	0.006	0.01	20.00	0.00	3.60	0.40	4.00	0.00	0.00	8	2.54	5.55	+0.65	1.84	1.86
0.02		1.77	0.005	0.01	20.34	0.68	3.07	0.28	3.35	0.65	0.34	8	2.53	5.73	+0.67	1.805	1.81
0.05	0.07	1.62	0.05		20.41	0.82	2.89	0.29	3.18	0.82	0.41	8	2.42	5.58	+0.65	1.79	1.91
0.09	0.03	1.86	0.01		20.285	0.57	3.16	0.27	3.43	0.57	0.285	8	2.85	5.74	+0.91	1.99	2.03
0.04		1.65	0.02	0.01	20.24	0.48	2.92	0.60	3.52	0.48	0.24	8	2.25	5.56	+0.40	1.72	1.74
	0.01	1.66	0.004	0.01	20.10	0.20	3.48	0.32	3.80	0.20	0.10	8	2.48	5.66	+0.66	1.683	1.70
	0.01	1.69	0.006	0.01	20.22	0.44	3.23	0.32	3.55	0.45	0.22	8	2.48	5.62	+0.73	1.714	1.73

It is important to note appreciable variations in the occupancy of the octahedral layer (5.52-5.94). The proportions of the octahedral ions are shown as occupancy percentages, which are correlated with physical properties and give a convenient comparison of the content of the octahedral layer in different micas. However, in the study of the relation of the octahedral ions to the ions of other coordinations, the actual octahedral occupancy must be considered.

Some of the minor elements were included in the calculation of the structural formulae and were taken from the X-ray spectrographic analyses. Quantities of CaO determined by X-ray spectrography and by the classical method are different in some concentrates, because of the presence of inclusions. In such cases, the most probable values were selected for calculating the formulae and are marked with an asterisk in Table IV.

Differential Thermal and Thermogravimetric Analysis

Differential thermal analysis and thermogravimetric tests were carried out to study the dehydration phenomena observed in natural micas. This work was conducted in the Physical Chemistry section of the Mines Branch, under the supervision of N. F. H. Bright. A few characteristic DTA and TGB curves are shown in Figure 6 to illustrate the difference in the thermal behaviour of muscovite *1*, phlogopite *5*, blistered biotite *11Bl*, biotite *13*, and iron-rich biotite *33*. Portions of coarse muscovite (1 mm in diameter) and phlogopite (2 mm) were crushed to −150 mesh and analyzed for comparison with uncrushed material. DTA was carried out in air, in argon, and in vacuum.

Table VII

Concentrate		CATIONS									
		Tetrahedral Layer				Octahedral Layer					
No.	(Field No.)	Si	Al	Ti	Fe^{3+}	Al	Ti	Fe^{3+}	Fe^{2+}	Mg	Mn
1	1955-165a-RA not corr	79.5	20.5			86.8	1.6	5.5	3.0	3.1	0.1
1c	1955-165a-RA corr 2% Bio	79.8	20.2			89.6	0.3	5.6	1.5	3.0	0.1
2	SH-44-59	79.3	20.7			84.4	2.0	7.0	2.4	4.2	
3	56-RC-37	76.3	21.2	0.5	Fe^{2+} 2.0				2.9	97.1	
4	56-RC-40	76.8	21.4	0.3	1.5			0.3	1.7	98.0	
5	B-JR-1	68.8	31.2			8.65	0.96	1.7	2.49	86.1	0.14
6	55-SR-45 (IV p. occ)	75.1	21.8	0.6	2.5			3.5	8.8	87.2	0.5
6a	55-SR-45 (IV p. not occ)	75.1	21.8				0.7	6.7	8.6	83.6	0.4
7	56-RC-29	79.5	20.3	0.2			1.1	1.2	12.2	85.3	0.2
8	WED-3-30	74.3	25.5	0.2			2.1	3.6	14.4	78.9	0.2
9	SH-101-59 not corr	74.0	26.0			7.9	2.9	3.5	13.5	70.3	0.2
9c	SH-101-59 corr 3% Pl, 2% Q, 2% Ch	71.8	28.2			4.8	2.9	3.5	13.8	72.8	0.1
10	56-RC-17	77.4	22.3	0.3			0.5	4.2	30.5	64.0	0.8
11	60-RC-2 compact	77.0	22.7	0.3			1.2	12.4	22.5	55.4	1.1
11B	60-RC-2 Blistered	77.1	21.3	1.4	0.2			13.1	23.5	55.4	1.1
11Ba	60-RC-2 Blistered (IV p. not occ)	77.1	21.3				1.9	13.1	23.0	54.1	1.1
12	FB-3-59	72.5	27.3	0.2			6.4	2.2	32.3	59.0	0.6
13	56-RC-28	74.0	23.5	2.5			0.3	7.5	33.5	57.3	1.0
14	W-58-RA-1A not corr	70.5	29.5			6.1	3.2	6.4	33.8	49.8	0.7
14c	W-58-RA-1A corr 15% H, 10% Ch	70.7	29.3			6.4	3.7	5.6	35.2	48.4	0.7
15	FB-28-59 not corr	68.0	32.0			12.8	5.2	2.6	37.0	41.6	0.8
15c	FB-28-59 corr 2% Ch, 1% Fe_2O_3	68.5	31.5			13.9	5.2	1.1	37.4	41.9	0.5
16	W-58-RA-14 not corr	67.8	32.2			7.4	3.8	6.2	34.5	47.1	1.0
16c	W-58-RA-14 corr 4% Ch, 2% H	67.7	32.3			6.0	3.9	6.2	35.5	47.7	0.7
17	W-58-RA-1 not corr	69.7	30.7			4.9	3.7	7.3	35.3	47.9	0.9
17c	W-58-RA-1 corr 4% Ch	70.6	29.4			5.5	3.7	7.4	34.9	52.2	0.7
18	BL-9-157 corr Ap	69.0	31.0			6.0	4.0	7.9	36.7	44.7	0.7
18c	BL-9-157 corr 4% Ch, Ap	69.5	30.5			6.3	4.3	8.0	36.0	44.9	0.5
19	KG-306-59	68.8	31.2			2.8	8.4	5.9	35.3	47.1	0.5
20	SH-40-59 not corr	67.5	32.5			12.1	6.7	1.9	40.5	38.6	0.2
20c	SH-40-59 corr 5% Ch	69.6	30.4			10.5	7.8	1.6	42.0	38.0	0.1
21	5-RA-4	68.5	31.5			0.9	8.0	6.1	36.3	43.1	0.6
22	W-58-RA-9 not corr	68.3	31.7			6.0	4.7	7.0	37.8	43.6	0.9
22c	W-58-RA-9 corr 12% Ch	70.2	29.8			7.0	5.0	7.2	37.6	42.6	0.6
23	W-58-RA-19 corr Ap	68.8	31.2			6.5	5.1	7.6	38.5	41.4	0.9
23c	W-58-RA-19 corr 3% Ch, Ap	69.4	30.6			6.8	5.2	7.7	38.6	41.1	0.6
24	KG-58-59	69.4	30.6			7.5	5.7	7.0	42.4	36.6	0.7
25	W-58-RA-21 not corr	67.2	32.8			6.5	6.0	7.5	43.1	35.9	1.0

Unit Cell Content Expressed as Percentage Occupancy of Layers

CATIONS													ANIONS			
Octahedral Layer								Interlayer					(OH,F) Group			
Cr	Ni	Li	Zn	ΣFe	Fe / ΣGr Me	$\frac{Fe^{3+}}{Ti}$	$\frac{Fe^{3+}}{Fe^{2+}}$	Na	Ca	K	Ba	Rb	OH	F	de-hydr*	O†
				8.5	10.1	3.4	1.8	10.0	0.3	89.4		0.3	97.5	2.5	0.0	0.0
				7.1	7.4			10.0	0.3	89.4		0.3	98.0	2.0	0.0	0.0
				9.4	11.4	3.5	3.0	10.4	0.7	88.9			91.0	2.0	7.0	3.5
				2.9	2.9			10.0	0.7	88.3	0.5	0.5	50.5	49.0	0.5	0.25
				2.0	2.0		0.17	6.5	9.5	83.1	0.5		51.5	48.0	0.5	0.25
				4.2	5.3	1.7	0.7	5.5	2.2	91.3	1.0		67.5	25.5	7.0	3.5
				12.3	12.8		0.4	3.8	6.6	88.6	1.0		44.5	48.0	7.5	3.75
				15.3	16.4	9.6	0.8	3.8	6.6	88.6	1.0		44.5	48.0	7.5	3.75
				13.4	14.7	1.0	0.1	3.8	6.6	88.2	1.0	0.4	33.0	66.0	1.0	0.5
0.6	0.2			18.0	21.1	1.7	0.25	5.7	3.1	90.0	0.7	0.5	33.5	37.5	29.0	14.5
1.9	<0.1			17.0	22.1	1.2	0.26	7.6	5.2	85.5	1.4	0.3	70.0	8.1	21.9	11.2
2.1	<0.1			17.3	22.4			4.0	4.6	89.7	1.5	0.3	70.5	9.0	20.5	10.25
				34.7	36.0	8.4	0.37	4.5		95.0		0.5	48.5	45.0	6.5	3.3
	0.3	7.1		34.9	37.5	10.0	0.55	2.0	1.0	93.5	+Cs 0.5	3.0	35.0	42.5	22.5	10.5
	0.4	6.6		36.6	38.1		0.55	1.6	1.1	93.6	+Cs 0.5	3.2	40.5	42.5	17.0	8.5
	0.3	6.5		36.1	39.1	7.0	0.55	1.6	1.1	93.6	+Cs 0.5	3.2	40.5	42.5	17.0	8.5
				34.5	41.5	0.34	0.07	4.0	1.4	94.0	0.3	0.3	34.0	31.0	35.0	17.5
			0.3	41.0	42.3	25.0	0.23	4.6	1.5	92.4		1.5	37.2	43.0	19.8	9.9
				40.2	44.1	2.	0.19	2.24	6.30	83.5			83.0	5.0	12.0	6.0
				40.8	45.2	1.6	0.15	3.00	0.40	96.2	0.40		66.7	6.8	26.5	13.25
				39.6	45.6	0.5	0.07	1.80		98.0	0.20		76.5	7.0	16.5	8.25
				38.5	44.0	0.21	0.03	1.50	0.50	97.7	0.30		73.7	6.8	19.5	10.5
				40.7	45.5			1.10	2.60	96.3			75.0	5.8	19.5	9.5
				41.7	46.3	1.6	0.17	1.00	3.10	94.9	1.00		73.2	5.8	21.0	10.5
				42.6	47.2			1.50	3.60	93.9	1.00		95.0	5.0	+10.	−5.00
				42.1	46.5	2.0	0.21	1.50	2.00	96.00	0.50		94.0	6.0	+2.0	−1.0
				44.6	49.3	1.9	0.21	1.00		98.5	0.50		82.0	4.5	13.5	7.0
				44.0	48.8	1.8	0.22	0.50		99.0	0.50		73.5	4.5	22.0	11.2
				41.2	50.1	0.7	0.16	2.10		96.8	1.10		65.0	7.0	28.0	14.0
				42.4	49.3	0.28	0.05		6.00	93.0	1.00		80.0	2.5	17.5	8.8
				42.6	50.5	0.25	0.04		6.20	93.3	0.50		73.0	2.7	24.3	13.2
				42.4	51.0	0.76	0.17	1.10		97.3	1.10	0.50	61.7	4.9	33.4	16.5
				44.8	50.4			0.60		98.5	0.30	0.60	88.0	12.0	+11.0	−7.0
				44.8	50.4	1.44	0.19	0.50		98.8	0.20	0.50	76.0	16.0	8.0	4.0
				46.1	52.1			1.60		98.15	0.25		68.2	9.0	22.8	11.5
				46.3	52.1	1.50	0.20	2.20		97.5	0.30		62.2	9.0	28.5	14.5
				49.4	55.8	1.2	0.17	1.10		98.4	0.50		72.5	4.5	23.0	11.5
				50.6	57.6			0.60	0.60	98.2	0.60		88.8	11.2	+8.0	−4.2

Table VII

Concentrate		CATIONS									
		Tetrahedral Layer				Octahedral Layer					
No.	(Field No.)	Si	Al	Ti	Fe^{3+}	Al	Ti	Fe^{3+}	Fe^{2+}	Mg	Mn
25c	W-58-RA-21 corr 10% Ch	68.9	31.2			6.9	6.7	7.6	43.7	34.0	1.1
26	LA-2-59R	69.3	30.7			0.7	8.3	6.0	43.0	41.6	0.3
27	SH-52-59 not corr	66.5	33.5			15.2	6.3	4.0	47.7	26.2	0.1
27c	SH-52-59 corr 2% Ch, 1% Q	65.8	34.2			15.6	6.0	4.4	48.2	25.5	
28	1955-165a-RA	68.2	31.8			12.6	5.4	4.3	51.2	24.7	1.6
29	SH-58-59 corr Ap	68.4	31.6			3.5	5.8	7.5	51.4	30.7	0.8
30	SH-90-59	69.8	30.2			3.7	9.0	4.9	53.8	28.0	0.6
31	56-RC-41	64.4	35.6			4.5	3.1	15.0	51.5	23.9	2.0
32	LA-1-59R corr Ap	71.9	28.1			1.4	7.4	11.8	53.1	25.3	1.0
33	SH-95-59 not corr	69.0	31.0			4.6	6.7	7.4	67.1	13.1	1.1
33c	SH-95-59 corr 3% Ch	69.0	31.0			4.2	7.3	7.2	67.4	12.6	1.3

*Deficiency of (OH,F) or difference from 4 (4=100%)

TGB tests on all micas were carried out in air, and two additional tests on biotites *13* and *33* were made in argon atmosphere. Loss of weight after TGB tests is marked on the left side of the TGB curves (Fig. 6). Numbers in parentheses indicate total weight of water and fluorine obtained by chemical analysis of these micas.

DTA and TGB results can be summarized as follows:

(1) DTA curves (obtained in vacuum and in argon) show prominent humps in the temperature range of 200°-400°C. These humps are not yet fully explained and may be due in part to incipient dehydration.

(2) With the exception of crushed phlogopite, which most likely adsorbed water during preparation, loss of weight of all ignited samples after the TGB tests is less than the sum of the water and fluorine present in these micas. The difference between the loss of weight recorded on the thermobalance and total water and fluorine content increases with increasing iron and fluorine content of the mica.

(3) The TGB test that was carried out in argon confirmed the results obtained in air. Loss of weight of biotite *33* after ignition in air (1.2%) was found to be almost the same as that in argon (1.3%). These results suggest that at least part of the oxygen and some of the fluorine from the (OH,F) group remain in the mica after ignition.

(4) Chemical analysis of blistered biotite *11Bl* confirmed the presence of fluorine (1.25%) and of a small quantity of water (0.1%) after ignition to 1200°C. The difference in the ferric iron content after firing could not be checked because of insufficient quantity of material. This test, however, proved that at least one component (F) of the (OH,F) group forms a stable compound on ignition and is retained in the mica. These observations confirm DTA experiments of Tsvetkov and Valyashikhina (1956), who found that at least part of

Unit Cell Content Expressed as Percentage Occupancy of Layers—continued

CATIONS													ANIONS			
Octahedral Layer								Interlayer					(OH,F) Group†			
Cr	Ni	Li	Zn	ΣFe	Fe / ΣGr Me	$\frac{Fe^{3+}}{Ti}$	$\frac{Fe^{3+}}{Fe^{2+}}$	Na	Ca	K	Ba	Rb	OH	F	de-hydr*	O†
				51.3	59.1	1.1	0.18	1.00	0.50	98.0	0.50		75.5	13.5	11.0	5.5
0.1				49.0	57.7	0.72	0.14	4.50	4.00	90.4	1.10		74.5	2.7	22.8	11.5
0.5				51.7	58.5	0.60	0.08		2.20	96.8	0.50	0.50	93.0	6.0	1.0	0.5
0.3				52.6	58.9	0.73	0.09		2.30	96.9	0.50	0.30	91.2	6.3	2.5	1.5
			0.2	55.5	62.5	0.80	0.08		1.10	98.1	0.30	0.50	90.0	10.0	0.0	0.0
0.3				58.9	65.8	1.20	0.14	1.10		98.2	0.20	0.50	76.7	7.0	16.3	8.5
				58.7	68.3	0.54	0.09	2.80	3.90	90.5	2.80		72.3	7.2	20.5	10.25
				66.5	71.6	4.8	0.29	4.60	1.50	93.4	0.50		79.0	6.8	14.2	7.1
				64.9	73.3	1.6	0.22	2.30		96.0	1.10	0.60	73.0	15.0	12.0	6.0
				74.5	82.3				0.70	98.4	0.20	0.70	87.0	8.0	5.0	2.5
				74.6	83.2	1.0	0.11		0.50	98.6	0.30	0.60	80.8	8.0	11.2	5.5

†Excess oxygen (oxygen over 20+(OH,F)) is placed into deficient (OH,F) group.

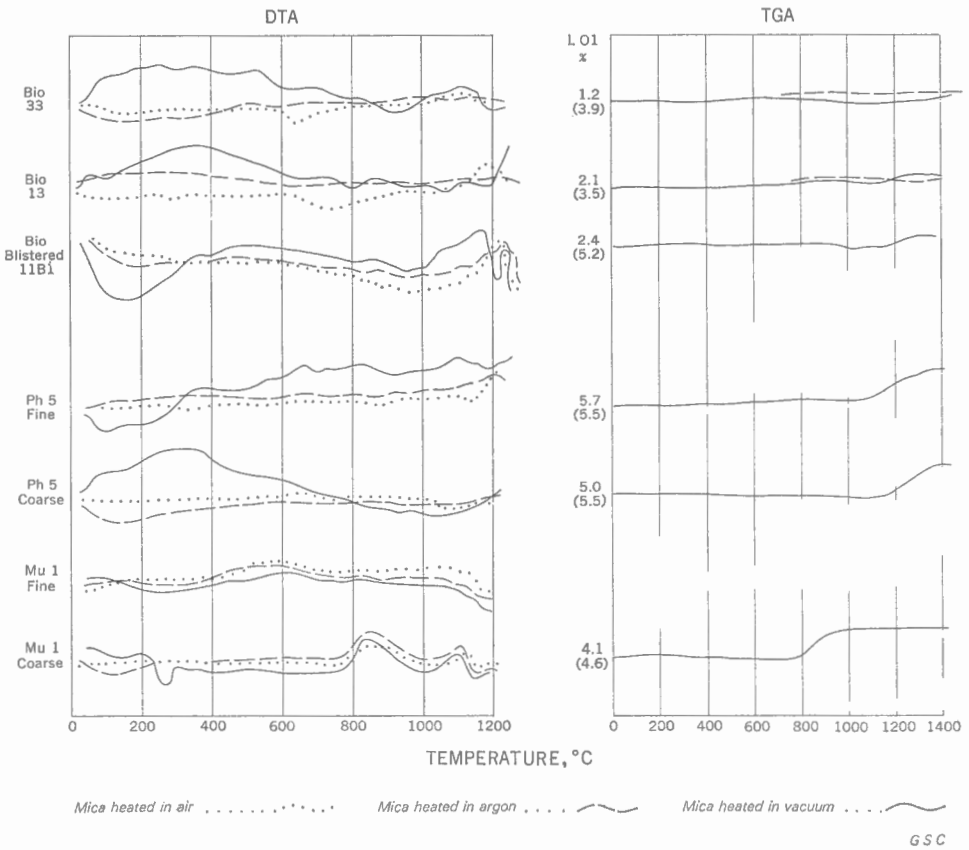

FIGURE 6. Differential thermal analysis and thermogravimetric analysis.

the oxygen from the (OH,F) group remains in the biotite lattice and causes self-oxidation of mica.

(5) The endothermal peak on the DTA curves of the coarse muscovite at 820°C (in air) and at 810°C (in argon and in vacuum) is correlative with expulsion of water. This peak corresponds to the loss of weight recorded on the TGB curve at 800°C. The second endothermal peak, at 1100°C, is correlative with decomposition and recrystallization of the coarse muscovite. Coarse muscovite fired to 600°C contains elongated blisters (Pl. III-6) and resembles in appearance blistered phlogopites (Pl. I-6).

(6) DTA curves of the crushed muscovite are much smoother. A weak endothermal peak at 600°C (in air) and at *ca* 580°C (in argon and in vacuum) is correlative with gradual expulsion of water, and a weak endothermal effect at 1000°-1100°C with decomposition and recrystallization.

(7) The coarse phlogopite shows greater thermal stability than the muscovite. The DTA curve (in air) is an almost straight line to 1175°C. The endothermal effect commencing at *ca* 1175°C is correlative with the loss of weight recorded on the TGB.

(8) The DTA curve (in air) of the crushed phlogopite shows three weak exothermal effects: one at 330°C, the second at 820°C, and the third at *ca* 1140°C. The last two exothermal effects are caused by oxidation of iron. The endothermal effect commencing at *ca* 1150°C and the loss of weight recorded on the TGB curve (1150°C) are correlative with the expulsion of water. The TGB curve shows gradual loss of small water content from *ca* 400°C. The comparison of thermal effects obtained on coarse and crushed phlogopite indicates that the crushed material is more susceptible to oxidation and loses water at slightly lower temperature than uncrushed mica.

(9) The behaviour of the blistered biotite is similar to that of crushed phlogopite, but shows a more distinct, sluggish, exothermal effect of oxidation (bumpy curve) in the temperature range 700°-1100°C. Endothermal effects at the lower temperature caused by the expulsion of water and fluorine, are probably masked by the exothermal effects of oxidation. A prominent endothermal effect, which is caused by expulsion of larger quantities of water and fluorine, and by decomposition, culminates at 1200°C (in air) and at *ca* 1170°C (in vacuum). The TGB curve shows a slight decrease in weight at *ca* 300°C, followed by a slight increase at 400°C, and a more prominent loss of weight at 1200°C.

(10) The DTA curve of biotite *13* shows two exothermal effects, at 300°C and at 720°C (the latter due to oxidation). The endothermal effect commences at 1130°C. The TGB curve shows a minor loss of weight at 1150°C (in air) and a very gradual loss of weight from *ca* 800°C (in argon).

(11) A distinct exothermal effect on the DTA curve (in air) of iron-rich biotite *33* occurs at 620°C, at a lower temperature than that observed on biotite *13*. Oxidation of iron-rich biotite at a somewhat lower temperature may be a

result either of its high FeO content or of its incipient alteration. Loss of weight on TGB curves, owing to the expulsion of water, is masked by oxidation, and the total loss of weight after firing is less than one third of the total water and fluorine content determined by chemical analysis.

A more detailed discussion of thermal effects and a description of mica properties after firing to several intermediate temperatures will be given in a separate report.

Chapter III

RELATIONS BETWEEN PHYSICAL PROPERTIES AND CHEMICAL COMPOSITION

In order to study the effect of octahedral Al, Ti, and Fe''' on the physical properties of the Mg-Fe series, micas with the following percentages of octahedral Al, Ti, and Fe''' were distinguished, and marked with corresponding symbols on the working curves (Figs. 7-15).

Symbol	Al	Ti	Fe'''	Symbol	Al	Ti	Fe'''	Symbol	Al	Ti	Fe'''
◆	0	0	0	◈	0-5	0-4	0-4	◇	5-10	4-10	4-10
♦	0	0	0-4	◈	0-5	0-4	4-10	◊	5-10	0-4	10
●	0	0-4	0-4	◐	0-5	4-10	4-10	○	10	4-10	0-4
■	0	0-4	0-10	◩	0-5	4-10	> 10	□	10	4-10	4-10
▲	0	4-10	0-10	◭	5-10	0-4	0-4	△	> 80	0-4	4-10
×	0	< 1	>10	+	5-10	0-4	4-10				

In the study of the relationship between the optical properties and the chemical composition, the refractive indices and the optic angles are plotted against: (1) per cent of total octahedral iron (Fe''' + Fe''), and (2) per cent of total iron group metals (Fe''' + Fe'' + Ti + Mn, etc.). A similar relationship is also sought between other physical properties and the chemical composition.

Optical Properties

Colour

The colour of mica depends on the amount of colouring ions present and on the proportion of Ti and Fe''' ions. Aluminum exerts a bleaching effect and yields brighter colours. Muscovite containing 7% of total octahedral iron appears almost colourless, whereas magnesium micas are more readily coloured and appear pale yellow with 2-4% of octahedral iron. Green, brown, greenish brown, and reddish brown colours,

commonly observed in the biotites, are related to the state of oxidation of iron and to the proportions of titanium and manganese in the octahedral layer. The main problem in correlating colour with the chemical composition arises from the fact that most concentrates are composed of multicoloured flakes. However, some of the concentrates consist predominantly of one-colour micas in different shades, and these will be considered first. A comparison of colour of mica with the ratios Fe'''/Ti and Fe'''/Fe'' is as follows:

Most prominent colour	Concentrate No.	Fe'''/Ti	Fe'''/Fe''
1. Reddish, bright.....	*15, 20*	0.25	0.05
2. Reddish brown, bright.....	*12, 27, 28, 30*	0.54-0.80	0.07-0.09
3. Brown-reddish, slightly dull.....	*19, 21, 26*	0.7-0.8	0.14-0.17
4. Brown-greenish, slightly dull.....	*9, 24*	1.2	0.17-0.26
5. Green.....	*13, 31*	4.8-25	0.23-0.29
6. Strongly pleochroic (γ brown)..... (β green).....	*6, 11*	10	0.55-0.80
7. Mixed brown and green flakes..... (γ, β non-pleochroic, unaltered)	*14, 16, 17, 18, 22, 23, 25, 29*	1.1-2.2	0.14-0.22

The relationship between the colour and the ratios Fe'''/Ti and Fe'''/Fe'' is quite obvious and confirms the observations of Hayama (1959), who correlated colour with TiO_2 content and the ratio $Fe_2O_3/(Fe_2O_3 + FeO)$. Ferric iron, when present in octahedral coordination in the proportions exceeding Fe'''/Ti = 1.0 and Fe'''/Fe'' = 0.17, imparts a greenish colour to mica. The green tone becomes more distinct with increasing proportions of the octahedral ferric iron and finally, when the ratio Fe'''/Fe'' reaches 0.30 or more, the mica becomes pleochroic with γ brown and β green. However, as soon as ferric iron separates from the mica lattice and crystallizes as tiny specks of Fe_2O_3, the mica becomes red-brown or brown. Mica *31* is mainly green, but alters in part to an orange-coloured anisotropic (γ, β) mica (*31a*). Although no distinct specks of ferric oxide could be identified optically, noticeable tiny specks along polygonal cracks in mica *31a* suggest that some Fe_2O_3 has separated from the lattice. In this connection, it can be pointed out that altered mica *31a* has a distinctly lower X-ray intensity ratio (004)/(005) and higher refractive indices than unaltered mica *31*. This suggests that some of the ferric iron is displaced from its octahedral sites, thus causing optical anisotropy on the (001) plane. Narrow bands of Fe_2O_3, which in many cases surround pleochroic haloes, are additional evidence for the relationship between separation of excess oxidized iron and optical anisotropy on the (001) plane. Inclusions of radioactive minerals and associated radioactive minerals may also cause oxidation of mica; e.g., mica *11*. Oxidation phenomena and displacement of atoms in mineral lattices as a result of radioactivity have been thoroughly discussed by Ellsworth (1932, p. 89).

The presence of green and brown mica flakes in some concentrates indicates a different state of iron oxidation in these micas. The difference in ferric iron content of the green and the brown mica flakes can be estimated by comparing colours with those of chemically analyzed homogeneous concentrates. The presence of reddish and brown flakes in a concentrate suggests variations in the titanium content of the octahedral layer, which may also be estimated by colour comparison.

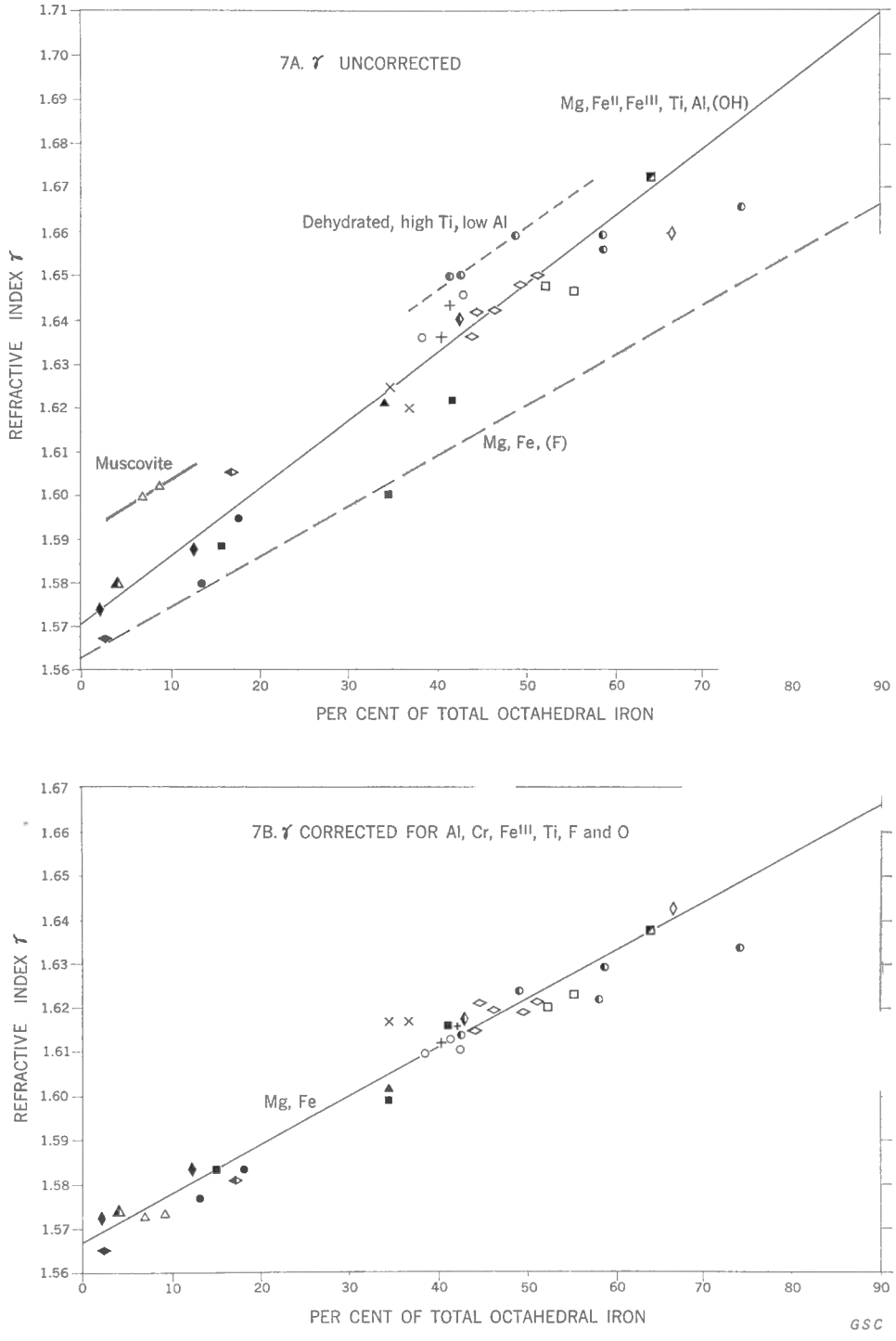

FIGURE 7. Relation between refractive index γ and iron content of the octahedral layer.

Refractive Indices

The refractive index γ plotted against %$\sum$oct.Fe[1] shows a general increase with increasing iron content, but with considerable scatter in the points (Fig. 7a). Considering the proportions of Al, Ti, and Fe''' in octahedral sites, and the composition of the (OH,F) group, it is possible to draw several lines connecting: (1) pure Mg-Fe-(F $\geq$ OH) members (with γ relatively low); (2) muscovites (γ relatively high); (3) partly dehydrated micas with high Ti and low Al (γ high); and (4) Mg-Fe''-(OH,O) micas containing octahedral Fe''', Ti, and Al (γ intermediate). By comparing micas with similar chemical compositions that differ in one component only, it was possible to calculate the effect on the refractive index γ of the substitution of Al, Cr, Ti, Fe''' for Mg and Fe'', and the effect of F and O in the (OH,F,O) group. It was found that substitutions of one per cent Al, Ti and Cr, and Fe''' raise γ by 0.0002, 0.004, and 0.0002, respectively. One per cent F in the (OH,F) group lowers the refractive index by 0.0002 and one percent O in the 'oxidized' (OH,F,O) group raises γ by 0.0002. After introducing the above corrections, the points show much less scatter (Fig. 7b). The average deviation of the points from the curve is $\pm 2\%$ Fe. Some points, however, remain anomalous—biotite *11*, which has a high γ index, displays optical anisotropy in the (001) plane, and biotite *33*, which has a low γ index, contains partly chloritized flakes and segregations of iron. Some of the correction factors may require revision when more analyzed micas are studied. Furthermore, the heterogeneity of the concentrates and inexact corrections applied to the chemical analyses for impurities contribute to some extent to the scattering of the points.

Refractive indices γ and α plotted against the per cent of total octahedral iron group metals (Fig. 8) show similar relations to those found in Figure 7a. After correcting for the Mg-Fe-(OH) series (Fig. 9), they show less scattering than those before correction. Both indices of mica *11* are high. The characteristic index for the main portion of the flakes of concentrate *33* is low, but the extreme high index of some flakes in this concentrate (marked *33a* in Fig. 9) and γ index of mica *31a* are abnormally high. These extreme variations in refractive indices are caused by alteration of mica.

The extension of γ and α lines corrected for the Mg-Fe-(OH) series (Fig. 9) indicate the following indices: for the pure Mg-phlogopite $\gamma = 1.568$ and $\alpha = 1.532$, and for Fe-rich biotite $\gamma = 1.697$ and $\alpha = 1.628$. In the Mg-Fe-(OH) series, the γ index increases with increasing octahedral ferrous iron by 0.0014 for 1% Fe'', and the α index by 0.001. Maximum error in determination of the iron content from these curves for altered biotites is 15%$\sum$oct.Fe and =8% FeO by weight. The average error, including altered micas is 2%$\sum$oct.Fe and =1% FeO by weight. These curves are prepared for studies of fresh micas. Since none of the concentrates is entirely homogeneous and may contain some altered flakes, a careful examination for evidence of alteration should be made before attempting to use optical properties for the determination of chemical composition of micas.

Optic Angles

Optic angles, including the range of extreme variations, plotted against the per cent of total octahedral iron group metals (Fig. 8, top) show no relation to

[1]For explanation of this symbol see list of abbreviations, Chapter I.

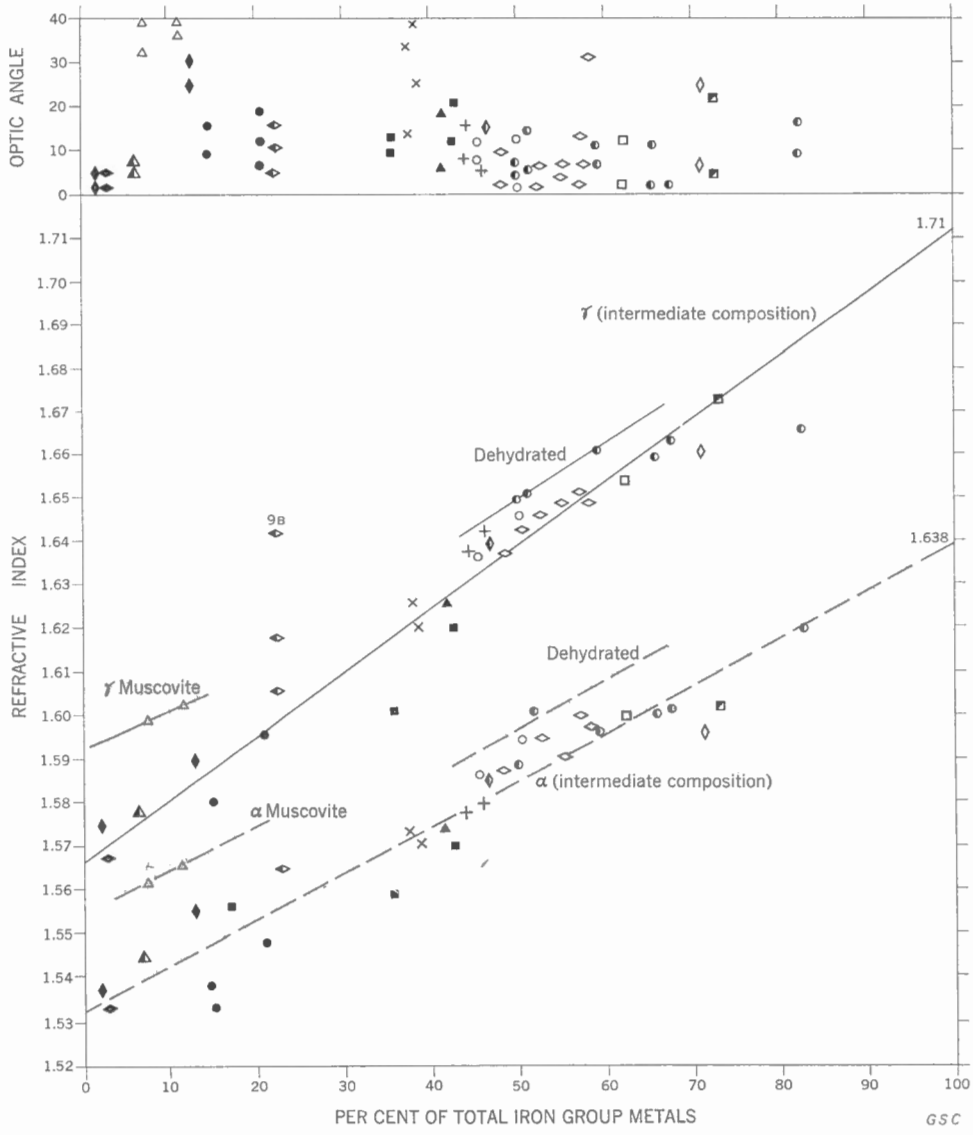

FIGURE 8. Relation between optical properties and content of iron group metals in the octahedral layer.

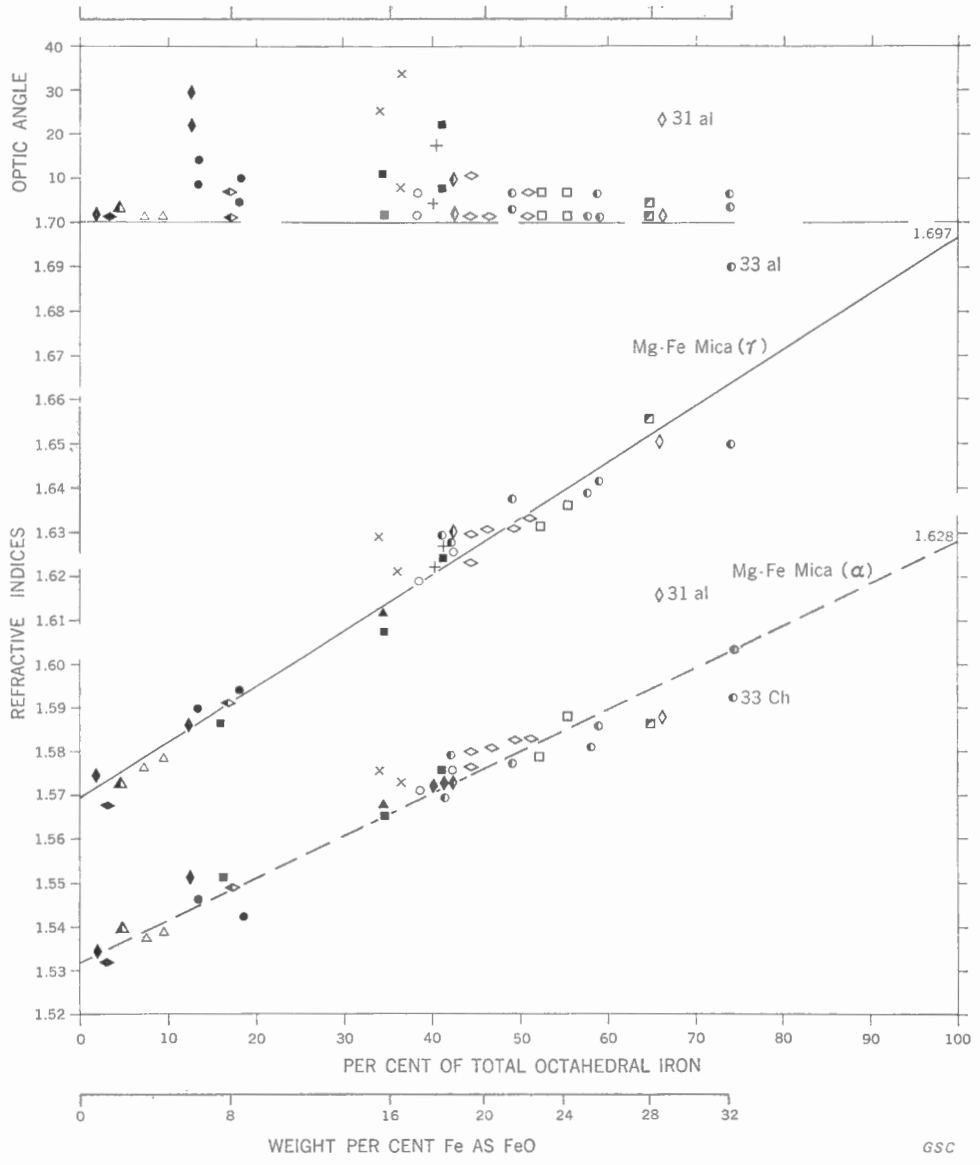

FIGURE 9. Relation between optical properties and iron content of the octahedral layer, corrected for Al, Fe‴, Ti, F, and O.

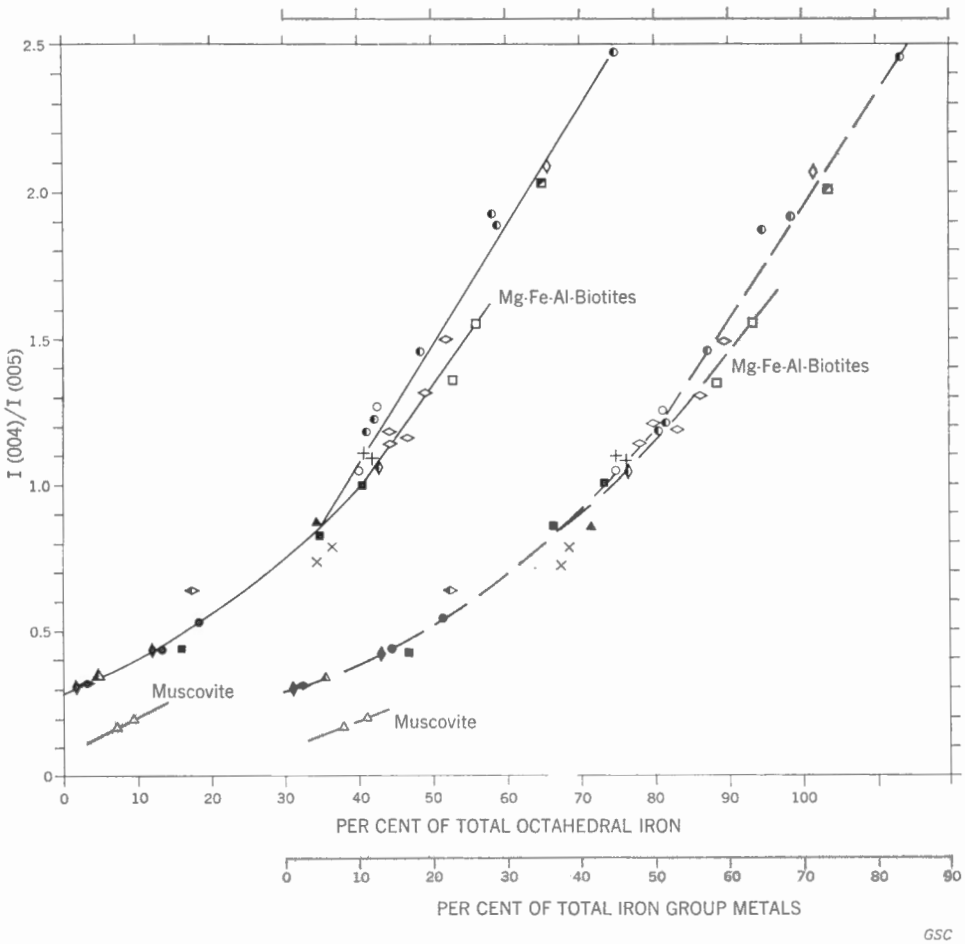

FIGURE 10. Relation between the X-ray intensity ratios $I_{(004)}/I_{(005)}$ and composition of the octahedral layer.

chemical composition. However, considering that the muscovites have larger optic angles than the biotites, which may be a result of the presence of trivalent aluminum and unoccupied positions in the octahedral layer, the optic angle was corrected for octahedral Al and Fe''' by subtracting 0.33° for each 1% of Al and Fe'''. Corrected 2V° and corrected refractive indices γ and α are plotted against the per cent of total octahedral iron and approximate weight per cent iron in Figure 9. After correcting for octahedral aluminum and ferric iron, the optic angle becomes 0° in muscovites and in most of the biotites, but remains large in pleochroic haloes, in blistered areas, and in pleochroic (γ,β) phlogopites and biotites. This is further evidence that optical anisotropy may be caused by displacement of iron ions in the octahedral layer.

X-Ray Diffraction Properties

Intensity Ratios $I_{(004)}/I_{(005)}$

The relation between the intensities of X-rays diffracted by the basal planes of mica and the composition of the octahedral layer has been studied by plotting

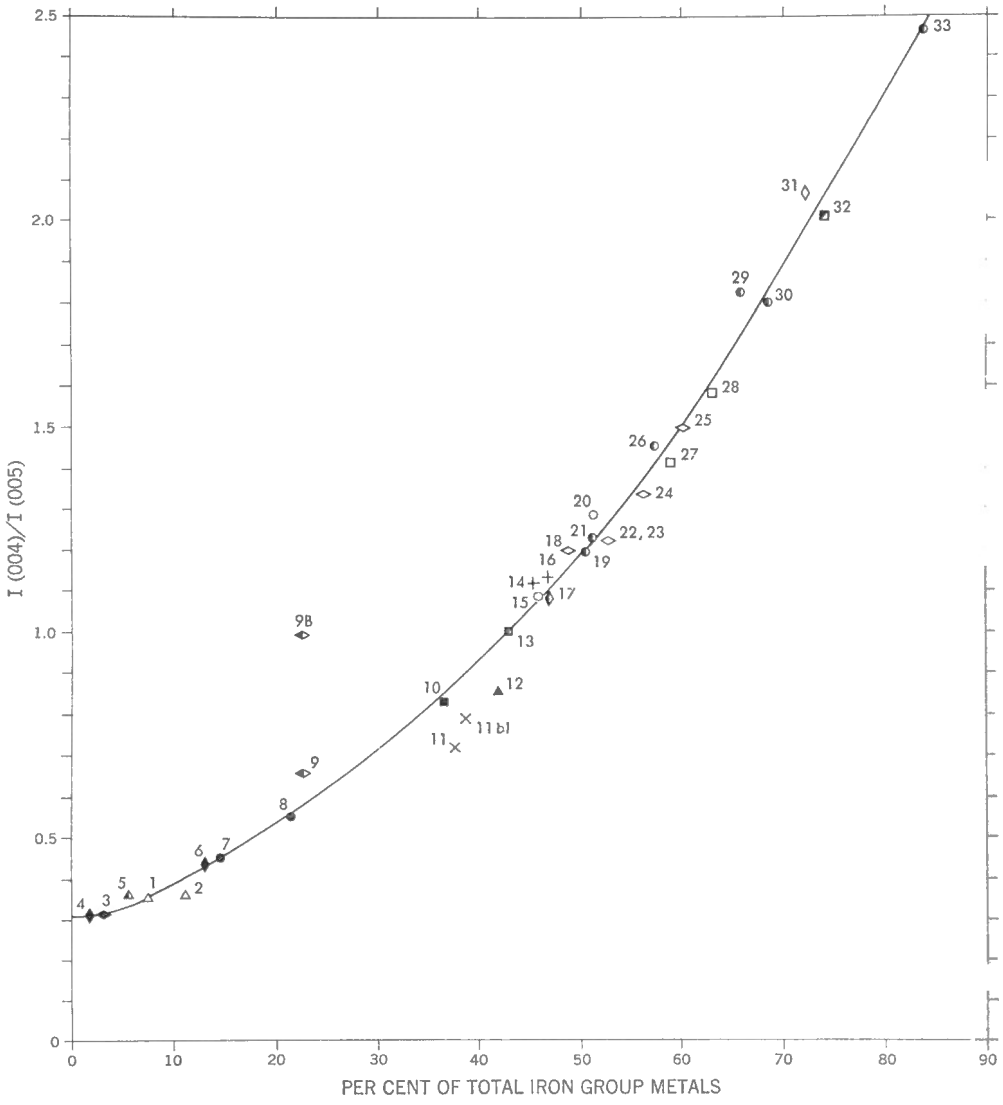

FIGURE 11. Relation between X-ray intensity ratios of $I_{(004)}/I_{(005)}$ and percentage of total octahedral iron group metals, corrected for Al, 1% Al^{vi} + 0.003 (area counts, Cu—radiation, Ni—filter, 45 kv, 16 mA).

$I_{(004)}/I_{(005)}$ against the percentages of total octahedral iron and of total octahedral iron group metals (Figs. 10 and 11). The curves show a gently curving slope between 0% and 35% octahedral iron. From about 35% total octahedral iron the curve splits into two almost straight lines (Fig. 10): the steeper slope refers to Mg-Fe biotites and the second to Mg-Fe-Al biotites. The presence of Al in the octahedral layer has the effect of lowering the intensity ratio by about 0.003 for each 1% Al. Thus, muscovite has a lower intensity ratio than phlogopite containing an equivalent amount of octahedral iron. In biotites, this effect results in the split curves shown

in Figure 10. When the intensity ratios are corrected for the octahedral aluminum content a single curve may be drawn (Fig. 11). Most of the points fall close to the curve. Heterogeneous mica *9* indicates a higher iron content; micas with variable optic angle and low octahedral occupancy (Nos. *11*, *11Bl*, and *12*) show lower total iron, possibly as a result of displacement of iron; and heterogeneous biotite *33* gives rather poor reproducibility (± 0.2). Including all erratic points, the average error in determination of $\%\sum$oct.FeGrMe[1] from Figure 11 is $\pm 2\%$. The intensity ratio (004/005) thus gives a close approximation to the composition of the octahedral layer. By this method it is possible to determine the quantities of ions actually present in the mica lattice, whereas chemical analyses give total amounts of elements present in the concentrate, which may include impurities, inclusions, and alteration products. It is important to point out that aluminum lowers the intensity ratio and raises the indices of refraction; therefore, by using both X-ray and optical methods, a fair estimation of octahedral aluminum can be made.

To check the accuracy of the curve, $\%\sum$oct.Fe was determined using the intensity ratios and chemical analyses published by Engel and Engel (1961). Results are as follows:

Chem. Anal. $\%\Sigma$oct.Fe (Engel)	42.0	42.0	45.0	45.0	44.0	33.0	36.0	32.0	33.7
Predicted from curve (Fe rad.) Gower (1957), av. Int. Ratio	53.5	49.0	59.5	64.0	56.5	49.0	55.0	46.5	49.5
Determined from curve (Cu rad.) Fig. 10, $\%\Sigma$oct.FeGrMe	40	38	44	46	41	36	40	34	36

This example shows that the percentages of iron obtained from the curve shown in Figure 10 of this paper (Cu radiation) are much closer to the iron values obtained by chemical analysis than the values predicted by Engel and Engel (1961), using the curve published by Gower (1957) for the ratios obtained with Fe radiation.

Lattice Spacings $d_{(001)}$ and $d_{(010)}$

In order to study the relationship between the spacings $d_{(001)}$ and $d_{(010)}$ and the chemical composition of micas, spacing measurements listed in Table II were plotted as a function of the per cent of total octahedral iron group metals (Fig. 12). Neither spacing shows any apparent relation to chemical composition, although average values, calculated for Mg-Fe micas in the following ranges of $\%\sum$oct.FeGrMe: 0-25%, 25-45%, 45-65%, and 65-85%, show a slight general increase with increasing iron (solid lines in Fig. 12).

The $d_{(001)}$ spacings of micas containing appreciable quantities of fluorine in the (OH,F) group lie below the solid line on Figure 12. Phlogopite *9*, which contains mainly OH in the (OH,F) group, falls above the average line, and biotite *9B*, which contains more iron, has a larger spacing than phlogopite *9*. This suggests that fluorine reduces the basal spacings and iron enlarges them. Biotites in the compositional range of 45-65% total octahedral iron group metals show the widest scatter, which may be related

[1]For explanation of this symbol see list of abbreviations, Chapter I.

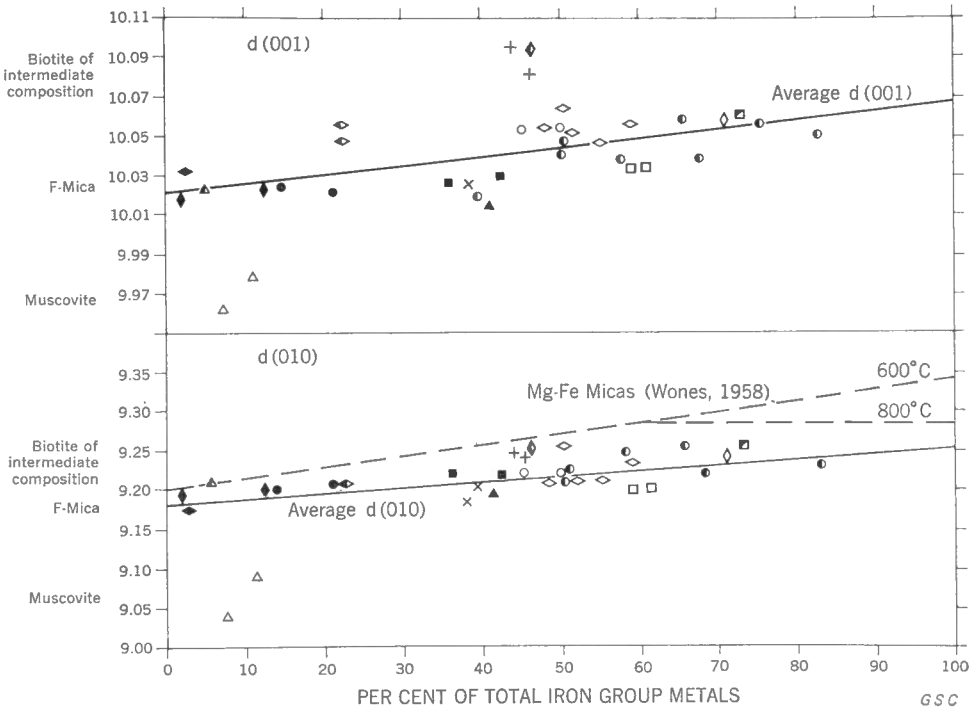

FIGURE 12. Relation between $d_{(001)}$, $d_{(010)}$ and composition of the octahedral layer.

to the presence of octahedral Al, Ti, and Fe‴, to the state of alteration of the biotite flakes, and to conditions of crystallization. All biotites from the White Creek Batholith fall above the average line, and those showing evidence of post-crystallizational alteration (chloritization and numerous inclusions, Pl. II-4) have the largest spacings. Biotite *27*, from a cordierite gneiss, and partly dehydrated biotite *12*, from paragneiss, have shorter spacings and fall below the average line. Micas containing relatively large quantities of octahedral aluminum and titanium, and thus a considerable proportion of unoccupied octahedral positions, also fall below the average line. The effect of Fe‴ is not quite clear. Fe‴ seems to enlarge the basal spacing when introduced under hydrothermal alteration conditions (partly chloritized flakes containing inclusions of epidote, Pl. II-4). Such micas show on X-ray diffractometer charts slightly enlarged basal spacings with distinctly separated chlorite reflections. However, the basal spacings of micas containing high ferric-iron contents not related to hydrothermal alteration, generally from alkalic environment, are not enlarged (biotite *32* and *11*).

Spacings $d_{(010)}$, determined in the present study on natural micas, were compared with those of synthetic Mg-Fe-(OH) biotites reported by Wones (1958, Fig. 14, p. 194) and by Eugster and Wones (1962, p. 96). It is important to point out that Wones (1958) observed the relationship that exists between the stability of iron-rich biotite and the temperature and pressure (O_2) of its crystallization. He found that

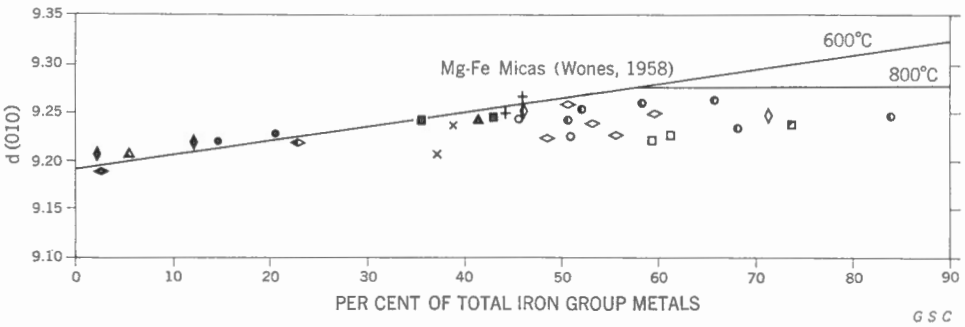

FIGURE 13. Relation between $d_{(010)}$ and chemical composition of the octahedral layer, corrected for F, Al, and vacant positions.

iron-rich biotites containing >80% octahedral iron are unstable at 800°C and recrystallize to form biotite, which contains less iron (60%), sanidine, magnetite, and vapour. The spacings $d_{(010)}$ of synthetic biotites (dotted line in Fig. 12) are somewhat larger than those observed in natural micas. However, after making the corrections for (1) the percentage of fluorine substituting for OH in the (OH) group, (2) the percentage of unoccupied octahedral positions, and (3) the percentage of octahedral aluminum ions substituting for magnesium in biotites (all corrections positive: 0.0005, 0.0005, and 0.00025 Å for 1% of each, respectively), the spacings of natural micas were found to be correlative with those reported by Wones (1958) in the range below 50% of total octahedral iron (Fig. 13). In the range from 50% to 83% ∑oct.FeGrMe, the spacings $d_{(010)}$ are smaller by *ca* 0.05 Å than those reported by Wones (1958) for synthetic micas. From 0 to 50% ∑oct.FeGrMe, the spacing $d_{(010)}$ increases from 9.188 to 9.263 Å, or by *ca* 0.0015 Å per 1% ∑oct.FeGrMe. In the iron-rich biotites the relationship between the $d_{(010)}$ spacing and the iron content is not apparent, probably because of the reduction and oxidation of iron. In this connection, it can be pointed out that micas fired to 600°C (in air) show inconsistency in spacing dimensions. In some micas the spacings decrease after firing; in others they increase. Study of fired micas is now under way and the results will be reported later. Radoslovich (1962) reported a similar variation in the b axis of micas before and after heating.

This is further evidence that the spacing of micas is not only a factor of structural composition, but depends also on the conditions of crystallization and subsequent alterations.

Specific Gravity

The relation between specific gravity and chemical composition is similar to that for refractive index and chemical composition. The Mg-Fe micas (Fig. 14, lower curve) are lighter than the Al-Fe micas (Fig. 14, upper curve), and the biotites containing Al, Ti, etc., fall between the upper and lower curves (intermediate curve in Fig. 14). The effect of Al becomes less prominent with increasing iron content, and most of the points in the range 50%-83% ∑oct.FeGrMe fall close to the intermediate curve for Mg-Fe″-(Al,Ti,Fe‴, etc.) biotites. One per cent of octahedral Al raises

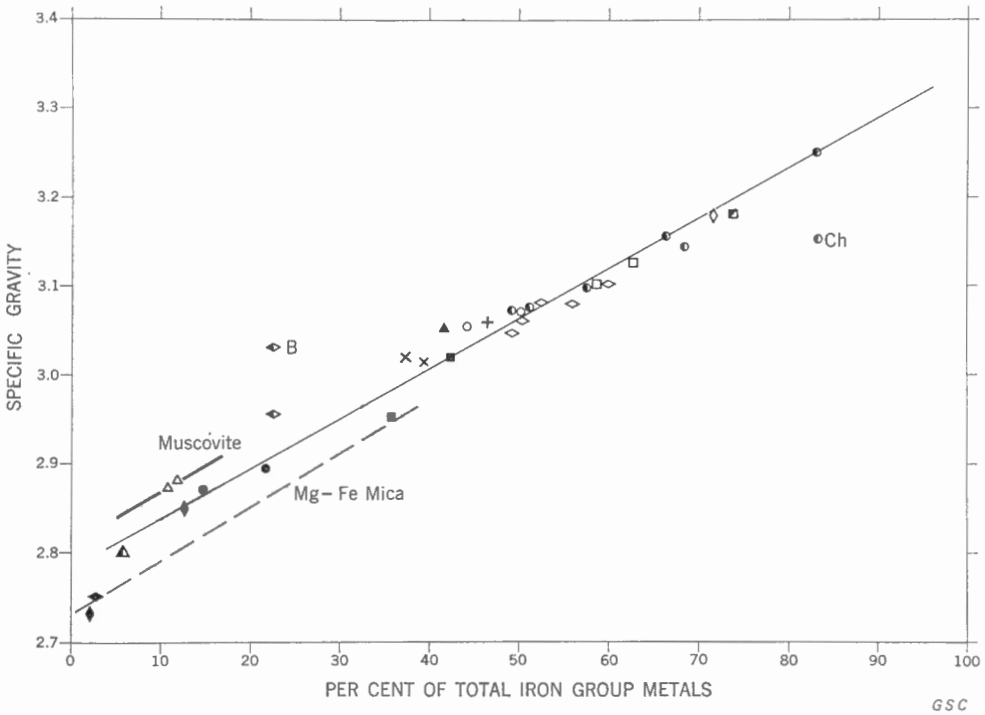

FIGURE 14. Relation between specific gravity and composition of the octahedral layer.

the specific gravity of Mg-mica by *ca* 0.0008, and 1% of octahedral iron by *ca* 0.006. Partly dehydrated micas containing low Fe''' seem to be slightly denser than those containing high Fe'''. Specific gravity measurements are useful in determining the homogeneity of partly altered micas and the chemical composition of fresh micas. In conjunction with the X-ray determination of the intensity ratio (004)/(005), where Al exerts an opposite effect by lowering the ratio (Al slightly raises R.I. and Sp.G. of Mg-micas), it is possible to estimate the content of octahedral Al in the biotites.

Magnetic Susceptibility

Magnetic susceptibility, measured with the Frantz Isodynamic Separator as the currents required to commence the separation of most and least magnetic flakes, gives a good indication of the homogeneity of the concentrates (Fig. 15).

The critical currents required to exert equal flow of mica through both channels of the Frantz Separator decrease with increasing iron content of Mg-Fe micas. The Al-micas show lower magnetic susceptibility than Mg-micas with equivalent iron content. The effect of Al on the magnetic susceptibility of mica is similar to that on the $d_{(001)}$ and $d_{(010)}$ spacings. The two critical currents measured on muscovites are 0.76 amp. and 0.66 amp. The large difference between the minimum and maximum currents is caused by the presence of magnetite and quartz inclusions in a few flakes.

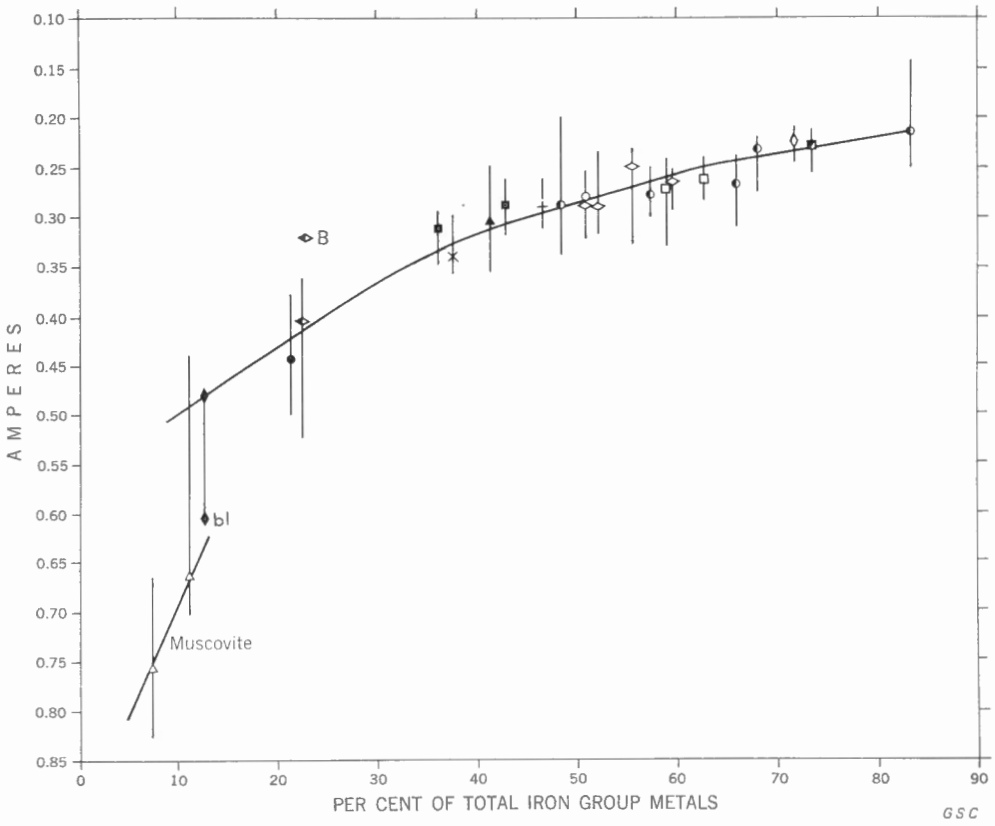

FIGURE 15. Relation between magnetic susceptibility and composition of the octahedral layer.

Phlogopite *6* is homogeneous in chemical composition but contains blistered flakes, which have low magnetic susceptibility. The critical current measured on phlogopite *6* is about 0.4 amp.; i.e., considerably lower than that measured on muscovite *2* (0.66 amp.), which contains a similar amount of octahedral iron. The difference in $\%\sum$oct.FeGrMe between phlogopite *9* and biotite *9B*, determined from the curve in Figure 15, is roughly 20% and is similar to that obtained from the optical data (curve in Fig. 8), from specific gravity (Fig. 14), and from X-ray intensity ratios (004)/(005) (Fig. 11). The highest magnetic susceptibility was shown by a few flakes with iron segregations from concentrate *33*. These flakes separated as a magnetic fraction at a current as low as 0.13 amp. However, these strongly magnetic flakes are an exception and the minimum current required for separation of iron-rich micas is approximately 0.20 amp.

As mentioned in Chapter II, the Frantz Separator was not calibrated in the present study, and thus the measurements are reported in amperes. The approximate magnetic susceptibilities converted into emu/g, employing the calibration chart published by McAndrew (1957, curve for transgressive slope 10°), are as follows:

	Critical Currents in amperes (present study)	Magnetic Susceptibility emu/g × 10^6 from calibration chart McAndrew (1957)
Muscovite (quartz inclusions)	0.83	4.5
Muscovite (clean)	0.76-0.66	5-8
Muscovite (magnetite inclusions)	0.44	18
Phlogopite (*ca* 12% Σoct.Fe, compact)	0.47	16
Phlogopite (*ca* 12% Σoct.Fe, blistered)	0.60	10
Biotite (*ca* 50% Σoct.Fe)	0.30	40
Biotite (*ca* 83% Σoct.FeGrMe)	0.21	80
Biotite (iron segregations)	0.13	180

These figures compare reasonably well with the following magnetic susceptibilities obtained on Australian biotites by Vernon (1961, Fig. 1, p. 1148):

Phlogopite	12 emu/g × 10^6
Biotite (40-45% FeMn)	35 emu/g × 10^6
Iron-rich biotite (*ca* 70% oct.FeMn)	50-55 emu/g × 10^6

Summary and Conclusions

Optical, X-ray diffraction, DTA and TGB analyses, as well as specific gravity and specific magnetic susceptibility measurements, were carried out on 34 chemically analyzed micas. A critical evaluation and re-examination of available methods was made in order to select the most suitable methods for determining the physical properties that are useful in correlating with the chemical composition. All correlations were made on the basis of the unit cell contents expressed as ionic percentages of IV, VI, and XII layers. Structural formulae were calculated on the basis of 44 cationic valencies, 24 anions, and 20 oxygens, in order to obtain the differences in the unit cell contents arising from the method of calculation.

Results of the present study are as follows:

1. None of the concentrates is entirely homogeneous. Individual flakes differ in chemical composition, state of oxidation of iron, morphological features, and degree of alteration.

2. The three methods used to calculate the structural formulae of mica give similar results when the proportions of the chemical components are equivalent to those of ideal mica. However, the structural formulae of partly dehydrated or 'oximicas' differ, depending on the method of calculation.

3. In most of the dehydrated micas the content of ferric iron is too low to account for the excess of oxygen. It is concluded that the deficiency of the OH group is a result of partial loss of water as H_2O. In such cases, the structural formula calculated on the basis of 44 cationic valencies is less distorted than those obtained on the basis of 24 anions and 20 oxygens. The excess oxygen in dehydrated micas is placed in the hydroxyl group.

4. The relations between physical properties and chemical composition, determined on the basis of present experimental data, are as follows:

(a) Colour of mica is a factor of the octahedral proportions of Ti, Fe''', and Fe''. Certain minimum quantities of each colouring ion must be present to produce colour of mica. The phlogopites seem to be more readily coloured than the muscovites. The relation of colour to the ratios of Fe'''/Ti and Fe'''/Fe'' observed on the present biotites is:

Fe'''/Ti	*Fe'''/Fe''*	*Colour*
10	0.5	strong pleochroism, γ brown, β green
5	0.2	green
1.2	0.14	greenish brown or a mixture of green and brown flakes
0.5-0.8	0.07-0.09	reddish brown
0.25	0.05	brownish red

Ti produces a reddish colour, Fe'' brown, and Fe''' green, if present in the mica lattice. Mn produces a reddish colour, but was not considered in the present study because it was present in small quantities only.

(b) The effect of different ions on the physical properties of pure Mg-mica is as follows:

Al raises the refractive indices and the specific gravity, but lowers the intensity ratio $I_{(004)}/I_{(005)}$ and reduces the spacing $d_{(010)}$.

F lowers the ratio $I_{(004)}/I_{(005)}$ and the refractive indices, and also reduces the spacing $d_{(010)}$.

Fe''' and *Ti* raise the refractive indices.

(c) The approximate interrelation of physical properties and the effect of ferrous iron on the properties of pure Mg-phlogopite are summarized in Table VIII. Properties of the muscovite (M) with 7%$\sum$oct.Fe are given for comparison.

5. A reasonably accurate estimation of the chemical composition of mica can be made on the basis of physical properties. Mg-Fe-OH members can be determined from the relations shown in Table VIII. The proportions of the octahedral Ti and Fe''' can be estimated from the colour, and Al and F by comparison of the refractive indices and $I_{(004)}/I_{(005)}$.

6. The spacings $d_{(001)}$ and $d_{(010)}$ are not only related to structural composition but also appear to be affected by the conditions of crystallization and subsequent alterations. Therefore, the use of the spacings in predicting the composition is limited until the effects of other factors (i.e., alteration) is fully understood.

7. The advantages of physical methods in determining the chemical composition are:

(a) relatively small quantities of material required;

(b) possibility of rapid identification of various mica types from the same rock;

(c) physical properties indicate the chemical constituents actually present in the mica lattice, whereas chemical analysis gives the composition of the bulk concentrate, including impurities and inclusions.

8. The interrelation of physical properties presented in Table VIII can be conveniently applied for practical purposes, such as concentration and separation of various mica types, homogeneity tests, etc.

Table VIII

Approximate Interrelation of Physical Properties and the Effect of Ferrous Iron on the Properties of Pure Mg-phlogopite

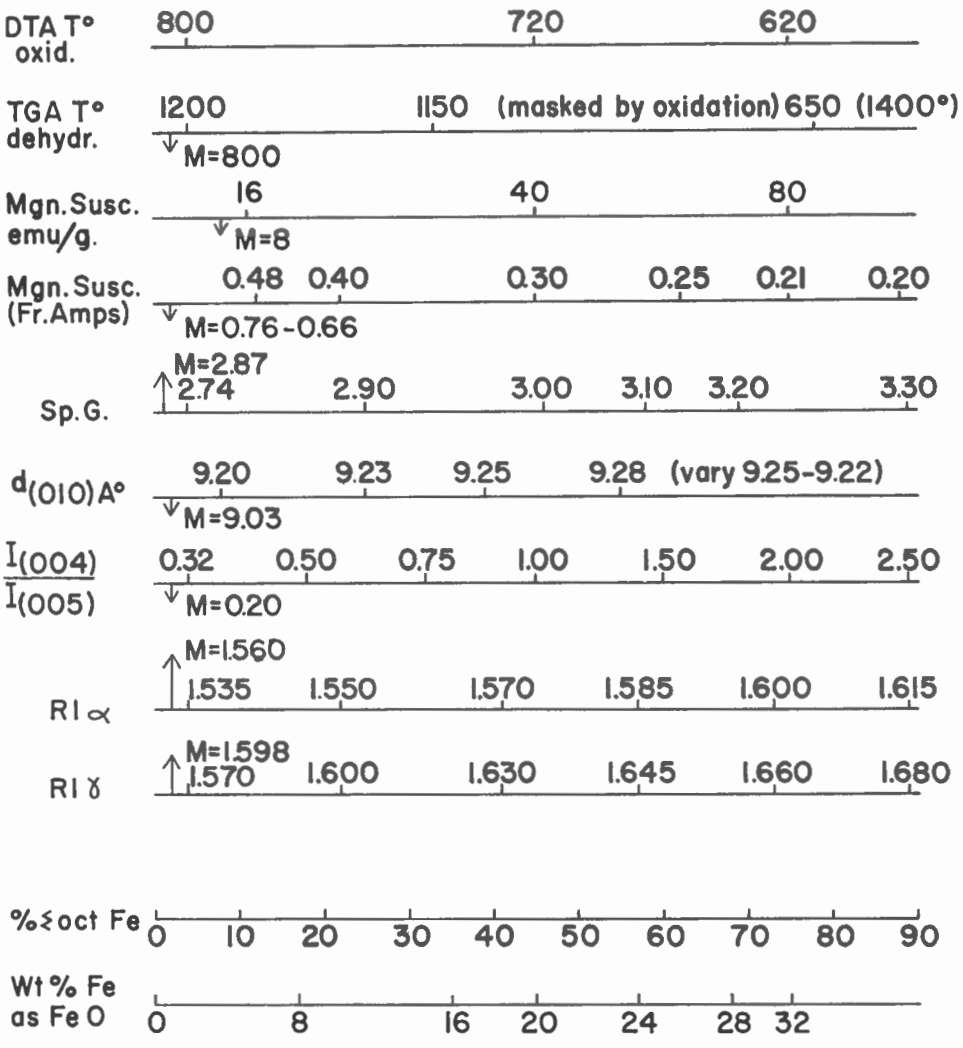

In above table, read "emu/g" emu/g $\times 10^6$

9. Considering the complexity of the chemical composition of micas, the present results on 34 chemically analyzed rock-forming (common) micas do not account for all possible mica varieties. The present study will be supplemented when more chemically analyzed mica varieties are available, particularly on Li-micas and iron-rich biotites.

Chapter IV

PETROLOGY OF MICA-BEARING ROCKS

The writer has studied the occurrence, paragenesis, sequence of crystallization, and alteration of the micas in thin sections of the 43 host rocks that formed the basis of this investigation. With the exception of eight specimens from the Bancroft area, nine specimens from the White Creek Batholith, and two specimens from the Mount Megantic complex, the rocks were collected from different localities and are unrelated.

Five specimens of granodiorites and four quartz monzonites representing rock-units 9 to 14 of the White Creek Batholith, including six analyzed mica concentrates, were made available for this study by J. E. Reesor, who described the geology and petrology of the area and presented a plan showing exact locations of the samples (Reesor, 1958; and 1961, pp. 88-89). Rock-units display a concentric arrangement grading from mafic-rich granodiorites (unit 9) into more leucocratic and acidic varieties of porphyritic quartz monzonite and leuco quartz monzonite towards the centre (units 12 and 14). Specimens from these rock-units were collected at different elevations. According to Reesor (1958), some minerals, particularly microcline phenocrysts, continued growing after emplacement of magma. In addition, two types of xenoliths were observed: (1) metamorphosed sedimentary rocks, and (2) fine-grained, mafic-rich inclusions.

Analyzed micas from skarn, schist and gneisses, pegmatite, and radioactive orebodies of the Bancroft area were made available for the present study by S. C. Robinson. The geology of the area has been described by Satterly (1956) and Hewitt (1957, map O.D.M. 1957-1). Rock-units distinguished in the Bancroft area from which micas were collected are:

Metasediments: paragneisses and amphibolite (unit 2), and marble (unit 3);
Precambrian plutonic rocks: older basic intrusive and meta-intrusive rocks (unit 4), syenitic rocks (unit 7), and granitic rocks (unit 8).

Petrographic Descriptions

In the following petrographic descriptions, the rocks are listed in the same order as in the location of samples (Table I) and in the description of concentrates (Table II). In Table II micas are listed in approximate order of increasing iron content in the octahedral sites. Thirty-three rocks from which micas were selected for complete chemical analysis are listed first. Micas from rocks *34* to *43* were analyzed by means of the X-ray spectrograph only. Numbers of concentrates and of host rocks are the same, with the exception of one quartz monzonite from which muscovite *1M* and biotite *28B* were concentrated.

1. *Quartz Monzonite* is composed of the following minerals, listed in approximate order of sequence of crystallization: zoned plagioclase, biotite, orthoclase, muscovite, strained quartz, microcline, perthite, myrmekite, fine-grained graphic quartz-muscovite intergrowths, and apatite. Biotite laths, *28B*, occur parallel with the foliation. They are surrounded and transected by muscovite (*2M*, Pl. VII-8), and locally replaced by chlorite and apatite. Muscovite occurs also in coarse composite porphyroblasts (Pl. I-2) and includes small euhedral plates of biotite (Pl. I-1). Some biotite crystals are interleaved with muscovite, which spreads along (001) sheets (Pl. I-3). Coarse-grained microcline displays discontinuous grid-twinning and replaces plagioclase in irregular patches. Some crystals of potassium feldspar are perthitic. Coarse composite muscovite crystals, formed by the growing together of several individual crystals, and shredded, fine-grained muscovite rims around coarse biotite and muscovite crystals indicate the presence of two generations of muscovite.

2. *Quartz Monzonite.* Minerals present in approximate order of crystallization include: biotite, plagioclase, microcline, quartz, coarse-grained muscovite, calcite, and fine-grained muscovite in calcite veinlets. Biotite is altered to chlorite and to a fine-grained aggregate of sphene. Plagioclase crystals display weak zoning. They are altered to albite, muscovite, and carbonate, and include remnants of altered biotite in the cores. Microcline includes partly resorbed crystals of plagioclase. Some grains are perthitic. Quartz is strained and filled with small inclusions of biotite, zircon, and apatite. Coarse-grained muscovite (*2M*) that replaces altered biotite (Pl. VIII-5, 6), is probably earlier than the finer-grained muscovite that replaces feldspars. Muscovite that occurs in rock-fractures with calcite (Pl. VIII-7) is apparently the youngest. Biotite was probably already altered before it was replaced by muscovite. This rock was affected by hydrothermal alteration. It shows very clearly the difference in stability between the early and late minerals under hydrothermal alteration conditions. The earliest minerals, biotite and plagioclase, underwent the greatest amount of alteration, whereas microcline, which was formed later, was only slightly altered, and muscovite remained unaltered even during crystallization of carbonate in the fractures.

3. *Marble.* Euhedral crystals of clear amber phlogopite occur in pink calcite. Phlogopite crystals carry subhedral to euhedral diopside in the cores, some of which are replaced by impure carbonate.

4. *Diopside Marble.* Phlogopite occurs in a coarse-grained calcite. It is associated with green diopside (Pl. I-5) and is partly replaced by apatite, allanite, and sphene. A few phlogopite crystals carry euhedral uraninite, which is surrounded by pleochroic haloes. Phlogopite containing uraninite is fractured and coated with orange-yellow crusts along (001) fractures.

5. *Metamorphosed Impure Limestone.* Coarse books of euhedral phlogopite, 4 inches in diameter, occur in impure limestone-tremolite rock near the contact with granite gneisses and pegmatites. Phlogopite displays inclusion zoning (Table II, Pl. I-7, 8) and contains adhering grains of greenish blue apatite. Complete chemical analysis was performed on clean phlogopite *5*. Phlogopite with acicular inclusions (*5a*) was analyzed by means of the X-ray spectrograph.

6. *Pyroxenite-Scapolite Rock.* Pale brown phlogopite crystals are disseminated in green massive pyroxene. Interstitial spaces are filled with scapolite and calcite. A few small grains of allanite and minute opaque specks occur in fractures of pyroxene.

7. *Calcite-Fluorite Dyke.* Pale buff phlogopite, greenish diopside, and colourless garnet occur in calcite-scapolite rock. Phlogopite is bent and peppered with iron oxides. This dyke also carries uraninite (Robinson, *in* Lowdon, 1960).

8. *Pyroxene-Hornblende-Biotite Gneiss.* This medium-grained, well foliated gneiss is composed of abundant pale green pyroxene, poikilitic amphibole, phlogopite, minor andesine, and interstitial quartz. Pyroxene, and to a lesser extent hornblende, crystals are fractured. Phlogopite is the chief constituent of the rock. It is fresh, only slightly bent, poikilitic, and contains inclusions of apatite and zircon, which are surrounded by pleochroic haloes (Pl. IX-1). Phlogopite engulfs pyroxene and occurs in hornblende along the cleavage planes. It spreads in net-like aggregates throughout the rock and apparently formed at the expense of other minerals, chiefly pyroxene, at the end of and after the deformation.

9. *Lamprophyre.* The rock is composed of early phenocrysts (*ca* 30%, Pl. IV-7), which are present in a fine-grained groundmass of fan-shaped aggregate of feathery, twinned albite with some epidote and magnetite (Pl. IV-8). Phenocrysts are zoned ortho- and clinopyroxenes and zoned phlogopite (*9Ph*, Pl. II-1). The lamprophyre is fractured and contains dark brown biotite *9B* and coarse epidote in the fractures (Pl. II-2). Phlogopite phenocrysts are also fractured, and are altered along the fractures to darker brown biotite (Pl. IV-7). Mica is present in two generations: euhedral zoned phlogopite phenocrysts associated with pyroxenes (pre-albitic), and anhedral biotite patches in the fractures transecting the groundmass (post-albitic). Epidote crystals scattered throughout the groundmass and in the fractures of early minerals might possibly be an alteration product of more calcic plagioclase. The early phlogopite has been slightly altered to chlorite and biotite during the late stages of crystallization.

10. *Schist and Hybrid Gneiss cut by Pegmatite Granite.* Coarse books of green mica, about 6 inches in diameter, contain small adhering fragments of purple fluorite and apatite.

11. *Orebody.* This rock consists of coarse-grained biotite, green pyroxene, albite, reddish microcline, perthite, and quartz with accessory allanite, uraninite, and uranothorite. Compact (*11*) and blistered (*11Bl*) biotites were concentrated for chemical analysis.

12. *Hornblende-Biotite Gneiss.* Brown biotite, green hornblende, magnetite, and apatite with interstitial quartz and myrmekite occur in roughly parallel bands. Light bands consist of coarse-grained, fractured, poikilitic antiperthite, perthite, and quartz, which display porphyroblastic growths. Fractures in porphyroblastic crystals are healed by their further growth and can be distinguished by rows of black minute inclusions. Oligoclase-antiperthite porphyroblasts push aside and in part replace larger biotite crystals (Pl. II-3), and include small biotite laths, suggesting their growth after crystallization of biotite. Biotite is also partly replaced by quartz, which enters into (001) fractures of the biotite, forming graphic intergrowths with it. Biotite

in dark bands replaces hornblende and transects some of the magnetite crystals, and is replaced by apatite. The mode of occurrence of biotite in this rock indicates that it continued to grow after crystallization of hornblende and magnetite, and was succeeded by porphyroblastic growth of feldspars and by crystallization of late quartz. The type of perthite and antiperthite resembles that of granodiorite *19* (Pl. V-7). Antiperthite is only slightly altered to sericite in areas adjacent to late quartz.

13. *Pegmatitic Segregations in Skarn.* Coarse-grained brown biotite with calcite specks along (001) cleavage planes occurs in pegmatitic segregations in skarn. Calcite is associated with violet fluorite and red syenite that carries uraninite.

14. *Inclusion in Granodiorite, Rock-Unit 9.* The mafic-rich inclusion is composed of a medium- to coarse-grained mosaic of impure, poikilitic plagioclase, hornblende, and biotite, with numerous inclusions of epidote, sphene, apatite, microcline, and quartz (Pls. VI-4 and II-4).

15. *Biotite-Muscovite Paragneiss.* Muscovite and reddish brown biotite *15* occur in roughly parallel flakes in a medium-grained mosaic of quartz, microcline, and albite. Biotite is 'pushed aside' by quartz and is in part replaced by muscovite, magnetite, and apatite (Pl. IX-8). Late microcline and myrmekite replace both muscovite and biotite.

16. *Biotite Granodiorite* displays a hybrid appearance. It is composed of coarse impure plagioclase and microcline crystals with interstitial patches of ferromagnesian minerals, resembling in texture partly resorbed mafic-rich inclusions, which are surrounded by a fine-grained mosaic of dusty quartz, feldspar, and minor biotite. Plagioclase (An_{44-10})[1] occurs in zoned, broken crystals and in composite aggregates, which are healed and overgrown with sodic feldspar. Mafic patches are composed of subhedral hornblende, coarse anhedral poikilitic biotite with inclusions of apatite, and of fine-grained, green biotite, which occurs in patches with apatite, epidote, and sphene (Pl. VI-5). Some calcic zones in plagioclase are altered to coarse-grained sericite.

17. *Hornblende-Biotite Granodiorite, Rock-Unit 10.* This rock is composed of medium-grained intergrowths of hornblende, biotite, microcline, quartz, sphene, epidote, and apatite, which surround relatively coarse impure plagioclase crystals (Pl. VI-8). Plagioclase crystals are composite and zoned (An_{43-5}) (Pl. VI-9). They contain inclusions of apatite and muscovite. The distribution of biotite and of other mafic minerals is reasonably uniform throughout the rock.

18. *Hornblende-Biotite Gneiss.* Mafic minerals—olive-green biotite, blue-green hornblende, coarse-grained apatite, epidote, allanite, and minorsphene—occur in roughly parallel bands and streaks. Light bands are composed mainly of coarse- and fine-grained quartz, some poikilitic albite, and minor interstitial microcline. Biotite is partly resorbed and replaced by quartz, albite, apatite, allanite, and epidote. Long biotite laths are rimmed with thin films of impure potassium feldspar (Pl. IX-2). Some poikilitic albite crystals contain euhedral inclusions of epidote, rounded grains of quartz, mica flakes, and a few patches of potassium feldspar (Pl. IX-3).

[1]Maximum and minimum anorthite content, as determined by optical methods. Intermediate compositions are also present.

19. *Granodiorite.* Biotite (*ca* 10%) occurs in partly resorbed laths and is associated with altered remnants of greenish blue amphibole (Pl. V-5). Biotite is in part replaced by potassium feldspar, either at the ends or along the margins and (001) fractures (Pl. V-6). Microcline also replaces oligoclase along the twinning planes and fractures, and forms thin crusts surrounding earlier minerals (Pl. V-7). Some fractures are coated with orange-yellow crusts. The mode of replacement of plagioclase and biotite by potassium feldspar, and almost complete resorption of amphibole indicate potassium metasomatism.

20. *Biotite Paragneiss.* Red-brown shredded biotite occurs in partly resorbed flakes, which surround coarse-grained plagioclase and quartz. Bunches and streaks of biotite are engulfed by cloudy, cataclastic and recrystallized quartz, plagioclase, and fresh microcline. Biotite contains acicular inclusions and opaque fine-grained rims along fractures and margins (Pl. IX-9). Acicular inclusions (Pl. III-2), dark rims that are composed mainly of sphene and hematite, and chlorite are alteration products of biotite.

Biotite was formed early, but was later deformed, pushed aside by growing minerals (mainly plagioclase), and partly resorbed. Still later, as a result of hydrothermal action, it was altered in part to chlorite, hematite, and sphene. The evidence of this later alteration is provided by the black rims formed along the margins of already resorbed, ragged flakes. Plagioclase is slightly antiperthitic, and clouded by small opaque specks and white mica.

21. *Hornblende-Biotite Porphyroblastic Gneiss.* Small, roughly parallel flakes of brown biotite and remnants of hornblende occur in irregular, roughly parallel mafic streaks. Light minerals consist of coarse porphyroblastic oligoclase, potassium feldspar and strained quartz, fine-grained interstitial quartz-plagioclase, amoeboid poorly-twinned microcline, and minor myrmekite. Porphyroblastic feldspars 'push aside' and in part replace hornblende and biotite (Pl. IX-4). Biotite is also replaced by very coarse grains of apatite and allanite (Pl. IX-5).

22. *Porphyritic (Microcline) Quartz Monzonite, Rock-Unit 11, Elevation 8,000'.* Biotite occurs in interstices of feldspars and also in coarse porphyroblasts of microcline, which engulf small crystals of plagioclase and biotite (Pl. VII-1). Plagioclase crystals (An_{32-7}) are zoned and composite, consisting of altered cores and clear albitic and myrmekitic rims that spread into the microcline. Microcline is perthitic along the grain boundaries (Pl. VII-2). Large areas consist of strained anhedral quartz. Biotite crystals are associated with apatite, sphene, and allanite that is rimmed by epidote. Locally, biotite alters to chlorite and muscovite (Pl. VII-3) and displays a colour-zoning. It is brown in the core and becomes green towards the periphery.

23. *Porphyritic Quartz Monzonite, Rock-Unit 11, Elevation 4,500'.* This rock resembles in texture and mineral composition quartz monzonite *22*, but contains more myrmekite and consists of less altered minerals. Myrmekitic edges of plagioclase invade biotite and microcline (Pl. VII-4). In areas adjacent to myrmekite, biotite is partly replaced by quartz, which enters into (001) fractures.

24. *Biotite-Quartz-Feldspar Veined Gneiss.* Biotite occurs in roughly parallel dark streaks, in interstices of feldspar and quartz, and as partly resorbed inclusions

in quartz. This rock displays cataclastic, poikilitic, and micropegmatitic textures. Quartz is strained, fractured, and full of minute opaque grains. Fractures are filled with secondary quartz, microcline, and myrmekite. Biotite is in part replaced by plagioclase, microcline, apatite, epidote, and allanite, and by minor chlorite and sphene (Pl. IX-6).

25. *Medium-grained Quartz Monzonite, Rock-Unit 14, Elevation 7,500'.* This rock-unit is located in the northwestern part of rock-unit 10 and is surrounded by the mafic-rich granodiorites of rock-units 9 and 10. Quartz monzonite contains more quartz than the granodiorite, and in some features resembles the rocks of rock-units 9, 10, and 11. Zoned plagioclase crystals (An_{40-0}) are altered in varying degrees to saussurite and muscovite (Pl. VII-6), thus resembling in composition and mode of alteration those of granodiorite *21*. Biotite occurs in disseminated flakes throughout the rock. It varies in colour from olive-brown to greenish, and contains numerous inclusions of apatite, epidote, and sphene, which are also common in mafic-rich granodiorites. However, coarse anhedral patches of microcline with engulfed plagioclase crystals, and abundant quartz-alkali feldspar intergrowths that invade and replace other minerals, including biotite, resemble those observed in quartz monzonite *23*.

26. *Anorthositic Gabbro.* The rock consists of subhedral coarse plagioclase (*ca* 65%) and of interstitial patches of ferromagnesian minerals (*ca* 30%). Coarse-grained massive apatite, sphene, and opaque minerals occur in large fractures and interstices. Small fractures are filled with potassium feldspar and quartz. Plagioclase displays signs of resorption and further growths, changing in composition from labradorite to oligoclase (Pl. V-1). Pyroxene is replaced by green and brown hornblende, which is further replaced by anhedral patches of biotite (Pl. V-2). Biotite is the latest ferromagnesian silicate in the sequence of crystallization.

27. *Biotite-Cordierite Schist.* Roughly parallel streaks of orange-red biotite are interbanded with quartz-microcline-cordierite and plagioclase layers. Cordierite is poikilitic and contains rounded inclusions of quartz, apatite, and biotite, and small specks of zircon surrounded by zoned, isotropic haloes. Cordierite is isotropic along the fractures. It replaces biotite and locally alters to secondary colourless mica (Pl. IX-7). Biotite contains minute specks of zircon surrounded by dark brown pleochroic haloes. Biotite flakes adjacent to altered cordierite are slightly altered to chlorite. The presence of secondary hydrous silicates suggests superimposed mild hydrothermal alteration of this rock.

28. *Quartz Monzonite.* The same as specimen *1*.

29. *Quartz Monzonite.* This rock displays a seriate amoeboidal texture and is composed of coarse-grained plagioclase (Pl. VII-9), checkerboard albite, strained quartz, orthoclase, microcline perthite, biotite, and hornblende, with interstitial fine-grained quartz, microcline, and myrmekite (Pl. VIII-1). Hornblende and biotite occur in small groups and are partly replaced by quartz and microcline of the mesostasis. Biotite is poikilitic. It contains numerous inclusions of apatite and sphene, and locally displays micrographic intergrowths with potassium feldspar (Pl. VIII-2). Calcic cores of plagioclase are altered to saussurite and sericite. Albitic and myrmekitic rims invade earlier orthoclase. All primary minerals are altered in varying degrees, and partly

replaced by deuteric minerals. Coarse anhedral perthitic patches of microcline with engulfed plagioclase and biotite, thin microcline rims bordering quartz, and the poikilitic character of biotite suggest metasomatic growth of potassium-bearing minerals.

30. *Gneissic Quartz Monzonite.* This rock displays heterogeneous distribution of mafic minerals and cataclastic seriate texture. Coarse-grained andesine and orthoclase are fractured and include broken fragments of mesostasis. Fractures are filled with microcline, strained quartz, partly decomposed ferromagnesian minerals (remnants of hornblende and biotite), coarse-grained epidote, apatite, and sphene. Ferromagnesian minerals are 'pushed aside' into interstices and occur in discontinuous bands, which gives the gneissic appearance to the rock. Mafic-rich zones consist of hornblende, biotite, apatite, sphene, opaque grains, and interstitial microcline, quartz, and poikilitic checkerboard albite. Biotite occurs in coarse, roughly parallel laths (Pl. VIII-3). Locally brown biotite laths recrystallize into an aggregate of reddish brown flakes, which occur in bunches and replace hornblende. Small anhedral specks of biotite and hornblende are scattered throughout the fractured areas of the rock (Pl. VIII-4).

31. *Radioactive Syenite Pegmatite.* Coarse-grained, massive, bent biotite *31* is intergrown with reddish pink microcline and altered to orange-yellow mica *31a* along the fractures. The properties of green and altered orange-yellow mica are given in Table II. Syenite pegmatite also contains tourmaline, uraninite, and thorianite.

32. *Granodiorite* (*Granite*). This rock is composed chiefly of alkali feldspar and quartz (total about 95%), with a small amount of biotite scattered in small groups. Alkali feldspar consists mainly of a patchy mixture of potassium feldspar and albite, perthite, and antiperthite. Some feldspar crystals resemble in appearance patchy plagioclase of associated anorthosite gabbro *26* (Pl. V-3; compare Pl. V-1). Biotite is partly resorbed and replaced by alkali feldspar and quartz, which suggests its early crystallization. Biotite varies in colour from reddish brown to greenish and alters along (001) fractures to hematite, chlorite, and minor muscovite (Pl. V-4). These alteration products were formed during the latest stages of crystallization. Feldspars are locally sericitized and contain scattered aggregates and small crystals of epidote, hematite, apatite, and sphene, which indicate an alteration of the original more calcic plagioclase and of former ferromagnesian minerals. A comparison of mineral assemblages and textures of anorthositic gabbro *26* and granite *32* suggests that the granitic material is a residual differentiate of anorthositic gabbro *26*. The biotite is the only FeMg mineral that is present in appreciable quantities in both rocks and shows a definite trend in chemical differentiation (*see* Chapter V). The nature of alteration of biotite in granite to hematite and to hydrous silicates, chlorite, and muscovite is in agreement with the experimental data of Eugster and Wones (1962, Fig. 4) and can be attributed to increasing oxygen pressure. They found that with increasing oxygen pressure, iron-rich biotite decomposes to sanidine + hematite + vapour. In the case of this granite, oxidation of biotite is indicated by a variable greenish colour and by the following alteration products: hematite, muscovite, and chlorite. The latter two crystallize instead of sanidine + vapour + some hematite.

33. *Quartz Monzonite.* This coarse-grained rock is a product of a residual granitic magma and consists of sodic plagioclase, antiperthite, perthite, microcline, quartz, biotite, and fluorite. The biotite is coarse-grained, brown to opaque along fractures and around inclusions of allanite, sphene, apatite, and chalcopyrite. It occurs in small groups and contains narrow reaction rims of epidote and chlorite at the contact with perthite. In areas adjacent to fluorite, biotite is in part replaced by subhedral to euhedral quartz and anhedral microcline (Pl. III-3). Fluorite occurs in interstices and in fractures of biotite. It succeeded quartz in the sequence of crystallization. Most of the plagioclase crystals, particularly those enclosed in quartz and those adjacent to fluorite and rock fractures, are altered to an aggregate of sericite and minor epidote. The nature of alteration is greisenization and sericitization. All feldspars are peppered with minute red iron oxides.

34. *Anorthosite.* Coarse patches of orange-brown phlogopite occur at the contact between ilmenite and plagioclase (Pl. IV-3). Plagioclase, commonly labradorite, is fractured and locally replaced by oligoclase along the fractures. Phlogopite is post-plagioclase and pre-ilmenite-hematite. Alteration products of plagioclase, phlogopite, and ore minerals include zeolites, sapphirine, and chlorite.

35. *Lamprophyre.* Phlogopite occurs as large, zoned euhedral phenocrysts and as coarse, slightly flexed laths in a groundmass of medium-grained pyroxene, feldspar, and fibrous amphibole (Pl. IV-9). Phlogopite crystals, and inclusions of apatite and sphene in phlogopite, are rimmed with dark-brown to black iron-rich biotite, which indicates changes in chemical composition during the later stages of crystallization. Locally, phlogopite is replaced by fine-grained fibrous amphibole.

36. *Porphyritic Basalt.* Mica occurs in two generations: early coarse-grained phenocrysts of phlogopite *36Ph*, which are associated with augite, and late fine-grained flakes of biotite *36B* in the groundmass (Pl. IV-4). The phlogopite phenocrysts are subhedral, ragged, bent, and in part recrystallized to scaly aggregates (Pl. IV-5); some of them contain numerous inclusions of anhedral quartz between (001) sheets (Pl. IV-6), and opaque specks. The fine-grained biotite in the matrix is relatively fresh and is associated with pigeonite. The rock is traversed by fractures, which are filled with fibrous chloritic material. The early phlogopite phenocrysts were apparently unstable during crystallization of the groundmass and were further altered during the deuteric stage.

37. *Picrite.* Red-brown biotite occurs in coarse anhedral patches surrounding sulphides in a groundmass of altered olivine and pyroxenes (Pl. IV-1). The picrite is severely altered to serpentine. Serpentine partly replaces biotite along the edges. Biotite contains numerous inclusions of sulphides, particularly along (001) fractures, and crenulated veinlets of serpentine transecting the entire flake (Pl. IV-2). Biotite crystallized after olivine and pyroxenes and was succeeded by sulphides and serpentine.

38. *Radioactive Orebody.* The rock is composed of coarse-grained anhedral microcline that includes subhedral albite, green pyroxene, biotite, apatite, euhedral zoned zircon, allanite, sphene, uraninite, and uranothorite. Biotite is blistered and split along (001) fractures (Pl. I-6), and readily crumbles. It displays γ, β pleochroism, perhaps due to displacement of iron from the octahedral positions, and is surrounded

by a thin rim of minute specks of hematite, which apparently were removed from the mica (Pl. VIII-8). Uraninite commonly occurs as euhedral crystals and as small rounded grains in uranothorite and in biotite (Pl. VIII-9). Uraninite produces distinct pleochroic haloes in biotite, and causes fracturing of the surrounding minerals as a result of its radioactivity. Uranothorite is heterogeneous, semitranslucent brownish, filled with minute opaque specks. Zircon consists of concentric alternating anisotropic and isotropic zones. Two concentrates were analyzed by means of the X-ray spectrograph—relatively compact biotite *38c*, and blistered biotite *38Bl*. Radioactive minerals were identified in autoradiographs that were prepared employing the procedure devised by Robinson (1952).

39. *Mafic-rich Inclusion in Granodiorite* resembles specimen *14*.

40. *Biotite Granodiorite* resembles in texture granodiorite *16*, but all minerals are coarser and cleaner. Plagioclase crystals are zoned (An_{34-8}) and display altered cores (Pl. VI-6) and myrmekitic edges, which spread into microcline. Microcline is slightly perthitic and contains partly resorbed inclusions of zoned plagioclase. Coarse-grained biotite contains numerous prisms of apatite and is associated with hornblende, coarse epidote, and sphene. Biotite is also present in irregular interstitial patches that suggest porphyroblastic growth at the expense of the former small flakes (Pl. VI-7).

41. *Leuco Quartz Monzonite, Rock-Unit 12, Elevation 5,000'*. The leuco quartz monzonite resembles in texture and mineral composition the surrounding rock of unit 11. It is composed of abundant, very coarse poikilitic crystals of microcline, strained quartz, plagioclase, and plentiful biotite and muscovite. Biotite *41B* is present in small groups and is partly replaced by later muscovite *41M* (Pl. VII-5) and minor chlorite. Plagioclase is zoned (An_{25-13}) and rimmed by albite and myrmekite that spreads into microcline (Pl. VII-6). Some of the plagioclase crystals are almost entirely replaced by fine-grained muscovite. The main difference between this rock (unit 12) and the surrounding rock of unit 11 is its higher acidity and greater abundance of hydrous silicates, especially muscovite.

42. *Granodiorite*. This rock is composed essentially of the same minerals as those in granodiorite *43*, but contains more secondary unstrained quartz in coarse-grained patches and veinlets, and less microcline and mica. It contains chiefly antiperthite, instead of perthite, and some chlorite, which was not observed in thin section of granodiorite *43*. Plagioclase is only slightly altered to sericite and zoisite. Biotite *42B* and muscovite *42M*, totalling *ca* 2%, are scattered throughout the rock. Coarse-grained muscovite is slightly flexed. Most of the biotite flakes are composite, consisting of recrystallized areas (Pl. VI-1) and are locally replaced by chlorite with minor muscovite, quartz, potassium feldspar, and iron oxides (Pl. VI-2, 3). Brown biotite alters through green biotite to bright green chlorite with minor hematite, muscovite, and potassium feldspar. This type of alteration is a result of oxidation, already discussed in sample *32*, and deficiency of potassium, which aided in the formation of chlorite from the biotite. Both granodiorites *42* and *43* contain hydrous alteration products and were affected by hydrothermal alteration under different concentrations of alkalis. Granodiorite *43*, with abundant sericite and recrystallized biotite, contained plentiful potas-

sium. Granodiorite *42*, with predominant hydrous alteration product chlorite, indicates a deficiency in potassium at the final stage of alteration.

43. *Granodiorite.* The mineral constituents of this rock in approximate order of crystallization are: (1) plagioclase and coarse-grained biotite (*43BI*); (2) coarse-grained muscovite (*43MI*); (3) microcline and microcline perthite with engulfed, partly resorbed plagioclase crystals; (4) coarse-grained (strained) quartz; and (5) myrmekite. Secondary minerals include: in part myrmekite, which forms along the edges of plagioclase adjacent to microcline; fine-grained biotite (*43BII*) and iron oxides; aggregates of recrystallized muscovite; micrographic muscovite-quartz intergrowths (*43MII*); fine-grained muscovite and epidote (resulting from saussuritization and sericitization of plagioclase); secondary quartz; secondary potassium feldspar; and sericite as fracture fillings transecting older minerals. Coarse-grained biotite is present in anhedral laths and patches, which are transected by coarse muscovite and rimmed by fringes of sericite. Adjacent to muscovite, biotite recrystallizes to an aggregate of iron oxides and fine-grained biotite (Pl. V-8). Small flakes of euhedral biotite with some iron oxides and rutile can be observed along the fractures of some coarse biotite flakes (Pl. V-9). Optical properties of primary, coarse-grained, and secondary, fine-grained biotite and muscovite are given in Table II. Refractive indices indicate that secondary biotite and muscovite are somewhat enriched in iron. Mode of alteration of this rock indicates high mobility of potassium. The original biotite was apparently unstable under these conditions and partly recrystallized to the iron-rich variety.

Chapter V

RELATIONS BETWEEN PETROLOGY AND CHEMICAL COMPOSITION OF MICAS

In the previous chapters, the micas and their host rocks examined for this report were listed in approximate order of increasing iron content in the octahedral sites of the micas. In this chapter, however, it is more convenient to discuss them in relation to the origin and type of the rock and associated minerals in the following order:

1. Basic igneous rocks: picrite *37**, anorthosite *34*, porphyritic basalt *36*, lamprophyres *9* and *35*.
2. Anorthositic gabbro *26* and associated granodiorite (granite) *32*.
3. Granodiorites *16*, *39*, *40*, *14*, *17* and associated quartz monzonites *22*, *23*, *25*, *41*, (*1M*, *28B*).
4. Granodiorites *19*, *42*, *43*; quartz monzonites *29*, *30*, *33*, *2*; and syenite pegmatite *31*.
5. Skarn rocks *3*, *4*, *6*, *7*; related rocks *10* and *13*; and radioactive orebodies *11* and *38*.
6. Metamorphic rocks: metamorphosed argillitic limestone *5*; pyroxene-hornblende-biotite gneiss *8*; hornblende-biotite gneisses *12*, *18*, *21*; biotite gneiss *24*; paragneisses *15* and *20*; and cordierite schist *27*.

Rock Type and Sequence of Crystallization

Basic Igneous Rocks

In the basic igneous rocks picrite and anorthosite, phlogopite is associated with sulphides and ilmenite-hematite. It occurs relatively late in the sequence of crystallization of silicates and is succeeded by the ore minerals. In anorthositic gabbro from the Mount Megantic igneous complex in southern Quebec, biotite is the latest ferromagnesian silicate. Porphyritic basalt *36* and lamprophyre *9* contain two paragenetically different micas: early phlogopite, and late biotite. Lamprophyre *35* is composed of abundant zoned phlogopite, which is rimmed with dark iron-rich biotite. Because it was not possible to obtain a sufficient quantity of clean micas for a complete chemical analysis, eight of these concentrates were analyzed with the X-ray spectrometer. Complete chemical analyses are available for two concentrates only: (1) the early phlogopite from lamprophyre *9*; and (2) the late biotite from anorthositic gabbro *26*.

*Number of specimen is the same as in Table I.

In order to show the difference between the chemical composition of an early mica, which represents the basic phase of magmatic crystallization, and that of the late mica, which represents more acidic, residual magma, two groups of micas will be compared: (1) phlogopites from picrite *37* and anorthosite *34*, early phlogopite from porphyritic basalt *36Ph* and lamprophyre *9Ph*, and phlogopite from lamprophyre *35*; (2) late biotites from porphyritic basalt *36B*, from lamprophyre *9B*, and from anorthositic gabbro *26*.

Results of this comparison are presented in Table IX.

Table IX

*Average Composition of Micas from Basic Igneous Rocks**

Specimens	Weight %							ppm					
	Total Fe as FeO	TiO_2	Cr_2O_3	MnO	K_2O	CaO	BaO	SrO	Rb_2O	Ga_2O_3	NiO	CuO	ZnO
Average (basic rocks) *37, 34, 36Ph, 9Ph, 35.*	8.0	3.5	0.45	0.06	8.6	0.57	0.40	108	505	36	1470	100	260
Average (basic rocks) Late mica *36B, 9B, 26.*	17.5	3.9	0.12	0.13	8.0	1.60	0.52	213	680	20	150	<50	330

*Averages calculated from XRS data, Table IV.

Some of the concentrates show erratic variations in quantities of CaO and of related oxides BaO and SrO, which can be accounted for by the presence of epidote inclusions. A few erratic values of CuO can be accounted for by the presence of sulphides.

A comparison between the phlogopites and the late biotites from basic igneous rocks (Table IX) shows the following general trend: iron content, manganese, zinc, and rubidium (and calcium, strontium, and barium) increase in late biotites, whereas chromium and nickel are more abundant in the phlogopites. A comparison between the early phlogopite and the late biotite from the same rock *36Ph*, *36B* and *9Ph*, *9B* (Fig. 16, *in pocket*) indicates very distinct differences in chemical composition between the early and late phases. In this connection, it is important to point out that the phlogopite concentrate was not entirely free from the late biotite flakes, and vice versa, and that some of the phlogopite crystals showed a distinct compositional zoning (Pl. II-1). Nevertheless, X-ray spectrographic analysis indicated 3 to 6 times the Cr_2O_3 content and 4 to 10 times the NiO content in the early phlogopite, and 2 to 9 times as much strontium, 1.5 to 2 times as much iron and manganese, and 2 to 5 times as much CaO in the late biotite. The variation in Rb_2O content is inconsistent: it is 4 times as much in the late biotite of sample *36* as in the phlogopite from the same rock, and it is slightly lower in biotite *9B* than in phlogopite *9Ph*. The variation in abundance of Rb and Sr in early and late micas from the same rock indicates the difference in geochemical behaviour of these elements, which might be significant in the interpretation of Rb-Sr ages. The obvious relation of Sr and Ca to the calcium-bearing mineral impurities might in part account for the inconsistency of Rb/Sr ratios in these micas.

The differences in chemical composition obtained on early and late micas from the same rock are similar to those recently published by Métais, Ravier and Phan-Kien-Duong (1962), who analyzed rimmed mica crystals from lamprophyres with the electron microprobe. They found the following proportional differences in chemical composition between the phlogopitic centre and the iron-rich border:

	Border	*Centre*
Si	16.4	18.4
Al	6.7	6.7
Mg	9.9	12.1
Fe	13.0	4.7
Ti	3.3	1.8
K	8.0	8.3
Cr	—	<1

Zoned and rimmed phlogopite crystals, described in the present study (Pls. II-1, IV-9), have also been submitted for electron microprobe analysis.

The complete chemical analysis and the structural formula of phlogopite *9* are presented in Tables III, VI, and VII. This phlogopite contains some octahedral alumina, moderate titanium and ferric iron, relatively low ferrous iron and manganese, high magnesium, relatively high chromium and nickel, relatively low fluorine, and a deficient (OH,F) group.

Partial dehydration of phlogopite and the development of iron-rich dark rims occurred, probably during crystallization of feathery alkali feldspar in the groundmass. Crystallization of late biotite in the fractures that transect the groundmass took place after consolidation of the lamprophyre during the late deuteric stage. At this stage, phlogopite phenocrysts became slightly altered to chlorite.

The present study of micas from certain basic rocks indicates that the chemical composition of such micas depends chiefly on their place in the sequence of crystallization and on the degree of magmatic differentiation. The early-formed micas are magnesium-rich phlogopites containing appreciable quantities of nickel and chromium, whereas the late micas, formed during the deuteric stage, are enriched in iron and manganese and contain much less nickel and chromium. Early-formed phlogopite phenocrysts can be affected during the crystallization of the (alkalic) groundmass (partial dehydration) and during the deuteric (hydrothermal) stage (chloritization).

Anorthositic Gabbro and Associated Granodiorite (Granite)

Anorthositic gabbro *26* and related granite *32* from the Mount Megantic complex show distinct textural similarities. The granite contains more abundant alkali feldspar and hydrous silicates. The biotite in the anorthositic gabbro is one of the latest ferromagnesian minerals, and in granite *32* it is the only primary, relatively fresh ferromagnesian silicate. A comparison of the chemical composition of micas from these related rocks (Tables III, IV, VI, and VII, and Fig. 16, *in pocket*) shows an interesting trend in chemical differentiation from the biotite of the anorthositic gabbro to the biotite of the granite: total iron content, zinc, silica, and the octahedral alumina slightly increase; ferric iron increases about two times; manganese, rubidium, gallium, and fluorine increase about four to five times; sodium and magnesium decrease; calcium, barium, and strontium decrease about three times. The (OH,F) group is only

slightly deficient in the biotite from the granite, and it is much more deficient in the biotite from the anorthositic gabbro. It is important to note that the deficiency of the (OH,F) group in this case is not related to the quantity of the ferric iron of the biotite, and thus cannot be accounted for by the oxidation of ferrous iron at the expense of the (OH,F) group. Biotite *32* contains more ferric iron and shows less deficiency in the (OH,F) group than biotite *26*. Partial loss of the (OH,F) group from biotite *26* occurred, probably during crystallization of the granitic phase *32*, and oxidation of biotite *32* (after its crystallization), which is indicated by the distinct variation in colour and characteristic alteration products. On the basis of these observations, oxidation of ferrous iron and partial loss of the (OH,F) group seem to be separate and unrelated results of different types of alterations.

Granodiorites and Associated Quartz Monzonites

Granodiorites and quartz monzonites of the White Creek Batholith are related hybrid rocks, in part contaminated by inclusions of the country rock. They show evidences of thermal metamorphism and of alkali metasomatism. These rocks vary in texture, and in abundance of alkalic minerals and quartz. The abundance of mafic minerals decreases towards the centre of the batholith and secondary hydrous silicates (chloritization and sericitization) increase in samples collected at higher elevations.

Average chemical compositions of biotites from granodiorites *16*, *40*, *14*, *17*, and from quartz monzonites *22*, *23*, *41*, *25* are presented in Table X, columns 4 and 5.

The composition of the tetrahedral layer in biotites from granodiorites and from quartz monzonites is almost identical. The tetrahedral positions are filled with silica and alumina. Silica is slightly lower than in the "ideal" mica and a fairly high excess of alumina is placed into the octahedral layer.

Major components of the octahedral layer differ: aluminum, titanium, ferric and ferrous iron are higher in biotites from quartz monzonites, and magnesium is accordingly lower. However, the average ratios of ferric to ferrous iron are almost the same, thus indicating a proportionate increase of ferric iron with increasing ferrous iron and similar general oxidation conditions of the granodiorites and quartz monzonites. Chromium is low in both mica groups (<0.05). Nickel content is similar and low (*ca* 150 ppm). Average quantities of manganese, zinc, and gallium increase in biotites from quartz monzonites. Gallium increases more than two times; i.e., in a much greater proportion than the slightly increasing octahedral aluminum.

Potassium is the major constituent of the interlayer group and varies from 96% to 98%, depending on the sodium and calcium content. Calcium is twice as high in biotites from the granodiorites and shows erratic variations, depending on the quantity of apatite inclusions. Strontium varies with calcium, depending to a great extent on the presence of calcium-bearing inclusions. Average rubidium content is higher in micas from the quartz monzonites.

Biotite concentrates from different rock-units, and from rocks taken at different elevations of the same unit, show considerable variation, especially in the abundance of some minor alkali metals and volatiles. From chemical data summarized in Tables III, IV, VI, and VII, the following differences are of petrological interest.

1. Biotite *14* from the mafic inclusion in the granodiorite of rock-unit 10 shows a considerable deficiency in the (OH,F) group. It has the lowest quantity of ferric iron and also the lowest ratio of ferric to ferrous iron of all biotites of the batholith. Biotite *17* from the host granodiorite is in part altered to chlorite. It contains more ferric iron than the biotite from the inclusion, shows the highest ratio of ferric to ferrous iron, and contains an almost ideal (OH,F) group, after correcting the chemical formula for chlorite. Biotite *14* has the highest sodium and lowest total iron content of all the biotites of the batholith, thus indicating the most basic character of this biotite *14*. The deficiency in the (OH,F) group of biotite *14* is due to loss of water and hydrogen, probably as a result of elevated temperature of the host granodiorite *17*. The relatively high ratio of ferric to ferrous iron in biotite *17* seems to be related to chloritization of this mica.

2. Two biotite concentrates from quartz monzonite of rock-unit 11 show an interesting relationship between deficiency of the (OH,F) group (as well as minor alkali metals) and sampling elevation of the host rock. Biotite *23*, elevation 4,500 feet, contains higher sodium, less rubidium, less fluorine, and shows more distinct deficiency in the (OH,F) group than biotite *23*, elevation 8,000 feet. The degree of chloritization increases with increasing elevation, which indicates a decrease in temperature with increasing elevation, whereas the degree of dehydration increases with decreasing elevation, thus indicating a rise in temperature.

All biotites from quartz monzonites are to some extent altered to chlorite, and yet, after making proportionate corrections for chlorite, show considerable variation in deficiency of the (OH,F) group. This suggests that the process of dehydration (dry thermal alteration) must have preceded the process of hydrothermal alteration (chloritization).

3. Quartz monzonites of rock-units 12 and 14 also show some distinct differences. Biotite *25* from rock-unit 14, which is surrounded by granodiorite of rock-unit 10, has some features that are common to those of biotites from granodiorites, and others that are common to biotites from quartz monzonites. Biotite *25* contains relatively low zinc, gallium, and manganese, which are comparable to those of the biotites from granodiorites. Deficiency and composition of the (OH,F) group are similar to those of biotite *22*. Total iron content, however, is somewhat higher than in biotites *22* and *23*, and slightly lower than in biotite *41* of rock-unit 12.

4. Biotite *41* is associated with muscovite *41*. Complete chemical analyses of these micas are not available. A comparison of X-ray spectrographic analyses (Table IV) of this biotite *41* and of biotites *22*, *23*, and *25* shows that biotite *41* contains the highest total iron, titanium, manganese, rubidium, gallium, nickel, and zinc. A comparison of X-ray spectrographic analyses of biotite *41* and muscovite *41* shows that the muscovite contains ten times as much gallium, more strontium, and more potassium. Rubidium and all metals of the iron group are less abundant in the muscovite.

Complete chemical and X-ray spectrographic analyses of biotite *28* and muscovite *1* from quartz monzonite of the Fry Creek Batholith are presented in Tables III, IV, VI, and VII. A comparison of unit-cell contents of biotite *28* and biotite *25* shows that biotite *28* has similar composition of the tetrahedral layer, silica being somewhat

deficient, and alumina relatively high. The octahedral aluminum is twice as high, this feature being characteristic of all the biotites associated with muscovites. Ferrous iron and manganese are also higher. Ferric iron and the ratio of ferric to ferrous iron are lower. The (OH,F) group is filled. X-ray spectrographic analyses of biotite *28* and of biotite *41* (which is also associated with muscovite) indicate similar, relatively high quantities of total iron, titanium, manganese, zinc, gallium, and rubidium in these biotites.

A comparison of unit-cell contents of biotite *28* and muscovite *1* from the same quartz monzonite shows that the muscovite contains much more tetrahedral silica, and higher octahedral aluminum, ferric iron, potassium, sodium, gallium, and strontium, but much less ferrous iron and all metals of the iron group, and less zinc, barium, rubidium, and fluorine. Muscovite *28*, in comparison with muscovite *41*, contains slightly less rubidium, and much less zinc and nickel. The abundance of zinc and nickel in biotite *41* and muscovite *41* is a local characteristic feature of these related micas.

Granodiorites and Quartz Monzonites

Granodiorites and quartz monzonites from which mica was selected for the present study are from different parts of the Canadian Shield. Granodiorite *19* is from the Superior province, Quebec, 60 miles west of the Labrador Trough. Granodiorites *42* and *43* are from the District of Mackenzie, *ca* 1,500 miles west of specimen *19*, and were taken close to the boundary between the Bear and Slave provinces. All quartz monzonites are from the western Canadian Shield: *29* from the southwestern area of the Bear province; *30* and *33* from the Churchill province (*30* being *ca* 400 miles southeast of *29*, and *33* being *ca* 300 miles east of *30*).

In comparison with the average composition of biotites (*29*, *30*, and *33*) from quartz monzonites, biotite *19* from granodiorite contains a similar composition of the tetrahedral layer, but shows distinct differences in the contents of the octahedral layer (Table X, columns 6 and 7). Magnesium is twice as high, titanium is slightly higher, aluminum and ferric and ferrous iron are lower. Biotite *19* shows a slightly higher ratio of ferric to ferrous iron and has a more deficient (OH,F) group. Fluorine and sodium contents are similar. Average minor element content of biotites *19* and *42* in comparison to that of average biotites (*29*, *30*, and *33*) shows more nickel, rubidium, zinc, and gallium, and less calcium, barium, and titanium.

The difference between the chemical composition of Precambrian biotites from granodiorites and from quartz monzonites is more distinct than the difference between biotites from younger granodiorites and quartz monzonites (Table X, columns 4, 5, 6, and 7). The composition of the tetrahedral layer is almost the same in all biotites. Octahedral alumina and ferric iron are lower, and titanium is much higher, in biotites from Precambrian rocks. Ferrous iron is almost the same in biotite *19* and average biotites from younger granodiorites. However, average biotites from Precambrian quartz monzonites contain more ferrous iron and less magnesium than average biotites from younger quartz monzonites.

Individual biotite concentrates of the Precambrian granodiorites and quartz monzonites also show distinct variations in chemical composition. Biotite *19* shows

Table X

Chemical Composition of Micas from Various Rock Types and Mineral Assemblages

	Basic Rocks		Associated Gr.D. and Q-M.		Unrelated Gr.D. and Q-M.		Skarn	RA Ore	Lst. Gneiss	Pyrox. Gneiss	Gneiss	Para-gneiss	Biotite-Hornblende Rocks			Bio-Mus. Q-Monz.		B-F Q-M
	Early *9*	Late *26*	Gr.D. (Avg. 3)	Q-M. (Avg. 3)	Gr.D. *19*	Q-M. (Avg. 3)	(Avg. 4)	Avg.2 *11,11B*	*5*	*8*	Avg.2 *18,24*	Avg.2 *15,20*	Gr.D. (Avg. 4)	Q-M. (Avg. 2)	Gneiss (Avg. 3)	*B 28*	*M 1*	*33*
1	2	3	4	5	6	7	8	9	10	11	12	13	14	15	16	17	18	19
Tetrahedral layer (Cationic %)																		
Si	71.8	69.3	69.3	69.5	68.8	69.1	77.0	77.1	68.8	74.3	69.5	69.0	69.0	69.1	70.2	68.2	79.8	69.0
Al	28.2	30.7	30.7	30.5	31.2	30.9	21.2	22.0	31.2	25.5	30.5	31.0	31.0	30.9	29.8	31.8	20.2	31.0
Ti	—	—	—	—	—	—	0.4	0.8	—	0.2	—	—	—	—	—	—	—	—
Fe	—	—	—	—	—	—	1.4	0.1	—	—	—	—	—	—	—	—	—	—
Octahedral layer (Cationic %)																		
Al	4.8	0.7	6.0	6.9	2.8	3.8	—	—	8.65	—	6.9	12.2	4.4	3.6	2.4	12.6	89.6	4.2
Ti	2.9	8.3	3.6	5.6	8.4	7.4	0.4	0.6	0.96	2.1	5.0	6.5	6.0	7.4	6.2	5.4	0.3	7.3
Fe^{3+}	3.5	6.0	6.4	7.5	5.9	6.5	1.7	12.7	1.7	3.6	7.5	1.3	6.1	6.2	5.8	4.3	5.6	7.2
Fe^{2+}	13.8	43.0	35.2	40.0	35.3	57.2	6.1	23.0	2.5	14.4	39.2	39.7	35.3	52.6	34.9	51.2	1.5	67.4
Mg	72.8	41.0	48.4	39.2	47.1	23.8	91.9	55.4	86.1	78.9	40.7	40.0	48.3	29.4	50.4	24.7	3.0	12.6
ΣFe	17.3	49.0	41.6	47.5	41.2	63.7	7.80	35.8	4.2	18.0	46.7	41.0	41.4	58.8	40.7	55.5	7.1	74.6
ΣFeMe	22.4	57.7	45.6	53.9	50.9	72.4	8.2	37.8	5.3	21.1	52.3	47.6	47.1	67.0	47.1	62.5	7.4	83.2
Fe^{3+} /Ti	1.2	0.72	1.7	1.35	0.7	0.85	0.4	8.5	1.7	1.7	1.5	0.23	1.1	0.87	0.97	0.80	19.0	1.0
Fe^{3+} /Fe^{2+}	0.26	0.14	0.18	0.19	0.16	0.11	0.27	0.55	0.7	0.25	0.2	0.03	0.17	0.13	0.15	0.08	3.4	0.11
Interlayer (Cationic %)																		
K	89.7	90.4	95.7	98.4	96.8	95.8	87.1	93.5	91.3	90.0	98.7	95.5	96.9	94.4	96.6	98.1	89.4	98.6
(OH,F,O) Group (Anionic %)																		
(OH)	70.5	74.5	78.0	71.2	65.0	76.6	44.6	37.8	67.5	35.5	73.0	73.3	74.7	74.5	56.4	90.0	98.0	80.8
F	9.0	2.7	6.2	12.9	7.0	7.4	52.7	42.5	25.5	37.5	4.5	4.7	6.4	7.1	13.5	10.0	2.0	8.0
O	10.25	11.4	7.9	8.0	14.0	8.0	1.3	9.5	3.5	13.5	11.2	11.0	9.4	8.7	15.0	0.0	0.0	5.5
% Dehydration	20.5	22.8	15.8	15.9	28.0	16.0	2.6	19.0	7.0	27.0	22.5	22.0	18.8	17.4	30.1	0.0	0.0	11.2
*Oxides (XRF, weight % and ppm)**																		
Wt % FeO	8.0	17.5	18.6	21.6	20.0	27.1	3.8	16.1	2.0	8.6	20.3	18.9	18.5	26.0	17.5	23.9	2.0	29.3
Wt % Cr_2O_3	0.45	0.12	<0.05	<0.05	<0.05	<0.05	<0.05	<0.05	<0.05	0.25	0.05	0.05	<0.05	<0.05	<0.05	0.05	0.05	<0.05
ppm NiO	1470.	150.	150.	138.	300.	63.	200.	1250.	100.	1000.	100.	75.	120.	100.	150.	200.	50.	50.
Wt % TiO_2	3.5	3.0	1.65	2.65	2.0	3.77	0.47	1.15	0.90	1.20	2.50	2.10	2.4	4.0	3.2	2.8	0.65	3.3
Wt % MnO	0.06	0.13	0.37	0.53	0.38	0.40	0.10	0.40	0.05	0.05	0.27	0.22	0.32	0.35	0.27	0.70	0.05	0.50
ppm ZnO	260.	330.	450.	825.	820.	500.	475.	1270.	400.	150.	625.	500.	530.	350.	467.	1300.	50.	800.
ppm Ga_2O_3	36.	20.	25.	80.	90.	57.	40.	100.	30.	<20.	55.	35.	28.	40.	35.	110.	190.	90.
Alkali Metals (Weight % and ppm)																		
Wt % K_2O	8.6	8.0	8.9	8.8	8.5	8.4	9.8	9.1	10.4	9.2	9.6	9.4	9.1	8.4	9.3	9.2	9.8	8.3
Wt % Na_2O	0.55	0.27	0.10	0.06	0.13	0.11	0.50	0.12	0.34	0.40	0.05	0.1	0.11	0.12	0.12	0.2	0.76	<0.2
Wt % CaO	0.57	1.60	1.14	0.56	0.05	0.40	0.50	0.70	0.40	0.55	0.12	0.25	0.92	0.50	0.15	0.30	0.05	0.20
Wt % BaO	0.40	0.52	0.16	0.19	0.15	0.39	0.14	0.10	0.25	0.20	0.15	0.17	0.14	0.52	0.20	0.10	<0.05	0.10
ppm SrO	108.	213.	18.	<10.	15.	16.	30.	<10.	70.	60.	10.	10.	18.	20.	10.	50.	<10.	10.
ppm Rb_2O	505.	680.	681.	1006.	1675.	900.	1010.	6000.	570.	850.	505.	612.	635.	750.	703.	1125.	775.	1200.

*These are the average figures and include XRF analyses of additional micas from similar rocks (analyses of individual concentrates are given in Tables III and IV).

relatively high deficiency of the (OH,F) group, which can be accounted for by its partial dehydration during replacement by feldspar (Pl. V-5, 6). X-ray spectographic analysis of biotites *19* and *42* indicates the following differences: biotite *42*, which is associated with muscovite *42*, contains more total iron; almost twice as much manganese; five times as much rubidium and gallium; and ten times as much nickel; whereas titanium and barium are ten times as low. Biotite *42* is altered and in part recrystallized. Some of these differences in chemical composition can be accounted for by loss of titanium (as indicated by decoloration and chloritization). Relatively high content of iron, manganese, rubidium, and gallium may possibly be a result of recrystallization in granitic environment. Manganese, nickel, gallium, and rubidium content of biotite *42* is similar to that of biotite *41* and, to some extent, biotite *28* of younger, muscovite-bearing quartz monzonites. Because of the small quantity of concentrate, X-ray spectographic analysis of biotite *42* was performed on a heterogeneous sample. Separate analyses of each biotite type of this concentrate *42* would give more conclusive data on the behaviour of different constituents during metamorphic processes.

Muscovite *42* contains much less total iron and manganese, slightly less rubidium and zinc, and more potassium and gallium than biotite *42*. In comparison with X-ray spectrographic analysis of other muscovites (Table IV), muscovite *42* contains similar quantities of potassium, calcium, and barium; higher total iron, rubidium, gallium, nickel, and zinc; and less manganese.

Biotites *29* and *33* from Precambrian quartz monzonites in general are similar in chemical composition. Biotite *33* from fluorite-bearing quartz monzonite contains more ferrous iron, manganese, and titanium. Manganese and ferric iron contents of these biotites (*29* and *33*) are comparable to those of average biotites from quartz monzonites from the White Creek Batholith, and relatively high total iron, rubidium, and gallium contents are almost the same as in biotite *32* from Mount Megantic granite.

Biotite *30* is in part recrystallized and, although it contains relatively high total iron, shows some significant differences, and in some features resembles biotites from more basic rocks. Biotite *30* contains relatively high titanium, barium, and strontium, comparable to those of biotite *26* from anorthositic gabbro of Mount Megantic, and relatively low manganese and rubidium. It contains relatively low ferric iron and a deficient (OH,F) group.

Muscovite *2* from Precambrian quartz monzonite from the south shore of Great Slave Lake is similar in composition to muscovite *1* from younger quartz monzonite of the Fry Creek Batholith. Muscovite *2*, which replaces altered biotite (Pl. VIII-5, 7), contains slightly more titanium, as well as more ferric and ferrous iron. Trace element content of these muscovites (*1* and *2*) is almost the same.

Biotite *31* from syenite pegmatite, Bancroft area, contains the following: high iron, comparable to that of average biotites from quartz monzonites; about twice as much manganese and ferric iron as in average biotites from quartz monzonites; relatively high copper and nickel; and relatively low titanium, barium, strontium, and rubidium. The deficiency in the (OH,F) group and the fluorine content are slightly less than those in biotites from Precambrian quartz monzonites. The most outstanding feature of biotite *31* from syenite pegmatite is its low silica content, high manganese

content, and relatively high ferric iron content, the ratio of ferric to ferrous iron being 0.29.

Skarn Rocks and Radioactive Orebodies

Micas from skarn, from related rocks, and from radioactive orebodies of the Bancroft area show some similarities and will be discussed together.

Phlogopites *3* and *4* are associated with diopside and occur in marbles. Phlogopite *6* occurs in green pyroxene in skarn, which is composed of pyroxene, scapolite and calcite. Phlogopite *7* is associated with pale greenish diopside that occurs in calcite-scapolite rock. Average composition of these four phlogopites is presented in Table X, column 8. Characteristic features of these phlogopites are: a slight excess of tetrahedral silica (77%), and deficient alumina, which is insufficient to fill the tetrahedral positions; very low titanium and low iron, some of which are placed to fill the tetrahedral positions. The ratio of tetrahedral silica to alumina is 3.6 to 1; i.e., higher than in the 'ideal' mica, 3 to 1. Average magnesium content is very high, *ca* 92% of the octahedral layer, and approximately one half of the (OH,F) group is filled with fluorine. The ratio of the octahedral ferric to ferrous iron is relatively high, and it is to some extent distorted because some iron is placed into the tetrahedral positions. The octahedral layer of these phlogopites carries a negative charge (Fig. 5, *in pocket*). Potassium and sodium contents are relatively high, and rubidium content moderate, comparable to those of biotites from granitic rocks. Phlogopites *3* and *4* contain very low iron and manganese, and relatively high sodium. Calcium shows distinct variations, which may be accounted for by the presence of calcite and apatite impurities. Zinc and manganese increase with increasing iron content. Phlogopite *7* contains very high fluorine. High fluorine content is the distinctive property of metasomatic micas.

Biotite *10* from schist and hybrid gneiss contains more iron, manganese, and rubidium, and less magnesium, but in other features resembles phlogopites *6* and *7* from the skarn.

Biotite *13* from pegmatitic segregations in skarn contains slightly deficient silica and alumina, which are too low to fill the available tetrahedral sites. The ratio of silica to alumina is 3.1 to 1, almost that of the ideal mica (3 to 1). Iron, titanium, and barium contents are slightly higher than in biotite *10*. Relatively high rubidium and zinc are almost the same as in biotite *10*. Manganese content is comparable to that of biotite *10* and to average biotites from quartz monzonites. Biotite *13* has a deficient (OH,F) group.

Biotites *10* and *13*, in some features, resemble phlogopites from marbles and, in others, resemble biotites from silicate rocks.

Biotites from the radioactive orebodies *11* and *38* show extreme variations in physical properties, in some cases within a single flake; some are compact, others are blistered (Pl. I-6). They vary in the degree of pleochroism and in the magnitude of the optic angles. Chemical analyses of blistered and compact portions of biotite (*11Bl* and *11C*) indicate small differences in chemical composition: alumina, potassium, and lithium are slightly higher in the compact biotite, whereas constitutional water and ferric iron are somewhat higher in the blistered biotite. Compact biotite contains a more deficient (OH,F) group. Other major constituents are almost identical.

X-ray spectrographic analysis of blistered and compact portions of biotites *11* and *38* indicates slightly higher iron, zinc, and calcium, and slightly lower nickel content in biotite *38*. Average unit-cell contents of biotites *11C* and *11Bl*, and average minor element contents of biotites *11* and *38* are shown in Table X, column 9. The composition of the tetrahedral layer, the deficiency of alumina and excess of fluorine in biotites from the radioactive orebodies are very similar to those of biotites from skarns (Table X, column 8). Biotites from the orebodies contain more total iron and rubidium, and less magnesium; they have a very high ratio (0.55) of ferric to ferrous iron; they contain relatively high quantities of alkali metals (rubidium, lithium, and cesium); and they contain titanium, manganese, and zinc comparable to the content of biotites *10* and *13*.

General common features of micas from skarns and from associated pegmatites, radioactive orebodies, and schists are: deficient alumina, relatively high fluorine, and very low chromium. The octahedral layer of phlogopites from iron-poor marbles is composed chiefly of magnesium (*ca* 98%). These phlogopites contain relatively high strontium, very low titanium, low nickel, zinc, and gallium. Biotites from the radioactive orebodies are very complex in chemical composition, and, in addition to common constituents, contain appreciable quantities of rubidium, lithium, and cesium. Biotites *11* and *38* contain relatively high nickel, comparable to that of early phlogopites from basic rocks, relatively high gallium and zinc, and very low strontium. It can be pointed out that high gallium content in the biotites from radioactive orebodies does not bear any direct relationship to the alumina content that was observed in the biotites from muscovite-bearing granodiorites and quartz monzonites. An increase in gallium content with increasing alumina is even more distinct in the muscovites than in associated biotites, which suggests a close geochemical relationship between these two elements. However, the biotites from radioactive orebodies, which show distinct metasomatic features, indicate an independent variation in the abundance of gallium and aluminum.

Gneisses and Schists

Phlogopite *5* from metamorphosed argillitic limestone of the Grenville subprovince, north of Hull, Quebec, differs from phlogopites from the skarn of the Bancroft area, chiefly by its high alumina content and about half the amount of fluorine and rubidium (Table X, column 10).

Phlogopite *8* from pyroxenite gneiss of the Churchill province, Labrador, resembles, in some chemical features, phlogopites from basic rocks and, in others, those from metasomatic skarns. The composition of the tetrahedral group is almost that of the ideal mica. Ferric and ferrous iron, magnesium, chromium, nickel, and titanium contents are comparable to those of phlogopite *9* from lamprophyre and to other phlogopites from basic rocks, while relatively high fluorine content is comparable to that of metasomatic phlogopites. The (OH,F) group is deficient.

Biotites *18* and *24* from gneisses of the Churchill province in northern and eastern Labrador are similar in chemical composition. Average composition of these biotites, presented in Table X, column 12, is very similar to that of biotites from quartz monzonites of the White Creek Batholith (Table X, column 5). Composition of the tetra-

hedral and octahedral layers of these biotites is very similar. Octahedral alumina is relatively high. Biotites from gneisses contain slightly less fluorine, and less calcium, rubidium, nickel, manganese, zinc, and gallium. Biotites *18* and *24* contain a deficient (OH,F) group.

Biotite *24*, in comparison with biotite *19* from gneissic granodiorite of the Superior province, *ca* 200 miles southeast of *24*, contains more total iron, higher ferric iron, much higher octahedral aluminum, lower titanium, manganese, sodium, three times as low rubidium and nickel, and lower gallium.

Biotite *12* from Grenville gneiss in eastern Quebec resembles, in major components, biotite *10*, also from the Grenville gneiss, in the Bancroft area; and in minor elements it resembles, to some extent, phlogopite *5*, except that the biotite *12* has a much higher content of titanium, and a lower ratio of ferric to ferrous iron. Biotite *12* has somewhat deficient silica and alumina, which are insufficient to fill the tetrahedral positions. Fluorine content is high and equivalent to that of biotite *10*. The (OH,F) group is more deficient than in biotite *10*. Biotite *12* contains much less gallium than biotite *10* and in this feature resembles phlogopite *5*, which contains low gallium but relatively high octahedral alumina. The high fluorine content in biotite *12* suggests its metasomatic origin.

Biotite *21* from porphyroblastic gneiss resembles in chemical composition biotite *19* from granodiorite, but contains less octahedral alumina and a more deficient (OH,F) group (Tables III, IV, VI, and VII).

Biotites *15* and *20* from paragneisses contain slightly deficient silica, high tetrahedral and octahedral alumina, very low ferric iron, similar quantities of ferrous iron and manganese, moderate titanium, relatively low fluorine, and a deficient (OH,F) group. The ratio of tetrahedral silica to alumina is 2.2 to 1. Average composition of biotites *15* and *20* is presented in Table X, column 13. Sodium, calcium, barium, strontium, rubidium, chromium, nickel, manganese, and gallium contents are relatively low. Biotites *15* and *20* show minor differences in chemical composition. Biotite *15* from the Penokean fault belt, Ontario, contains slightly less iron, titanium, and barium, half the amount of calcium and gallium, twice as much manganese and zinc, and slightly more rubidium than biotite *20* from the Churchill province. Biotite *20*, in comparison with biotite *30* from gneissic quartz monzonite, about 100 miles east of *20*, contains similar composition of the tetrahedral layer, less total iron, much less ferric iron, less fluorine, titanium, calcium, barium, and strontium, more octahedral alumina and more gallium. Both biotites contain similar and relatively low quantities of manganese, rubidium, nickel, and zinc. The outstanding feature of biotites from paragneisses is high aluminum content and very low ferric iron. Although octahedral alumina is high in both micas, gallium is twice as high in biotite *20*.

Biotite *27* from cordierite schist, Bear province, contains deficient silica and the highest alumina content of all the micas. The ratio of silica to alumina is 1.8 to 1; i.e., lower than in biotites from paragneisses. Octahedral aluminum is slightly higher, and the deficiency in the (OH,F) group is less, than in biotites from paragneisses. Biotite *27* contains relatively high chromium. In comparison with biotite *29* from porphyroblastic quartz monzonite *ca* 100 miles to the southwest, biotite *27* contains: slightly lower total iron; ten times as low a ratio of ferric to ferrous iron; less silica; much

more alumina; less magnesium and calcium; similar fluorine content; similar barium, strontium, gallium, and zinc; higher nickel and chromium. High octahedral aluminum in biotite *27* indicates its origin from sedimentary rocks. Biotites from gneissic rocks are characterized by the high deficiency of the (OH,F) group.

Associated Minerals

Pyroxene-Mica

Phlogopite *37* from picrite is an example of mica that is associated with olivine, pyroxene, serpentine, pyrrhotite and other sulphides. Phlogopite *37* is the latest primary silicate in the sequence of crystallization. It contains moderate quantities of iron, chromium, gallium, and strontium, relatively high titanium, copper, and nickel, and low manganese. Phlogopites *36Ph*, *9Ph*, and *35* from porphyritic basalt and lamprophyres are associated with pyroxene in the early stage of crystallization. They contain relatively low iron, manganese, zinc, and gallium, and the highest chromium content of all the micas. The late biotite from these rocks, which is associated with the deuteric minerals fibrous amphibole, epidote, and alkali feldspar, contains more iron, manganese, and strontium, and much less chromium. It is important to point out that micas that crystallize early display a compositional zoning, and dark brown iron-rich rims that are similar in composition to that of the late biotite. Change in composition from early phlogopite to late biotite is not gradual, as could be expected in a continuous phlogopite-biotite series. A distinct difference in composition between the early and late micas from these basic rocks points out the differences in the crystallizational environment of these micas.

This suggests either a break between the early magmatic stage and the deuteric stage of crystallization, or a discontinuity in the phlogopite-biotite series in the range from *ca* 25% to 40% of total octahedral iron.

Micas from the diopside-phlogopite assemblage in crystalline limestones (*3*, *4*, *6*, *7*, Table I; skarn, Table X) are deficient in alumina and contain high fluorine. They differ from phlogopites from basic igneous rocks in their low chromium, nickel, and titanium content.

Biotites *11* and *38* from radioactive orebodies (pegmatites) are associated with green pyroxene, titanium-, and rare-earth-bearing minerals. They contain moderate quantities of total iron, high ferric iron, low titanium and strontium, very low chromium, relatively high manganese, gallium, nickel, zinc, and fluorine, and abundant alkali metals (lithium, rubidium, and cesium).

Micas from pyroxene-bearing rocks (Table X, columns 2, 8, and 11) contain low to moderate iron and alumina, and relatively high magnesium. Minor elements and fluorine content vary, depending on the origin of the rock.

Pyroxene-Hornblende-Mica

Biotite *26* from anorthositic gabbro, which succeeds pyroxene and hornblende in the sequence of crystallization, contains a moderate quantity of ferrous iron, relatively high ferric iron, very high titanium, and low manganese. Phlogopite *8* from pyroxenite-hornblende-biotite gneiss forms at the expense of pyroxene and hornblende and is

associated with apatite and pyrite. This phlogopite contains low iron, titanium, manganese, zinc, and gallium, relatively high chromium and nickel, and high fluorine.

Micas from basic igneous rocks (Table X, column 1) vary in chemical composition, depending on the sequence of crystallization. Iron content increases in late biotites, whereas magnesium, chromium, and nickel are higher in early phlogopites. Metamorphic phlogopite, which crystallizes at the expense of pyroxene, contains low iron, relatively high chromium and nickel, and high fluorine. Biotites from radioactive orebodies are associated with radioactive and rare-earth-bearing minerals. They are very complex in chemical composition. Micas from marbles are associated with diopside and apatite. They contain high magnesium and fluorine, relatively low aluminum and iron, and low metals of the iron group.

Amphibole-Biotite

Biotite is associated with hornblende in granodiorites of the White Creek Batholith, in Precambrian granodiorite *19*, and in quartz monzonites *29* and *30*. The chemical composition of biotites from different amphibole-bearing rocks is presented in Table X. Column 2 in this table shows the chemical composition of biotite that is associated with pyroxene and hornblende, column 14 shows the average chemical composition of biotites from hornblende-bearing granodiorites, and column 15 shows biotites from quartz monzonites. The composition of the tetrahedral layer of these biotites is very similar. Silica is slightly lower than in the ideal mica, and alumina fills the remaining tetrahedral positions. Octahedral aluminum is highest in biotites from granodiorites and lowest in the biotite from anorthositic gabbro. Titanium is relatively high in all biotites. Ferric iron is relatively high and almost the same in all biotites. Ferrous iron is lowest in biotites from granodiorites and highest in those from quartz monzonites, whereas the magnesium content is highest in biotites from granodiorites and lowest in those from quartz monzonites. The ratios of ferric iron to titanium and of ferric to ferrous iron are higher in biotites from the granodiorites. Sodium content is slightly higher in the biotite from anorthositic gabbro. The composition of the (OH,F,O) group is similar in all biotites: the group is composed of *ca* 75% hydroxide; fluorine is slightly higher in the biotites from quartz monzonites; oxygen content and the deficiency of the (OH,F) group is highest in the biotite from anorthositic gabbro and in biotite *19* from gneissic granodiorite.

Micas from amphibole-bearing metamorphic rocks show considerable differences in chemical composition depending on the origin and type of the host rock. Chemical composition of phlogopite *5* from tremolite-bearing argillitic limestone is given in Table X, column 10, and the average chemical composition of biotites *12*, *18*, and *21* from hornblende-bearing gneisses, in column 16. In general, average chemical composition of biotites from gneisses is very similar to that of biotites from granodiorites; however, calcium and strontium are lower, and fluorine and deficiency of the (OH,F) group are higher in biotites from gneisses. Phlogopite *5* from metamorphosed argillitic limestone differs from biotites of hornblende-bearing gneisses in its higher deficiency of tetrahedral silica, much higher quantities of octahedral aluminum and magnesium, low iron, titanium, manganese, and calcium, and higher sodium, stron-

tium, and fluorine contents. The (OH,F) group is less deficient in phlogopite *5* than in biotites from gneisses.

Individual concentrates from hornblende-bearing rocks show more distinct variations than the average figures, particularly in the abundance of trace elements, deficiency of the (OH,F) group, and fluorine content (Tables IV, VI, and VII).

Biotites from granodiorites of the White Creek Batholith and from radioactive orebodies that are associated with the abundant titanium-bearing mineral, sphene, contain less titanium than other biotites from similar rocks.

Biotites associated with hornblende contain, in general, more iron than those associated with pyroxene. However, members of pyroxene and amphibole families vary in chemical composition, and occur in a great variety of igneous and metamorphic rocks. Composition of associated biotite also varies with the origin and type of the host rock. Deficiency of the (OH,F) group is independent of the chemical composition of mica and is correlative with the grade of thermal and regional metamorphism.

Biotite-Muscovite

Biotite and muscovite are plentiful in quartz monzonite *41* (rock-unit 12, White Creek Batholith), and in gneissic quartz monzonite (*1M*, *28B*) from Fry Creek Batholith. Quartz monzonite *22* also contains some muscovite that, with chlorite, replaces biotite. Partly altered biotite and muscovite are present in granodiorites *42* and *43*, and an entirely altered biotite and fresh muscovite occur in quartz monzonite *2*. In paragneiss *15*, muscovite partly replaces biotite.

Chemical composition of biotite *15* from paragneiss is similar to that of biotite *22* from quartz monzonite. In both these rocks biotite shows incipient alteration to muscovite. Biotites *15* and *22* are similar in chemical composition. They contain almost the same quantities of octahedral magnesium, ferrous iron, and titanium. However, ferric iron is six times as low and aluminum is twice as high in biotite *15* from paragneiss. The (OH,F) group is more deficient and fluorine content is lower in the biotite from paragneiss. The trace-element content of biotites *15* and *22* is very similar.

Chemical composition of biotite that is present with muscovite *2* in quartz monzonite is not known, because the biotite is altered to chlorite and sphene. It can be pointed out, however, that this biotite was not stable under conditions favouring crystallization of muscovite, which suggests that only the very special type of biotite with a limited compositional range is stable in association with muscovite. A complete chemical and X-ray spectrographic analysis of biotite *28*, which coexists with muscovite *1*, shows the following differences in comparison with the biotites from hornblende-bearing rocks (Table X, columns 14, 15, 16, and 17): Biotite *28* contains three to five times higher octahedral aluminum; slightly lower titanium, ferric iron, and magnesium; relatively high ferrous iron, comparable to that of biotites from quartz monzonites; at least twice as high manganese, zinc, gallium, and strontium; and higher rubidium. The main differences in chemical composition between biotite *28* and muscovite *1* have already been pointed out. A comparison of biotite *28* with other biotites, and of muscovite *1* with muscovites from muscovite-biotite-bearing rocks,

has also been made. The distinctive properties of biotite that coexists in association with muscovite are:

1. relatively high tetrahedral and octahedral aluminum, the ratio of tetrahedral silicon to aluminum being 2.2:1, and the ratio of octahedral magnesium to aluminum being 2:1 to 3:1.
2. moderate to high ferrous iron, the ratio of ferrous iron to magnesium varying from 2:1 (in igneous rocks) to 1:1 (in paragneiss).
3. relatively high manganese, zinc, gallium, and rubidium content, particularly in biotites from muscovite-bearing igneous rocks.

Biotite-Fluorite

Biotite *33* occurs in fluorite-bearing quartz monzonite (Pl. III-3, 4). It contains the highest quantity of ferrous iron and the lowest magnesium content of all the biotites. In comparison with the biotites from hornblende-bearing quartz monzonites and granodiorites, biotite *33* contains slightly more ferric iron and fluorine, and more manganese, zinc, gallium, and rubidium; therefore, in abundance of these elements, it resembles biotite *28*, which is associated with muscovite. Nickel, calcium, barium, and strontium content in biotite *33* is low. It is interesting to note that fluorine content in biotite *33* from fluorite-bearing quartz monzonite is slightly lower than in biotites *28* and *32* from granitic rocks, which do not carry fluorite.

A decisive factor in the chemical composition of biotite members that coexist with fluorite is their origin. Late magmatic biotite from quartz monzonite contains high iron, relatively high manganese, zinc, and gallium, thus resembling biotites which crystallize from residual magmas enriched in these elements. Metasomatic phlogopites from skarns and associated dykes contain very high quantities of fluorine, which in phlogopite *7* is twice as high as hydroxyl and high magnesium.

Biotite-Cordierite

Biotite *27* from cordierite schist contains the highest quantity of tetrahedral and octahedral aluminum, thus resembling aluminum-rich biotites from paragneisses and biotite *28* from quartz monzonite, which is associated with muscovite. The high aluminum and low silica content of biotite from metamorphosed sediments can be explained by its origin from argillaceous layers that originally consisted of alumina-rich clay minerals, and by the presence of unreactive quartz, which is not so readily incorporated into the biotite lattice, and frequently remains in the form of small rounded inclusions.

Summary and Conclusions

The present study of 50 micas, which was carried out on the basis of 34 complete chemical and 47 X-ray spectrographic analyses and optical examination of textures, has shown that the main factors determining the chemical composition of micas are:

1. chemical composition of the source material;
2. origin (type of host rock);
3. physical-chemical conditions of crystallization;
4. associated minerals; and
5. post-crystallizational alteration.

The crystal structure of micas provides accommodation for a great variety of elements; thus, depending on physical-chemical conditions of crystallization, some micas are chemically simple, others complex. The extreme high and low quantities of major components and of trace elements in the mica lattice determined in the present study are presented in Tables XI and XII.

Table XI

Range in Chemical Composition of Micas Studied

Oxide or Element	Weight % or ppm	Biotites and Phlogopites		Muscovites
		Minimum	Maximum	Maximum
SiO_2	(weight %)	32.8 (*31B*)	43.4 (*7Ph*)	47.6 (*1M*)
Al_2O_3	(weight %)	9.4 (*7Ph*)	19.8 (*27B*)	32.4 (*1M*)
TiO_2	(weight %)	0.35 (*3Ph*)	5.7 (*26B*)	0.8
Fe_2O_3	(weight %)	0.00 (*3Ph*)	7.2 (*31B*)	2.8 (*2M*)
FeO	(weight %)	0.79 (*4Ph*)	28.8 (*33B*)	0.96 (*1M*)
MgO	(weight %)	3.2 (*33B*)	26.8 (*3Ph*)	0.87 (*2M*)
MnO	(weight %)	<0.05 (*Ph*)	0.9 (*31B*)	0.05
Cr_2O_3	(weight %)	<0.05	0.93 (*9Ph*)	<0.05
NiO	(ppm)	50	2,300 (*36Ph*)	250 (*41M*)
CuO	(ppm)	<50	250 (*37Ph*)	<50
ZnO	(ppm)	250 (*4Ph*), 50 (*M*)	1,800 (*31B*)	500 (*42M*)
Ga_2O_3	(ppm)	<20	120 (*41B*)	260 (*42M*)
K_2O	(weight %)	7.2 (altered *41B*)	9.9 (*3Ph*)	10.2 (*2M*)
Na_2O	(weight %)	0.04 (*25B*)	0.9 (*3Ph*)	0.76
CaO	(weight %)	0.03 (*19B*)	1.3 (*4Ph*)	0.65 (*2M*)
BaO	(weight %)	0.05 (*10B*)	0.95 (*30B*)	0.03
SrO	(ppm)	<10	420 (*9B*)	50 (*1M*)
Rb_2O	(ppm)	220 (*26B*)	7,000 (*11B*)	2,000 (*42M*)
Li_2O	(weight %)		0.71 (*11B*)	
Cs_2O	(weight %)		0.1 (*11B*)	
As	(weight %)		trace (*38B*)	
Pb	(weight %)		trace (*38B*)	
Sc	(weight %)		trace (*42B*)	
V	(weight %)		trace (*17B*)	
H_2O+	(weight %)	1.32	4.07 (*17B*)	4.4 (*1M*)
H_2O-	(weight %)	0.04	0.88 (*10B*)	
F	(weight %)	0.23 (*20B*)	5.7 (*7Ph*)	0.28 (*1M*)
P_2O_5	(weight %)	0	0.29 (*23B* in apatite)	

Table XII

Variations in Unit Cell Contents of Micas Studied

Layer	Ion	Biotites and Phlogopites		Muscovites
		Minimum	Maximum	Maximum
Tetrahedral (%)	Si	64.4 (*31B*)	76.8 (*4Ph*)	79.8
	Al	20.3 (*7Ph*)	35.6 (*31B*)	
	Ti	0.0	2.5 (*13B*)	
	Fe‴	0.0	2.5 (*6Ph*)	
	Fe″	0.0	2.0 (*3Ph*)	
Octahedral (%)	Al	0.0	15.6 (*27B*)	89.6
	Ti	0.0 (*3Ph*)	8.3 (*26B*)	2.0
	Fe‴	1.1 (*15B*)	15.0 (*31B*)	7.0
	Fe″	1.7 (*4Ph*)	67.1 (*33B*)	2.4
	Mg	12.6 (*33B*)	98.0 (*4Ph*)	4.2
Interlayer (%)	K	83.1 (*4Ph*)	99.0 (*18B*)	89.4
(OH,F,O) Group (%	OH	33.0 (*7Ph*)	94.0 (*17B*)	98.0
	F	2.5 (*20B*)	66.0 (*7Ph*)	2.0
	O	0.0 (*28B*)	17.5 (*12B*)	3.5
% Dehydration		0.0	35.0 (*12B*)	7.0

Micas from pegmatites and from basic and metasomatic rocks display the greatest variation and complexity in chemical composition, whereas micas from some paragneisses that crystallized from well-sorted sediments are chemically least complex.

The chemical compositions of micas from diverse rocks and from different mineral assemblages described in the present report are summarized in Table X. Some of the most interesting relations follow:

1. In the basic magmatic rocks, an early, magnesium-rich phlogopite contains the highest quantities of chromium, nickel, and sodium, whereas the late biotite is enriched in iron, manganese, and rubidium. Quantities of calcium, strontium, and barium vary to some extent, depending on calcium-bearing inclusions, chiefly epidote and apatite, which are late deuteric, or form during post-crystallizational alteration. Titanium content varies depending on the presence or absence of sphene. If sphene is present, titanium preferentially concentrates in it, and the associated mica contains less titanium. In basic rocks, biotite that formed during the last stages of crystallization generally contains the highest quantity of titanium.

2. Biotites from granodiorites and quartz monzonites vary in chemical composition, depending on the presence of sedimentary or/and metasomatic components and on the sequence of crystallization (and, in some cases, recrystallization) of biotite. In general, fluorine content, ferrous and ferric iron, and manganese increase, and magnesium decreases, with increasing acidity of the rock. The difference in chemical composition between biotites from granodiorites and those from quartz

monzonites are more distinct in the biotites from the unrelated rocks of the Canadian Shield than in related rocks of the White Creek Batholith.

Biotites that are associated with muscovite contain relatively high iron and aluminum and are enriched in elements with large ionic radii, such as manganese, zinc, and rubidium. This suggests their crystallization from acidic residual magmas. High alumina content may be due to assimilation of sediments. All biotites from the hybrid granodiorites and quartz monzonites of the White Creek Batholith contain higher octahedral aluminum than biotites from similar Precambrian rocks. The difference between the biotite and the muscovite from the same quartz monzonite is illustrated in Table X, columns 17 and 18. Biotite contains more metals of the iron group and more rubidium, whereas muscovite contains more silica, alumina, and gallium.

3. Biotites from pegmatites differ in chemical composition, depending on the nature of the pegmatite and on its petrographic environment. Biotite from syenite pegmatite is similar in chemical composition to biotite from quartz monzonite, but contains very low silica and much more ferric iron. Biotite from the pegmatitic radioactive orebodies also contains relatively high ferric iron, very high rubidium and some rarer alkali metals (lithium and cesium), and high fluorine, which suggests its partly metasomatic origin. Phlogopite from pegmatitic segregations in skarn contains high magnesium and fluorine.

4. Phlogopites from skarn are deficient in alumina. They contain high magnesium and fluorine and vary in iron content, depending on the quantity of iron-bearing impurities present in the original limestone. They differ from the phlogopites from basic magmatic rocks, chiefly in the absence of chromium and in their high fluorine content.

5. Phlogopites from metamorphosed argillitic limestone differ from phlogopites from skarn in relatively high quantity of octahedral alumina.

6. Phlogopites from pyroxene-hornblende gneiss resemble in chemical composition phlogopites from basic magmatic rocks (in relatively high magnesium, chromium, and nickel content) and metasomatic phlogopites from skarn (in high fluorine content).

7. Biotites from gneisses vary depending on the origin of the gneiss. In general, they are similar in chemical composition to biotites from younger quartz monzonites. Some biotites from gneisses contain high fluorine and gallium, which indicates their metasomatic origin. The most distinctive feature of the biotites from gneisses is the deficiency of the (OH,F,O) group.

8. Biotites from paragneisses can be distinguished from biotites from orthogneisses by their high octahedral aluminum content, and from biotites from muscovite-bearing quartz monzonites (which also contain high aluminum) by lower quantities of ferrous iron and very low ferric iron. Trace elements vary depending on residual minerals present in the original sediments.

9. Chemical composition of micas from metamorphosed sediments depends on the composition of the original minerals present during crystallization and on the metamorphic grade; i.e., on the nature of the associated minerals. At the lower grade of metamorphism, some iron and titanium are present in goethite, hematite, sphene,

and epidote, which frequently occur as inclusions in biotite. As metamorphic grade increases, biotite recrystallizes and includes in the structure at least some components of the inclusions.

10. The early phlogopite and biotite are in many cases unstable during crystallization of later minerals. Phlogopite recrystallizes, or in part is replaced by chlorite, feldspar, and quartz during crystallization of late biotite and later alterations of basic magmatic rocks. During crystallization of muscovite, which normally succeeds biotite in the sequence of crystallization, biotite generally alters to chlorite, recrystallizes, and is in part replaced by muscovite. In magmatic rocks, only late iron- and aluminum-rich biotite is stable in association with muscovite. Alteration of biotite in sericitized rocks follows the alteration of feldspar, whereas muscovite remains unaffected during sericitization, which might take place much later, after crystallization of the primary minerals. This explains why the isotopic age of early phlogopite is younger than that of late biotite, and the isotopic age of paragenetically older biotite is less than that of muscovite.

11. Study of the deficiency of the (OH,F,O) group and of ferric iron content in the present micas indicates that about one-third of the micas show a deficiency of the (OH,F,O) group of from 20% to 35%. Octahedral ferric iron in these micas varies from 2% to 12%. These micas are from gneisses, from gneissic quartz monzonite, from anorthositic gabbro that was intruded by granite, from a radioactive orebody, and from a mafic inclusion in granodiorite. There is no apparent relation between the deficiency of the (OH,F) group and the quantity of ferric iron, which suggests that oxidation of ferrous iron and dehydration of these micas are separate and unrelated processes. Dehydration of mica is a result of regional metamorphism (in gneisses) and of thermal metamorphism; i.e., the effect of heat from surrounding and intruding rock.

12. The highest ferric iron content is present in the biotite from uraninite-bearing syenite pegmatite and in the biotite from the radioactive pegmatitic orebody, which suggests the relationship between the high quantity of ferric iron and the alkalic environment, and probable later oxidation of ferrous iron as a result of radioactive effect of associated minerals. Moderate quantities of ferric iron are present in micas in which the deficiency of the (OH,F) group varies from 0% to 30%. Ferric iron is relatively high in muscovites, in partly chloritized micas, and in related rocks; e.g., from the Mount Megantic complex in southwestern Quebec it increases with increasing ferrous iron content and with increasing acidity of the rock. In such rocks, the deficiency of the (OH,F) group is opposite to the increasing quantity of ferric iron. The lowest ferric iron content (*ca* 2% octahedral Fe''') was found in micas from paragneisses and in phlogopites from marbles, in which the deficiency of the (OH,F) group varies from 0% to 30% depending on the metamorphic grade.

The present study indicates that the deficiency of the (OH,F,O) group can be a result of partial loss of hydrogen and water due to elevated temperatures and pressure. This most probably reduces the total number of anions, with the negative charge of the (OH,F,O) group remaining the same and the cations being unaffected by oxidation. In rare cases, the number of anions remains constant, the negative charge of the (OH,F,O) group increases, and ferrous iron oxidizes to ferric iron at the expense of the hydroxyl group.

Chapter VI

NOTES ON THE INTERPRETATION OF ISOTOPIC AGES

Most isotopic ages are hybrid ages for the following reasons: (1) different geochemical behaviour of potassium and argon, and of rubidium and strontium; (2) the presence of more than one type of mica in a rock; and (3) different susceptibility of micas to alteration under diverse conditions. No published data are yet available on the time actually elapsed between crystallization of early and late minerals, on the duration of metamorphic processes, and on losses or gains of these radioactive and radiogenic elements. Recently Marmo (1960) pointed out that low K-Ar ages of potassium feldspar, which is often metasomatic, indicate actual time of its late crystallization rather than assumed loss of argon. In interpreting isotopic ages, it is important to determine the origin and sequence of crystallization of micas, their type, and degree and nature of alteration. Results of the present study indicate that most micas are affected by dehydration, by chloritization, or by both types of alteration. During the process of chloritization, potassium and argon are lost. If the losses are proportional, the age will not be affected; if differential (Ar > K), the age will be lower. Rubidium is bound more strongly than strontium (Goldschmidt, 1954), and strontium readily enters into the lattice of secondary calcium-bearing minerals that commonly contaminate micas. Ages of such micas are not reliable because strontium might also be concentrated from other minerals. Dehydrated micas occur in rocks that are affected by plutonic and contact metamorphism, which, according to Barth, Correns, and Eskola (1939), in most cases is allochemical. These rocks show evidences of replacement of biotite by potassium feldspar, by epidote, and by sphene. Biotite often recrystallizes. Such micas retain or gain potassium, and lose part of the (OH,F) group and some argon, owing to elevated temperature and pressure. In some cases, this type of alteration might have a more serious effect on isotopic ages than hydrothermal alteration.

Muscovites are stable during deuteric and hydrothermal alteration, whereas the stability of biotites under these conditions varies, depending on their chemical composition. During long-lasting hydrothermal alteration and cooling of the rock, biotite will be affected to a greater or lesser extent, while muscovite will remain stable.

Isotopic ages of the micas used in the present study are briefly discussed on the basis of the above mineralogical and petrological studies. Specimens are discussed in the same order as in Chapter V. Reference to ages is given in Table I.

Micas from Basic Rocks

Late Phlogopite *37:* Partly altered. Minimum age of picrite.

Late Phlogopite *34:* Minimum age of anorthosite.

Early Phlogopite *36Ph:* Recrystallized, unstable during crystallization of the matrix and post-crystallizational alteration. Probable loss of argon. Hybrid age of crystallization and last stage of alteration.

Late Biotite *36B:* More stable under cooling conditions than *36Ph.* Minimum age of diabase. This is an example of the difference between the stabilities of high-temperature phlogopite and low-temperature biotite as a result of different chemical composition.

Early Phlogopite *9:* Considerable loss of the (OH,F) group and probably of some argon. Minimum age of lamprophyre.

Zoned Phlogopite *35:* No evidence of alteration. Age of lamprophyre.

Late Biotite *26:* Considerable deficiency in the (OH,F) group. Minimum age of anorthositic gabbro.

Early Biotite *32:* Slight deficiency of the (OH,F) group, incipient alteration. Minimum age of granite.

Micas from Granodiorites and Associated Quartz Monzonites

Biotites from various rock-units of the White Creek Batholith differ in iron content, and those from the same rock-unit differ mainly in abundance of volatiles, depending on sampling locality. The most distinct deficiency in the (OH,F) group was observed in biotite from the mafic inclusion and in biotite *23* from rock-unit 11, elevation 4,200′. Biotite *22*, collected at a higher elevation, 8,000′, is partly altered to chlorite and contains a less deficient (OH,F) group.

In order to study the relationship between dehydration and possible loss of argon, a comparison of biotite ages from two inclusions, and from rocks sampled at higher and lower elevations of the same rock-unit is made.

	Elevation (in feet)	*Age (m.y.)*	
Rock-Unit 9			
Biotite *16*	7,500	79	partly dehydrated and chloritized
Biotite *40*	4,200	73	slightly chloritized (H_2O and F contents similar to those of biotite *16*)
Biotite *39*	from inclusion	56	not chloritized
Rock-Unit 10			
Biotite *17*			not dehydrated, chloritized
Biotite *14*	from inclusion		dehydrated and chloritized
Rock-Unit 11			
Biotite *22*	8,000	60	partly dehydrated and chloritized
Biotite *23*	4,500	29	dehydrated more than *22*, slightly chloritized
Rock-Unit 12			
Biotite *41*	5,000	82	slightly chloritized
Muscovite *41*	5,000	80	not chloritized
Rock-Unit 14			
Biotite *25*	7,500	18	partly dehydrated and chloritized

Biotites *22* and *23*, from the same rock-unit (11), show relative decrease in age with decreasing elevation and increasing dehydration. The degree of dehydration in this case seems to have relatively greater effect on age (loss of argon) than chloritiza-

tion. Biotites from rock-unit 9 show decreasing age in the same order as those of unit 11. However, since the water and fluorine content in biotite *39* was not determined, the relationship between loss of water and loss of argon was proved on one biotite pair only, and needs further study.

The age of the biotite from the mafic inclusion, which is less than that of the biotite of the surrounding rock, indicates greater stability of biotite that is richer in iron during post-crystallizational alteration. Muscovite *41* and biotite *41* (which contains the highest iron) were the most stable of all micas and gave the oldest ages. In general, all rocks were affected by alteration and all mica ages are hybrid, varying between the time of crystallization and the most likely long-lasting period of alteration.

Muscovite *1* from Fry Creek Batholith is present in two generations. Earlier flakes are associated with biotite, and the later muscovite forms composite porphyroblastic grains, indicating further growth of earlier flakes (Pl. I-2). The muscovite age is hybrid and higher than that of the associated biotite *28*. This suggests that older muscovite retained argon better than the biotite during further growth of muscovite, which occurred probably in a solid state.

Micas from Unrelated Granodiorites and Quartz Monzonites

Biotite *19* is in part replaced by potassium feldspar (Pl. IV-6). It shows a considerable deficiency in the (OH,F) group (28%), which suggests a partial loss of the volatiles and, perhaps, of some argon. The age is the minimum age of granodiorite.

Biotite *43* occurs in two generations (Pl. V-8). Older, coarse, partly resorbed flakes and fine-grained recrystallized biotite give a hybrid age of the period of crystallization and of recrystallization.

Muscovite *43*, which is paragenetically younger than the coarse-grained biotite, occurs also in two generations. The age of the muscovite is also hybrid. The age relation between biotite *43* and muscovite *43* is similar to that observed between micas *1* and *28*, which suggests that muscovite retains argon better during low-grade metamorphism and under hydrothermal conditions that favour crystallization of secondary white mica and chlorite.

Biotite *42* is in part recrystallized, altered, and replaced by secondary minerals (Pl. VI-1, 2, 3). The age of biotite *42* is a hybrid age of its crystallization and of superimposed alteration.

Muscovite *42* is only slightly flexed and gives the minimum age of granodiorite.

Biotite *29* is in part replaced and pushed aside by feldspar. It contains a deficient (OH,F) group, which suggests possible loss of some argon. The biotite age is the minimum age of the quartz monzonite.

Biotite *30* occurs in two generations (Pl. VIII-3). Early coarse-grained, roughly parallel laths are in part replaced by feldspar and by randomly oriented recrystallized flakes of biotite. The biotite contains a deficient (OH,F) group. The age of the biotite is hybrid, and gives the minimum age of crystallization and maximum age of recrystallization of the biotite.

Biotite *33* shows evidences of post-crystallizational alteration (Pl. III-3). The age indicates the minimum age of the quartz monzonite.

Biotite *31* contains very high ferric iron and a deficient (OH,F) group, suggesting partial loss of volatile components and, perhaps, of some argon. The K-Ar age is the minimum age of crystallization of the biotite.

Late Muscovite *2* gives the minimum age of the quartz monzonite.

Micas from Skarn Rocks

Phlogopite *7* contains extremely high fluorine and almost the ideal (OH,F) group. The age of this phlogopite is that of fluorine metasomatism in the Bancroft area.

Biotite *13* shows a considerable deficiency in the (OH,F) group, thus indicating partial loss of the volatiles, probably including some of the argon. The age is the minimum age of crystallization of this biotite.

Micas from Gneisses and Schists

Phlogopite *8* shows a high deficiency in the (OH,F) group, and thus gives a hybrid age; that is, a minimum age of crystallization and maximum age of dehydration.

Biotite *12* contains a deficient (OH,F) group (35%). The age indicates the minimum age of crystallization of biotite and the maximum age of porphyroblastic growth of feldspars.

Biotite *18* is in part replaced by potassium feldspar (Pl. IX-2), and contains a deficient (OH,F) group. It gives a hybrid age; that is, a minimum age of crystallization and maximum age of alteration and replacement by feldspar.

Biotite *21* is in part replaced and pushed aside by porphyroblastic feldspar and shows a high deficiency in the (OH,F) group (>33%). The age indicates the minimum age of crystallization of the biotite and the maximum age of porphyroblastic growth of the feldspar.

Biotite *24* is in part replaced by feldspar and by minerals of the epidote group (Pl. IX-5). It is in part dehydrated and indicates a hybrid age—minimum age of crystallization of biotite, and maximum age of deformation and porphyroblastic growth of feldspar and other minerals.

Biotite *27* is in part replaced by cordierite and slightly altered to chlorite. The age is hybrid and indicates the minimum age of crystallization of biotite and the maximum age of alteration.

Biotite *15* is in part replaced by muscovite and contains a deficient (OH,F) group. The age is the minimum age of crystallization of the biotite.

Biotite *20* is partly resorbed and subsequently altered (Pl. IX-9) and in part dehydrated. The age is the minimum age of crystallization of biotite and the maximum age of the final stage of its alteration.

The relationship between loss of water and loss of argon in micas was established in laboratory experiments by Amirkhanoff *et al.* (1961). Their laboratory results agree with the results obtained on natural micas in the present study. The most reliable determination of the deficient (OH,F) group is provided by the structural formula of mica, which is calculated on the basis of a complete chemical analysis. However, since a relationship was found between the metamorphic grade and the deficiency in the (OH,F) group in mica, the degree of dehydration can be roughly estimated by optical study. A study of the quantitative relationship between loss of water and loss of argon in natural micas that differ in chemical composition seems warranted.

REFERENCES

Abbey, S., and Maxwell, J. A.
1960: Determination of potassium in micas. A flame photometric study; *Chem. in Can.*, vol. 12, No. 9, pp. 37-41.

Amirkhanoff, K. I., Brandt, S. B., and Bartnitsky, E. N.
1961: Radiogenic argon in minerals and its migration; *Ann. New York Acad. Sci.*, vol. 91, art. 2, pp. 235-275.

Barth, T. F. W., Correns, C. W., and Eskola, P.
1939: Die Entstehung der Gesteine; Berlin, Julius Springer.

Bijvoet, J. M., Kolkmeijer, N. H., and MacGillavry, C. H.
1951: X-ray analysis of crystals; London, Butterworths Scientific Publications.

Bowen, N. L., and Tuttle, O. F.
1953: Beginning of melting of some natural granites; *Carnegie Inst. Washington*, Ann. Rept., Dir. Geophys. Lab., vol. 52, 1952-1953, p. 50.

Bradley, W. F., and Grim, R. E.
1951: High temperature effects on clay and related materials; *Am. Mineralogist*, vol. 36, pp. 182-201.

Braitsch, O.
1957: Ueber die natuerlichen Faser- und Aggregationstypen beim SiO_2, ihre Verwachsungsformen, Richtungsstatistik und Doppelbrechung; *Heidelberger Beitr. zur Mineral. u. Petrogr.*, vol. 5, pp. 331-372.

Brun, A.
1913: Note sur l'hydration des micas; *Bull. S.I. Soc. Franc. de Mineralogie*, vol. 36, p. 44.

Burckhardt, C.D.
1943: Zur Bestimmung der gesteinsbildenden Glimmer; *Schweiz. Mineral. u. Petrograph. Mitt.*, vol. 23, pp. 467-474.

Chayes, F., and MacKenzie, W. S.
1957: Experimental errors in determining certain locations and distance between peaks in X-ray powder diffractometer patterns; *Am. Mineralogist*, vol. 42, Nos. 7-8, pp. 534-548.

Courville, S.
1962: Apparatus for total water determination by the Penfield method; *Can. Mineralogist*, vol. 7, pt. 2, pp. 326-329.

Deer, W. A., Howie, R. A., and Zussman, J.
1962: Rock forming minerals. Vol. 3, Sheet silicates (Mica pp. 1-114); Longmans.

Ellsworth, H. V.
1932: Rare-element minerals of Canada; *Geol. Surv. Can.*, Econ. Geol. Ser., No. 11.

Engel, A. E. J., and Engel, C.
1961: Progressive metamorphism and granitization, Adirondack mountains. Part II; Mineralogy; *Bull. Geol. Soc. Amer.*, vol. 71, pp. 1-58.

Engelhardt von, W.
1943: Die Strukturen von Thueringit, Bavalit und Chamosit und ihre Stellung in der Chloritgruppe; *Zeitschr. Kristall.*, vol. 104, pp. 142-159.

Eugster, H. P., and Wones, D. R.
1962: Stability relations of the ferruginous biotite, annite; *J. Petrol.*, vol. 3, No. 1, pp. 82-125.

Foster, M.D.
1960: Interpretation of the composition of trioctahedral micas; *U. S. Geol. Surv.*, Prof. Paper 354-B.

Goldschmidt, V. M.
1954: Geochemistry; Ed. by Alex Muir; Oxford, Clarendon Press.

Goodspeed, G. E.
1959: Some textural features of magmatic and metasomatic rocks; *Am. Mineralogist*, vol. 44, Nos. 3, 4, pp. 211-250.

Gower, J. A.
1957: X-ray measurement of the iron-magnesium ratio in biotites; *Am. J. Sci.*, vol. 255, No. 2, pp. 142-156.

Harder, H.
1956: Untersuchungen an Paragoniten und an natriumhaltigen Muskoviten; *Heidelberger Beitr. Mineral. u. Petrogr.*, vol. 5, pp. 227-271.

Hayama, Yoshikazu.
1959: Some consideration on the colour of biotite and its relation to metamorphism; *J. Geol. Soc. Japan*, vol. 65, No. 760, pp. 21-30.

Heinrich, E. W.
1946: Studies in the mica group; *Am. J. Sci.*, vol. 244, pp. 836-848.

Heinrich, E. W., *et al.*
1953: Studies in the natural history of micas; Engineering Research Institute, Univ. Michigan, Ann Arbour.

Hendricks, S. B., and Jefferson, M. E.
1939: Polymorphism of the micas; *Am. Mineralogist*, vol. 24, No. 12, pp. 729-779.

Hewitt, D. F.
1957: Geology of Faraday and Cardiff Townships; *Ont. Dept. Mines*, Ann. Rept. 66, pt. 3.

Hirschi, H.
1901: Beitraege zur Kenntniss der gesteinsbildenden Biotite und ihre Beziehung zum Gestein; Zürich, Inaug. Dissertat.

Korzhinsky, D. S.
1960: Acidity-alkalinity in magmatic processes; *Proc. Int. Geol. Congr. NORDEN*, pt. 21, pp. 160-170.

Kunitz, W.
1924: Die Beziehungen zwischen der chemischen Zusammensetzung und der physikalisch-optischen Eigenschaften innerhalb der Glimmergruppe; *Neues Jahrbuch Mineral*, vol. 50, pp. 365-413.
1936: Die Rolle des Titans und Zirkoniums in den gesteinsbildenden Silikaten; *Neues Jahrbuch Mineral*, B. 70, pp. 385-466.

Lowdon, J. A.
1960: Age determinations by the Geological Survey of Canada, Report 1—Isotopic Ages; *Geol. Surv. Can.*, Paper 60-17.
1961: Age determinations by the Geological Survey of Canada, Report 2—Isotopic Ages; *Geol. Surv. Can.*, Paper 61-17.

Lowdon, J. A., *et al.*
1963: Age determinations and geological studies (Including Isotopic Ages—Report 3); *Geol. Surv. Can.*, Paper 62-17.

Marmo, V.
1960: On the K-Ar ages of the granite rocks; *Schweiz. Mineral. Petrogr. Mitt.*, vol. 40/1, pp. 17-36.

McAndrew, J.
1957: Calibration of a Frantz isodynamic separator; *Proc. Australian Inst. Min. Metall.*, No. 181, pp. 59-73.

Métais, D., Ravier, J., and Phan-Kien-Duong.
1962: Nature et composition chimique des micas des deux lamprophyres; *Bull. Soc. Franc. Mineral. Cristall.*, vol. 85, No. 4, pp. 321-328.

Nagelschnidt, G.
1937: X-ray investigations on clays, Part 3; *Zeit. Krist.*, vol. 97, p. 514.

Nockolds, S. R.
1947: The relation between chemical composition and paragenesis in the biotite micas of igneous rocks; *Am. J. Sci.*, vol. 245, pp. 401-420.

Platen von, H., and Winkler, H. G. F.
1961: Kristallisation eines Obsidians bei Anwesenheit von H_2O, NH_3, HCl und HF unter 2000 Atm. Druck; *Fortschr. Mineral.*, vol. 39, p. 355.

Radoslovich, E. W.
1962: The cell dimensions and symmetry of the layer lattice silicates, II. Regression Relations; *Am. Mineralogist*, vol. 47, pp. 617-636.

Ramberg, H.
1952: The origin of metamorphic and metasomatic rocks; Univ. Chicago Press.

Rankama, K., and Sahama, Th. G.
1950: Geochemistry; Univ. Chicago Press.

Reesor, J. E.
1958: Dewar Creek map-area, with special emphasis on the White Creek Batholith, British Columbia; *Geol. Surv. Can.*, Mem. 292.

Reesor, J. E., *in* Lowdon, J. A.
1961: Age determinations by the Geological Survey of Canada, Report 2—Isotopic Ages; *Geol. Surv. Can.*, Paper 61-17.

Ridgway, R.
1912: Color standards and nomenclature; Washington, D.C. (Published by the author).

Rimsaite, J.
1957: Ueber die Eigenschaften der Glimmer in den Sanden und Sandsteinen; *Beitr. Mineral. Petrogr.*, vol. 6, pp. 1-51.
1962: Studies of rock-forming micas (Abstract); *Am. Mineralogist*, vol. 47, p. 201.

Rinne, F.
1924: Roentgenographische Diagnostik beim Brennen von Kalkstein, Dolomit, Kaolinit und Glimmer; *Zeitschr. Kristall.*, vol. 61, pp. 113-124.

Robinson, S. C.
1952: Autoradiographs as a means of studying distribution of radioactive minerals in thin section; *Am. Mineralogist*, vol. 37, pp. 544-547.

Robinson, S. C., *in* Lowdon, J. A.
1960: Age determinations by the Geological Survey of Canada, Report 1—Isotopic Ages; *Geol. Surv. Can.*, Paper 60-17.

Satterly, J.
1956: Radioactive mineral occurrences in the Bancroft area; *Ont. Dept. Mines*, Ann. Rept. 65, pt. 6.

Schauberger, G.
1927: Biotit in tertiaeren Eruptivgesteinen Boehmens; *Centralbl. Mineral. Abt. A*, pp. 89-105.

Shell, H. R., and Craig, R. L.
1956: Synthetic mica investigations; VII, chemical analysis and calculation to unit formula of fluorsilicates; *U.S. Dept. Interior, Bur. Mines*, Rept. Invest. 5158.

Smith, J. V., and Yoder, H. S.
1956: Experimental and theoretical study of the mica polymorphs; *Mineral. Mag.*, vol. 31, pp. 209-239.

Stevens, R. E.
1946: A system for calculating analyses of micas and related minerals to end members; Contribution to geochemistry, 1942-1945; *U.S. Dept. Interior, Geol. Surv.*, Bull. 950.

Swanson, H. E., and Fuyat, R. K.
1953: *in*: Standard X-ray diffraction powder patterns; *N. B. S.* Circular 539, *3*, p. 24 (1954).

Szádeczky-Kardoss, E.
1960: A genetic system of igneous rocks; *Proc. Int. Geol. Congr. NORDEN*, pt. 13, pp. 260-274.

Troeger, W. E.
1952: Tabellen zur optischen Bestimmung der gesteinsbildenden Minerale; E. Schweizerbart'sche Verlagsbuchhandlung, Stuttgart.

Tsvetkov, A. I., and Valyashikhina, E. P.
1956: Data on thermal studies of minerals, III: Micas; *Trans. Inst. Geol., Ore Deposits, Mineral., Geoch., Ed. 4. Acad. Sci. U.S.S.R.*, Moscow.

Vernon, R. H.
1961: Magnetic susceptibility as a measure of total iron plus manganese in ferromagnesian silicates; *Am. Mineralogist*, vol. 46, pp. 1141-1153.

Winchell, A. N.
1935: The biotite system; *Am. Mineralogist*, vol. 20, pp. 773-779.

Winchell, A. N., and Winchell, H.
1951: Elements of optical mineralogy; Part II: Description of minerals; New York, John Wiley & Sons, Inc.

Wones, D. R.
1958: The phlogopite-annite join; *Carnegie Inst.*, Washington, D.C., Year Book 1957-1958, pp. 194-195.

Yoder, H. S., and Eugster, H. P.
1954: Phlogopite synthesis and stability ranges; *Geochim. et Cosmochim. Acta*, vol. 6, pp. 157-185.
1955: Synthetic and natural muscovites; *Geochim. et Cosmochim. Acta*, vol. 8, pp. 227-271.

Note: Since this bulletin was written in 1963; the writer published the following paper, in which reference is made to this bulletin as "Rimsaite 1963": Rimsaite, J. (1964): Micas in magmatic and metamorphic rocks; *Beitr. Mineral. Petrogr.*, vol. 10, pp. 152-183.

Related papers;

Rimsaite, J. and Lachance, G. R.
In press: Examples of heterogeneity in phlogopite, euxenite, and feldspar; *Indian Mineralogist*, IMA Volume.

Rimsaite, J. Y. H.
In press: Biotite intermediate between dioctahedral and trioctahedral micas; *Clays and Minerals* Proc. XV Nat. Conf., Pittsburg, Pa.

PLATES I to IX

Photomicrographs of concentrates and of textures of host rocks, by the author

PLATE I

1. Quartz monzonite *1*. Thin section. x50.
A large crystal of muscovite (M) with small euhedral crystals of biotite (B) on (001) cleavage planes. Left a large crystal of biotite.

2. Muscovite concentrate *1*. +N, x50.
A coarse composite flake of muscovite, suggesting further growth of small flakes.

3. Biotite concentrate *28*. x100.
A coarse flake of biotite with muscovite flakes between (001) cleavage planes. The biotite has compact (non-split) edges.

3A. Biotite from White Creek Batholith. x100.
A biotite flake with numerous long prismatic inclusions of zircon surrounded by dark pleochroic haloes. A few prisms of apatite (A).

4. Biotite concentrate 8 from pyroxenite gneiss. x500.
Edge of a phlogopite flake which displays a prominent splitting parallel to (001) cleavage.

5. Diopside marble *4*. Thin section. x50.
Diopside (D) and phlogopite (PH) crystals in crystalline limestone (C).

6. Phlogopite concentrate *6*. x500.
A blistered portion of a phlogopite flake. Small elongated blisters (X) project into a long channel.

7. Phlogopite *5* from metamorphosed argillitic limestone. + N, x100.
Central portion of zoned phlogopite *5* with needle-like inclusions which make a zoned appearance of the crystal.

8. Phlogopite *5*. x500.
Enlarged portion of Pl. I-*7*, showing rutile inclusions.

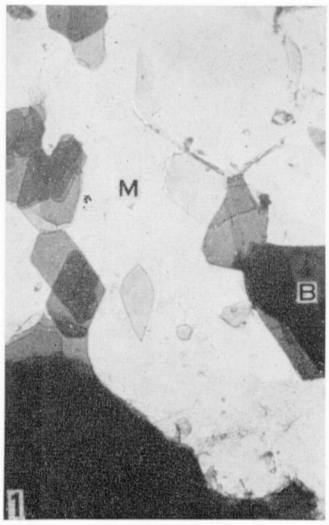
M
B
1

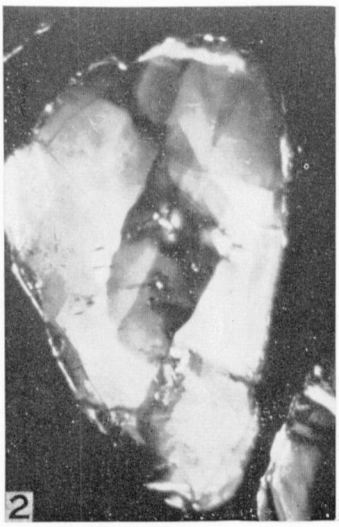
2

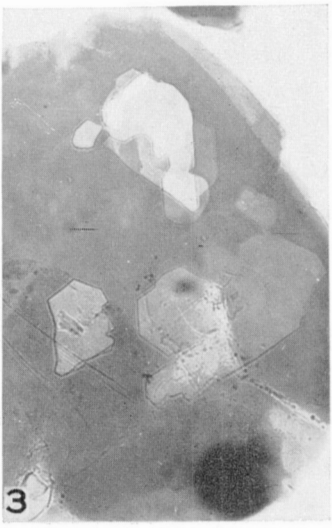
3

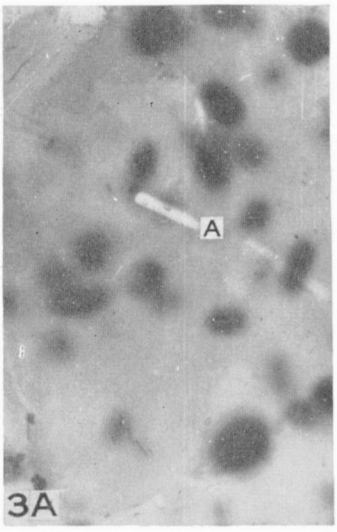
A
3A

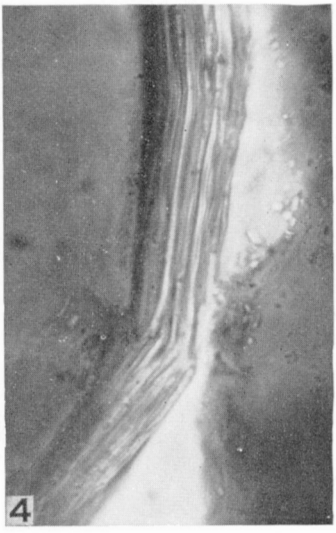
4

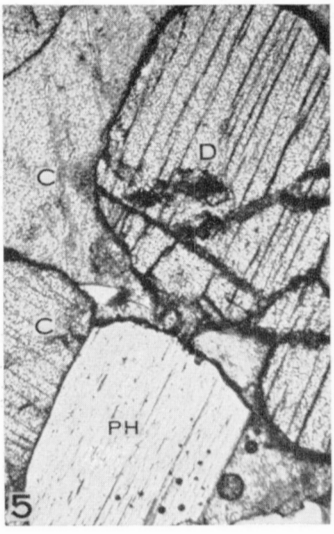
C
D
C
PH
5

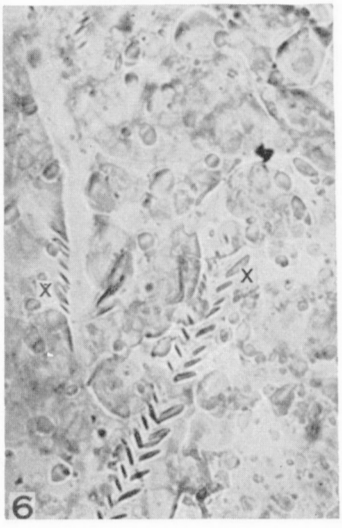
X
X
6

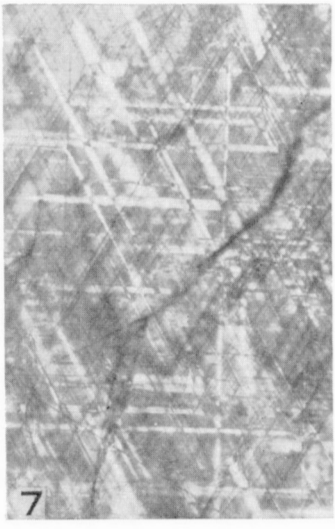
7

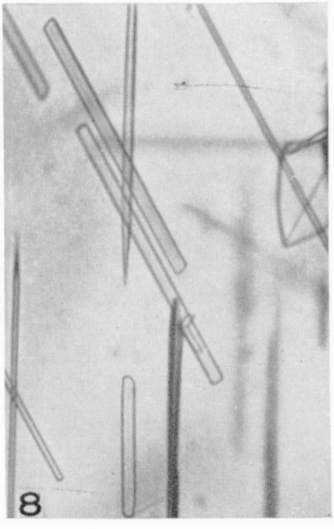
8

PLATE II

1. Phlogopite concentrate 9. Phenocrysts from lamprophyre. x100.
Zoned phlogopite flake with a dark rim of biotite.

2. Lamprophyre 9. Thin section. x100.
Biotite in the fracture of the lamprophyre. White area is feldspar.

3. Hornblende-biotite gneiss 12. Thin section. x100.
Partly resorbed biotite pushed aside by perthite and partly replaced by potassium feldspar (K).

4. Mafic-rich inclusion 14 from granodiorite. Thin section. x50.
Poikilitic, ragged biotite, intergrown with chlorite, containing inclusions of epidote, sphene and quartz.

5. Porphyritic quartz monzonite 23. Thin section. x100.
Biotite with a few inclusions of sphene.

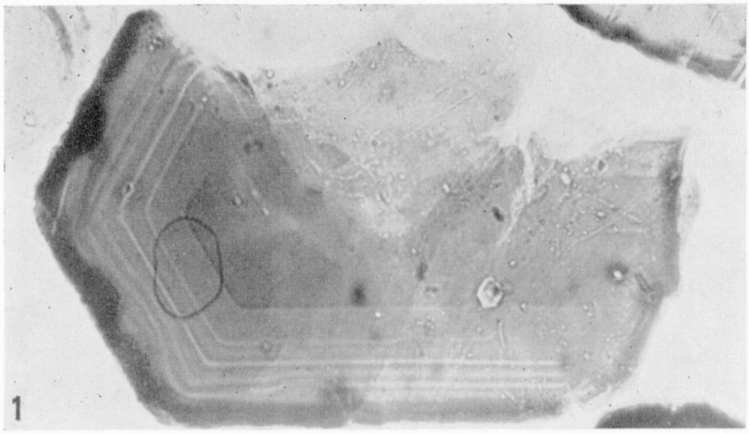
1

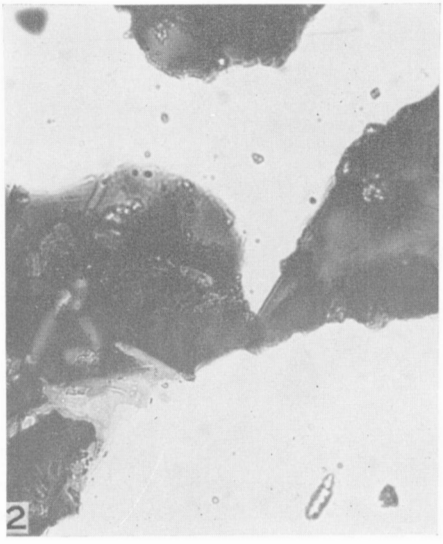
2


K
3

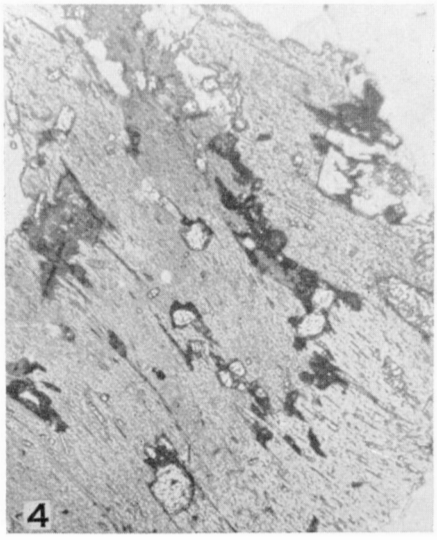
4

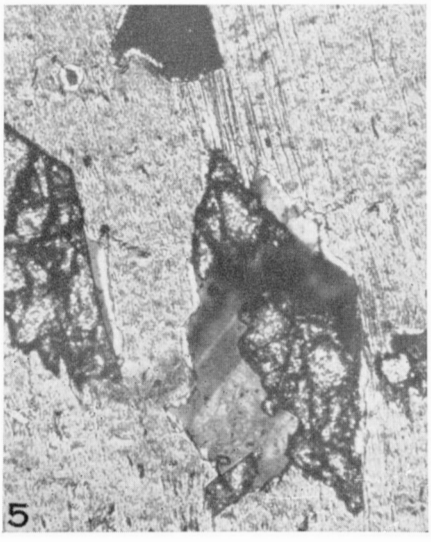
5

PLATE III

1. Biotite concentrate 23. x100.
Biotite flake with prismatic inclusions of apatite; split along (001) planes.

2. Biotite concentrate 20 from paragneiss. x100.
Biotite flakes with inclusions of rutile, ilmenite, sphene, epidote, zircon, and quartz.

3. Quartz monzonite 33. Thin section. x50.
Biotite (B), partly replaced by fluorite (F) and quartz with dark iron-rich patches along the (001) cleavage planes.

4. Biotite concentrate 33. x50.
Heterogeneous biotite concentrate. Some flakes are pale and bleached, others are almost opaque with black pleochroic haloes and segregations of iron.

5. Biotite 31*a*. x500.
Polygonal cracks at the surface of pleochroic altered biotite (γ reddish orange, β green). This altered mica has extremely high refractive index ($\gamma = 1.740$), probably as a result of exsolved sub-microscopic Fe_2O_3.

6. Muscovite concentrate 1. x100.
Muscovite flake with blisters and long channels after heating four hours at 600°C.

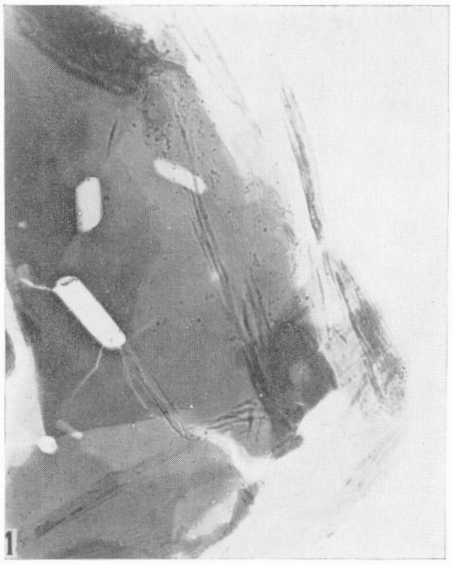
1

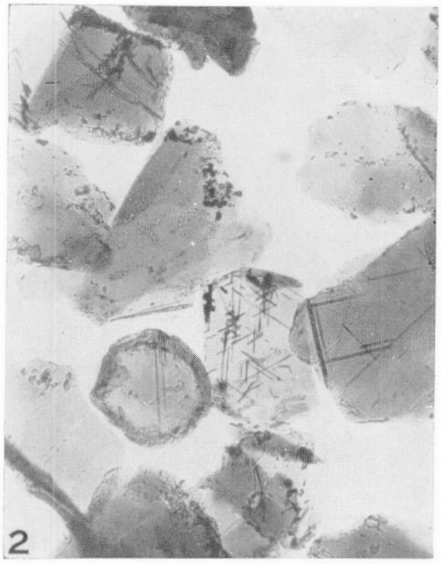
2

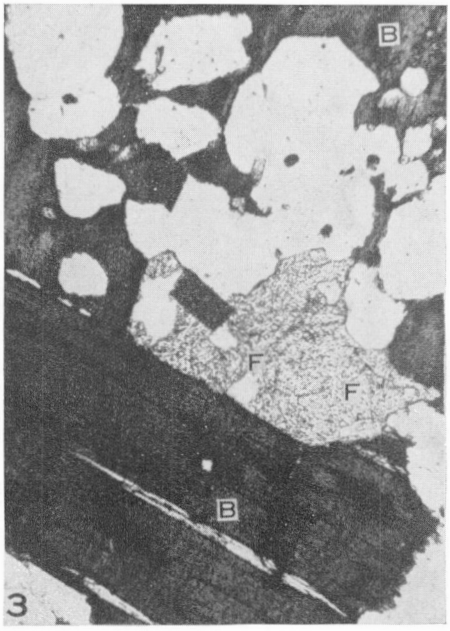

3


4

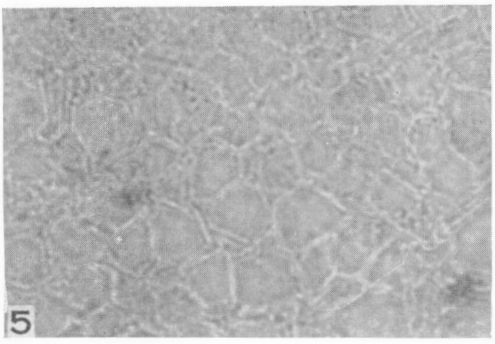
5

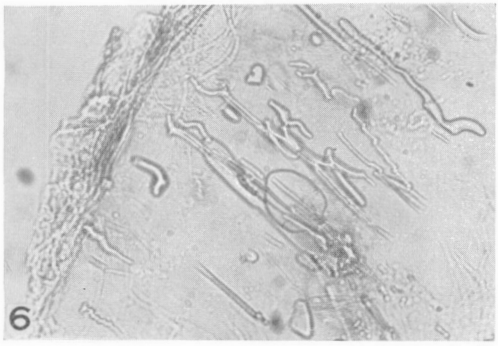
6

PLATE IV

1. Picrite 37. Thin section. x50.
Coarse patches of biotite (B) surround sulphides (opaque) and occur in a groundmass of altered olivine, pyroxenes, and patches of serpentine (S).

2. Picrite 37. Thin section. x540.
Biotite flake transected by a crenulated veinlet of serpentine (S) with opaque sulphide in (001) fractures.

3. Anorthosite 34. Thin section. x50.
Patches of red-brown phlogopite (P) between ilmenite (I) and fractured labradorite. Phlogopite contains opaque patches of ilmenite and chlorite (Cl) rimmed by opaque minerals.

4. Porphyritic basalt 36. Thin section. x50.
Phenocrysts of augite (A) and ragged phlogopite (P). Finer-grained dark brown biotite (B) occurs with pigeonite in the groundmass.

5. Porphyritic basalt 36. Thin section. x50.
Bent phenocrysts of phlogopite, recrystallized to fine-grained scaly aggregates.

6. Porphyritic basalt 36. Concentrate. x540.
Phlogopite flake with inclusions of quartz.

7. Lamprophyre 9. Thin section. x115.
Intergrowths of pyroxene and pale brown phlogopite phenocrysts. Phlogopite is fractured and is darker brown along the fractures grading into iron-rich biotite. Small crystals along fractures are epidote.

8. Lamprophyre 9. Thin section. x115.
Twinned phenocrysts of pyroxene in a groundmass of feathery albite.

9. Lamprophyre 35. Thin section. x50.
A coarse phenocryst of red-brown zoned phlogopite (P) with dark brown rims. Groundmass is composed of pyroxene, feldspar, and fibrous amphibole.

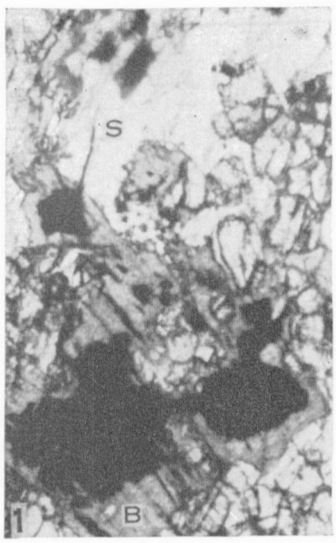
S
B
1


S
2

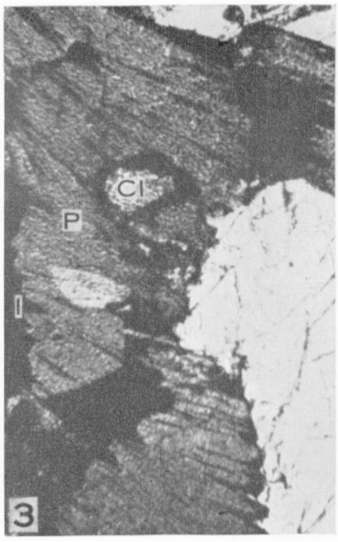
Cl
P
I
3

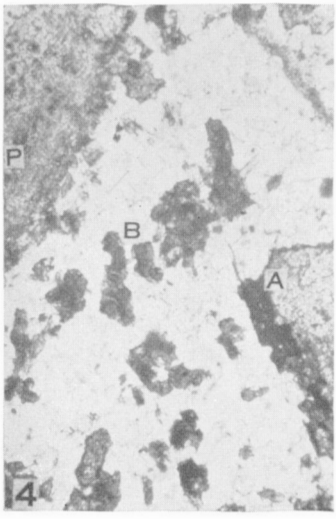
P
B
A
4

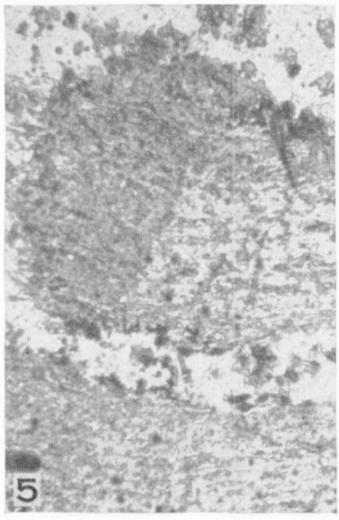
5

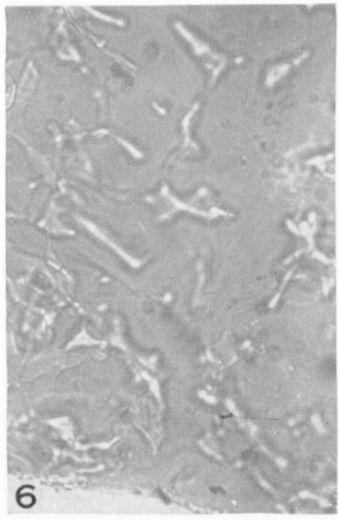
6

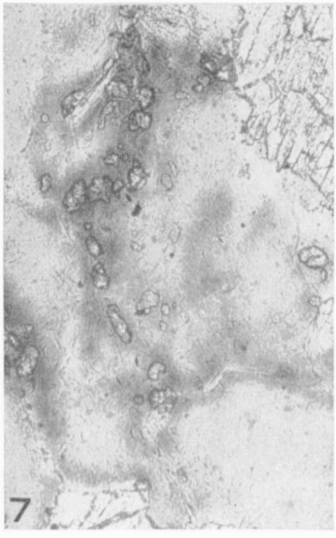
7


8


P
9

PLATE V

1. Anorthositic gabbro 26. Thin section. +N, x50.
Plagioclase crystals displaying signs of resorption and further growth.

2. Anorthositic gabbro 26. Thin section. x50.
A group of ferromagnesian minerals displaying clearly the sequence of crystallization from pyroxene (P, light remnants) through brown and green hornblende (H) to coarse patches of biotite (B).

3. Granodiorite (Granite) 32. Thin section. +N, x50.
A composite crystal of alkali feldspar resembling in appearance the plagioclase shown in Pl. V-1. Central portion consists chiefly of potassium feldspar (K) with a thin rim of quartz (Q) and an outer portion of antiperthite (AP). Alkali feldspar in the upper field consists of coarse patches of albite and K-feldspar. Coarse-grained mosaic of quartz fills the interstices.

4. Granodiorite (Granite) 32. Thin section. x115.
A group of partly resorbed biotite crystals, showing marginal areas partly replaced by quartz and feldspar. Small white crystals are apatite (A). Biotite alters along (001) fractures to hematite (H), chlorite (C), and muscovite (M).

5. Granodiorite 19. Thin section. x115.
Biotite laths (B) and partly resorbed hornblende (H).

6. Granodiorite 19. Thin section. x540.
Biotite surrounded and partly replaced along (001) fractures by potassium feldspar (K).

7. Granodiorite 19. Thin section. x115.
Replacement of antiperthite with patches of microcline adjacent to fractures.

8. Granodiorite 43. Thin section. x115.
Remnants of coarse biotite (B) transected by coarse muscovite laths (M). Biotite along muscovite contact recrystallizes to iron oxides (F) and fine-grained biotite flakes (R). Thin rims of sericite (S).

9. Granodiorite 43. Biotite concentrate. x540.
Biotite flake with small euhedral plates of secondary biotite, iron oxides, and rutile along the fracture.

1

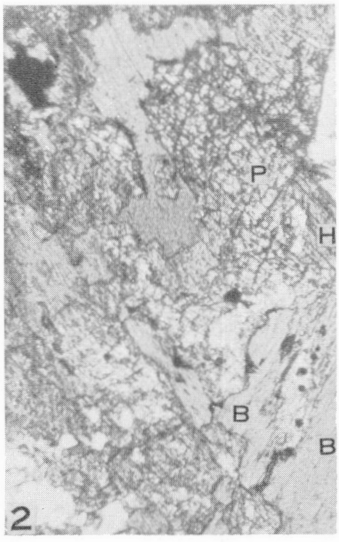

2

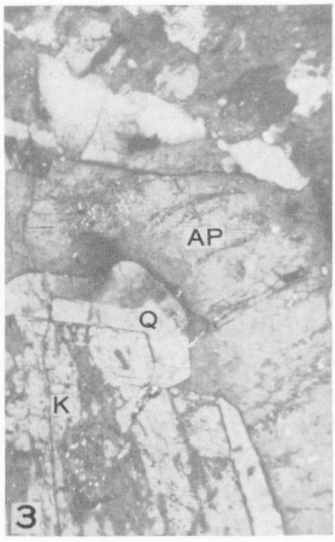

3

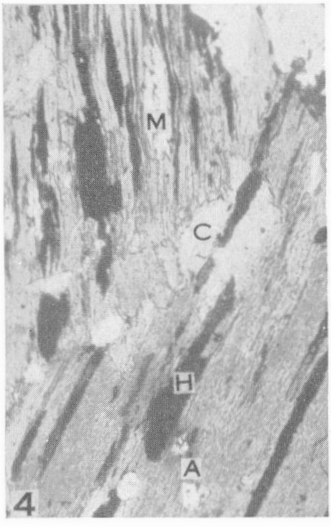

4

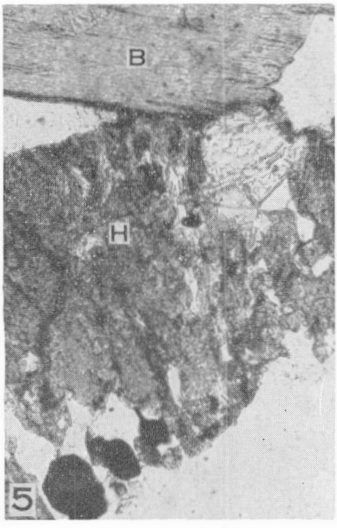

5

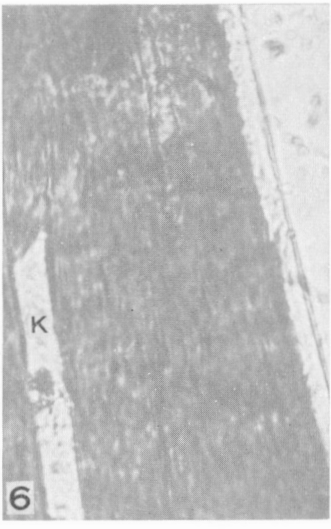

6

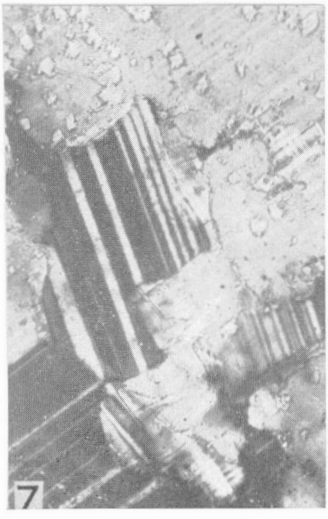

7

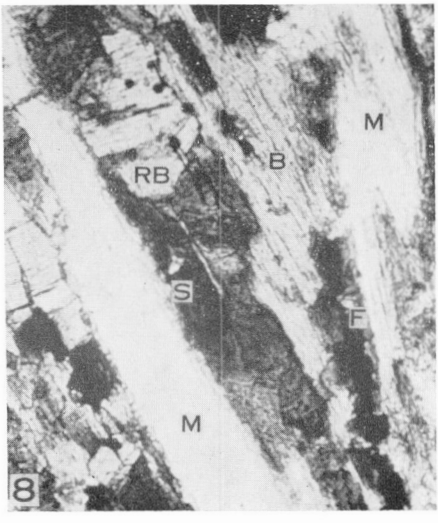

8

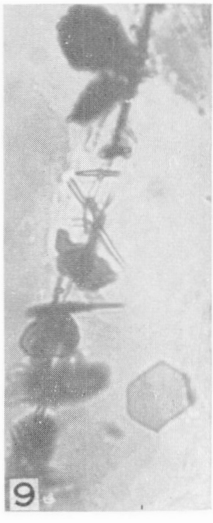

9

PLATE VI

1. Granodiorite *42*. Biotite concentrate. x540.
Biotite flake recrystallized to an aggregate of small flakes in random orientation.

2. Granodiorite *42*. Biotite concentrate. x540.
Biotite flake partly replaced by an aggregate of muscovite, chlorite, potassium feldspar, quartz, rutile, and iron oxides.

3. Granodiorite *42*. Biotite concentrate. x540.
Biotite flake displays distinct (001) splitting and micrographic intergrowths with quartz (Q) on (001) planes.

4. Mafic-rich inclusion from granodiorite *16*. Thin section. +N, x50.
Poikilitic checkerboard plagioclase with inclusions of biotite (B), epidote (E), opaque grains, and veinlets of quartz (Q).

5. Granodiorite *16*. Thin section. x115.
Mafic minerals: hornblende (H), coarse-grained poikilitic biotite (B), fine-grained biotite (BF), sphene (S), apatite (A), epidote (E).

6. Granodiorite *40*. Thin section. +N, x50.
Two small zoned crystals in the core of a coarse zoned plagioclase.

7. Granodiorite *40*. Thin section. x50.
Interstitial patches of biotite suggesting porphyroblastic growth of small grains.

8. Granodiorite *17*. Thin section. x115.
Plagioclase with inclusions of apatite (A) and muscovite (M) surrounded by biotite, hornblende (H), epidote (E), and sphene (S).

9. Granodiorite *17*. Thin section. +N, x50.
Zoned, composite plagioclase (An_{43-23}).

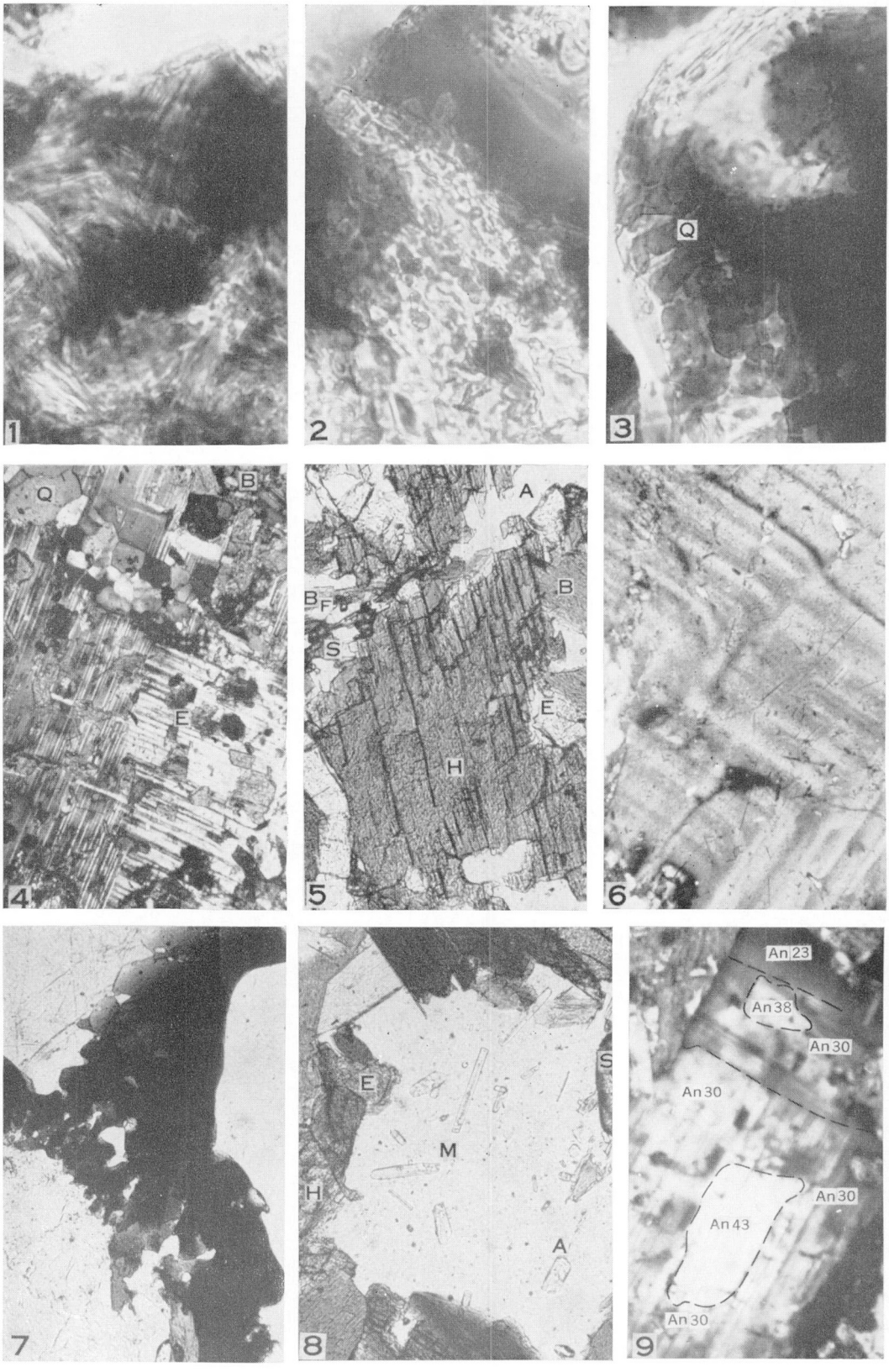
1
2
3
Q
4
Q
B
E
5
A
B
F
S
E
H
6
7
8
E
S
M
H
A
9
An 23
An 38
An 30
An 30
An 30
An 43
An 30

PLATE VII

1. Quartz monzonite 22. Thin section. +N, x50.
Microcline with altered inclusions of plagioclase, quartz (Q), and biotite (B). Biotite is replaced along the edges by muscovite (M) and iron oxides (opaque).

2. Quartz monzonite 22. Thin section. +N, x115.
Quartz and microcline with flame perthite along the grain boundaries. (M) is an interstitial muscovite.

3. Quartz monzonite 22. Thin section. x115.
Biotite with a few small pleochroic haloes partly replaced by muscovite (M).

4. Porphyritic quartz monzonite 23. Thin section. +N, x115.
Myrmekite spreading from albitic rim of plagioclase replaces microcline (M) and biotite (B). Note micrographic biotite-quartz intergrowths (Q) adjacent to myrmekite.

5. Leuco quartz monzonite 41. Thin section. x50.
Muscovite (M) replaces biotite (B). Biotite contains numerous zircon inclusions surrounded by dark pleochroic haloes.

6. Leuco quartz monzonite 41. Thin section. +N, x50.
Zoned plagioclase (An_{25-13}) with an altered core and albitic rim with quartz inclusions (Q) which grades into myrmekite (M). Myrmekite spreads into microcline. Microcline contains inclusions of biotite (B).

7. Medium-grained quartz monzonite 25. Thin section. +N, x115.
Zoned plagioclase crystal. Calcic zones are in part replaced by secondary white mica.

8. Quartz monzonite 28. Thin section. +N, x115.
Muscovite transects biotite. Muscovite ends are fibrous and shredded, and are intergrown with quartz.

9. Quartz monzonite 29. Thin section. +N, x50.
Coarse-grained plagioclase with an altered core (P) and ragged flake of biotite (B) in groundmass composed of granular and amoeboid quartz (Q), myrmekite (M), microcline, and fine-grained biotite (B).

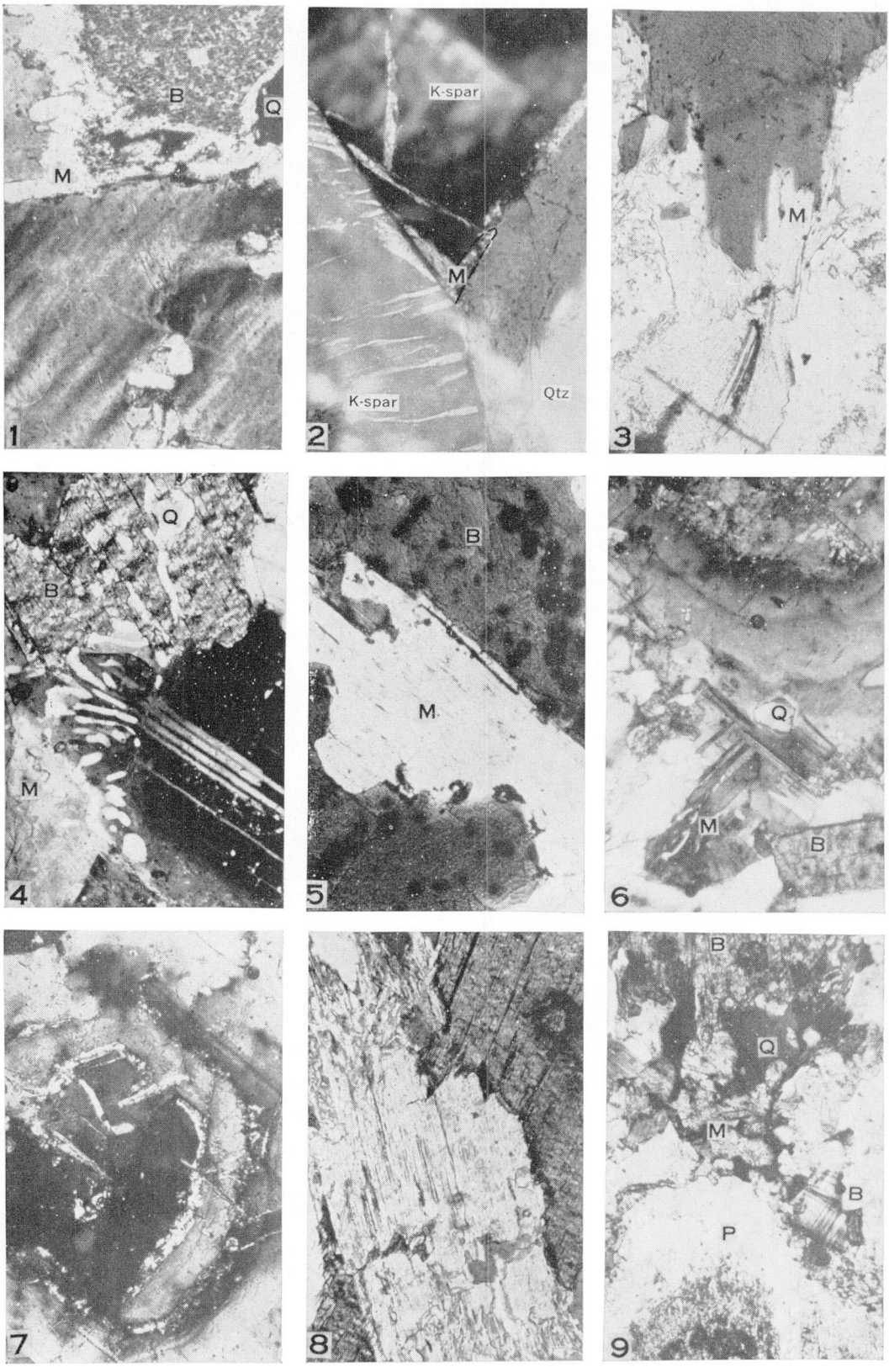
B
Q
M
1
K-spar
M
K-spar
Qtz
2
M
3
Q
B
M
4
B
M
5
Q
M
B
6
7
8
B
Q
M
B
P
9

PLATE VIII

1. Quartz monzonite 29. Thin section. +N, x50.
Checkerboard albite surrounded by fine-grained mosaic of quartz.

2. Quartz monzonite 29. Thin section. x115.
Biotite crystal with inclusions of apatite (A) and sphene (S), partly resorbed and replaced by quartz (Q), perthite and checkerboard albite (P). Biotite locally displays micrographic intergrowths with potassium feldspar (G).

3. Gneissic quartz monzonite 30. Thin section. x115.
Parallel laths of biotite (B), locally recrystallized to red-brown flakes (R), associated with hornblende (H), quartz (Q), and microcline (M).

4. Gneissic quartz monzonite 30. Thin section. +N, x115.
Small specks of biotite (B) and hornblende (H) associated with sphene (S), apatite (A), quartz, and plagioclase.

5. Quartz monzonite 2. Thin section. x115.
Biotite (B) altered to chlorite and to fine-grained aggregate of sphene, in part replaced by muscovite (M).

6. Quartz monzonite 2. Thin section. x540.
Muscovite with remnants of altered, resorbed biotite.

7. Quartz monzonite 2. Thin section. x115.
Calcite veinlet (C) containing muscovite (M) cuts across a coarse-grained microcline.

8. Radioactive orebody 38. Thin section. x115.
Biotite surrounded by a narrow rim of fine-grained hematite.

9. Radioactive orebody 38. Thin section. +N, x115.
Uraninite crystal on biotite surrounded by pleochroic halo.

10. Radioactive orebody 38. Thin section. x115.
Autoradiogram of uraninite crystal illustrated in Pl. VIII-9.

1

2

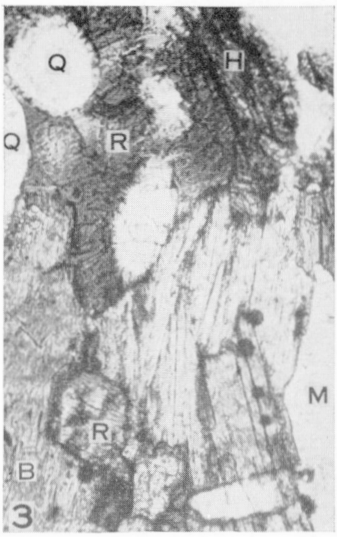

3

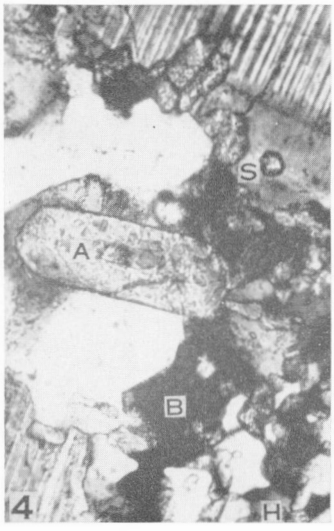

4

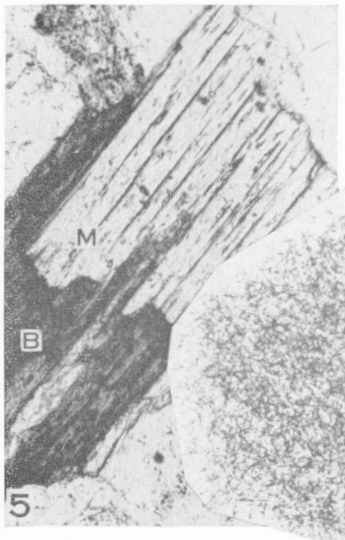

5

6

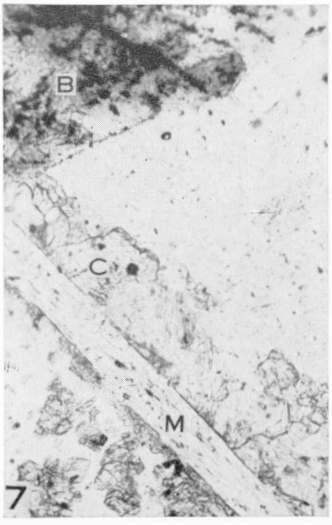

7

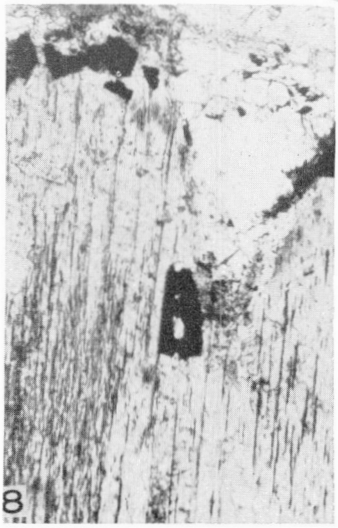

8

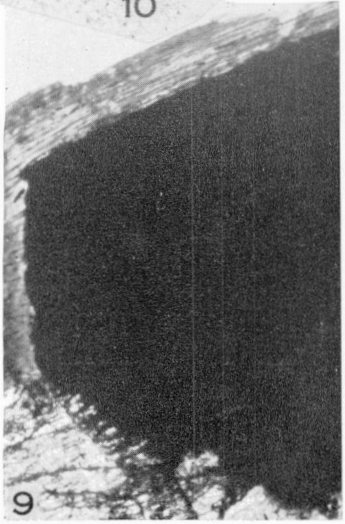

9

10

PLATE IX

1. Pyroxene-hornblende-biotite gneiss *8*. Thin section. x115.
Fractured pyroxene (P) in part replaced by biotite (B), which contains inclusions of apatite (A), surrounded by pleochroic haloes, and spreads into hornblende (H) and quartz (Q). Small opaque grains are pyrite crystals.

2. Hornblende-biotite gneiss *18*. Thin section. x115.
Long laths of biotite are partly replaced by quartz and are rimmed by thin films of impure potassium feldspar (K).

3. Hornblende-biotite gneiss *18*. +N, x50.
Twinned albite porphyroblasts with inclusions of epidote, biotite, and quartz.

4. Hornblende-biotite porphyroblastic gneiss *21*. Thin section. x50.
Biotite and hornblende (H) are partly replaced by porphyroblastic feldspar (F) and quartz.

5. Hornblende-biotite porphyroblastic gneiss *21*. Thin section. x50.
Remnants of biotite (B), hornblende (H), and coarse, porphyroblastic allanite (A).

6. Biotite-quartz-feldspar veined gneiss *24*. Thin section. x115.
Biotite (B), in part replaced by plagioclase (P), and epidote (E) that rims allanite (A).

7. Biotite-cordierite schist *27*. Thin section. +N, x115.
Cordierite (C) is slightly altered to colourless mica (M) and to isotropic material along fractures; cordierite and muscovite (white rim (X)) replace biotite (B).

8. Biotite-muscovite paragneiss *15*. Thin section. x115.
Muscovite (M) and magnetite (MG) replace biotite (B).

9. Biotite paragneiss *20*. Thin section. x115.
Ragged, partly resorbed patches of biotite with opaque rims along the margins and fractures, and surrounding a dark zircon inclusion (Z).

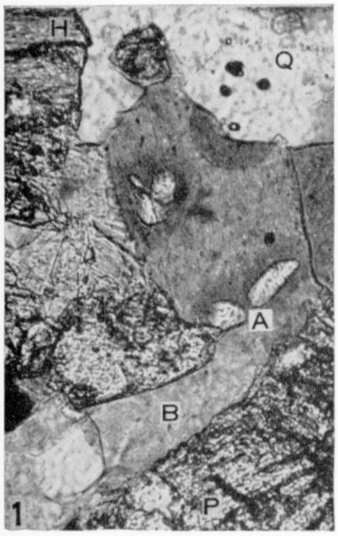
H
Q
A
B
P
1

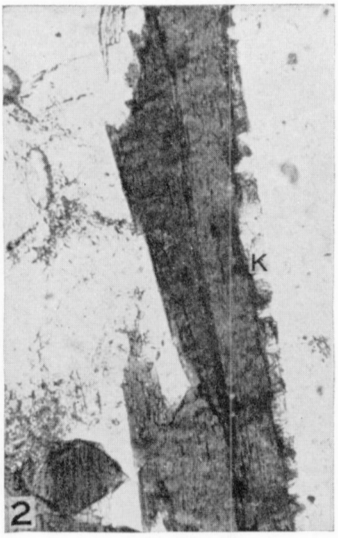
K
2


3


F
H
4

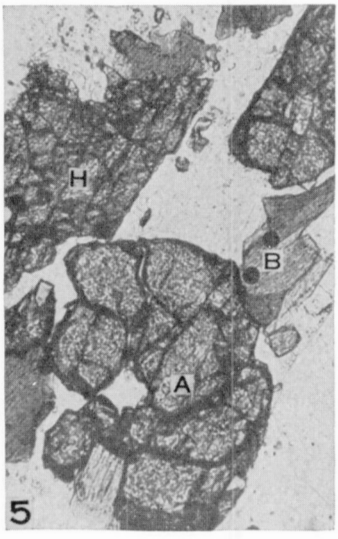
H
B
A
5

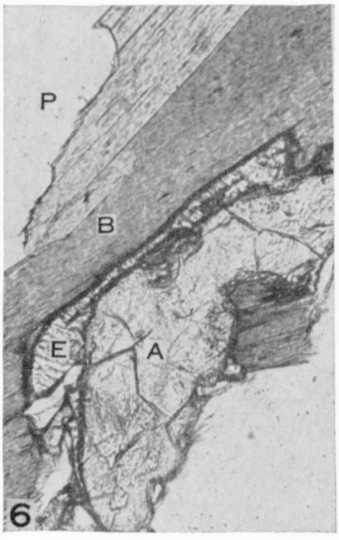
P
B
E
A
6

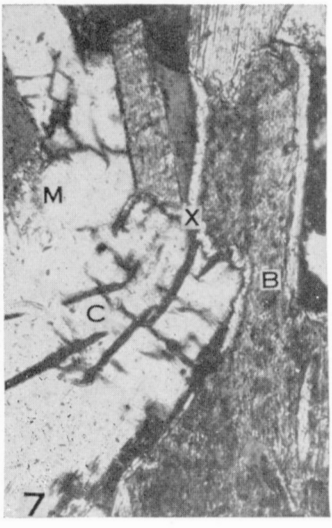
M
X
B
C
7

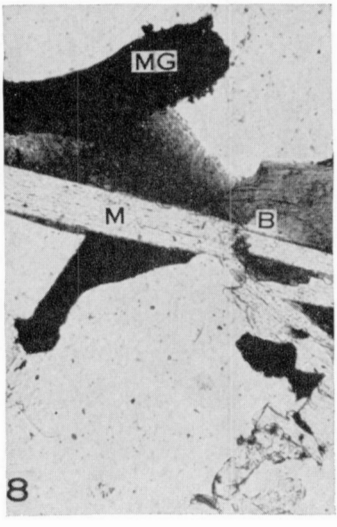
MG
M
B
8

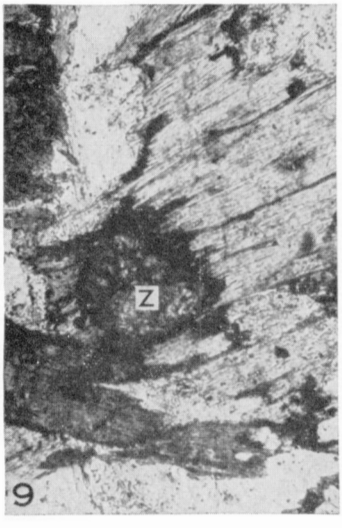
Z
9